

PROTEIN SELF-ORGANIZATION IN CYANOBACTERIA

By

Joshua Scott MacCready

A DISSERTATION

Submitted to
Michigan State University
in partial fulfillment of the requirements
for the degree of

Microbiology and Molecular Genetics — Doctor of Philosophy

2018

ABSTRACT

PROTEIN SELF-ORGANIZATION IN CYANOBACTERIA

By

Joshua Scott MacCready

Proteins from the MinD/ParA family of ATPases are ubiquitous across the microbial world. Primarily studied in *E. coli* for their ability to self-organize in space and time, these proteins control a wide range of cellular functions. Indeed, MinD is a critical component of the Min system, which defines the cell division plane, and ParA is a critical component of the Par system, which segregates plasmids, chromosomes and other large macromolecular structures in the cell. The capacity of these proteins to self-organize requires: (i) a biological surface - membranes for MinD and the nucleoid for ParA, (ii) ATP, and (iii) an additional protein to provide site specificity – MinE for MinD and ParB for ParA.

Cyanobacteria comprise a phylum of photosynthetic bacteria that have important ecological, bioindustrial and evolutionary significance. Despite their importance, how MinD/ParA family proteins behave in cyanobacteria has been understudied. Furthermore, cyanobacteria have a number of distinct cellular features relative to the classic prokaryotic models in which self-organizing protein systems have been studied. In this thesis, I used a combination of genetics, microscopy, and computational modeling in the model rod-shaped cyanobacterium *Synechococcus elongatus* PCC 7942 to study several aspects of protein self-organization in cyanobacteria.

I first show that the cyanobacterial Min system exhibits a robust self-organizing oscillation even in the face of the complicating architecture of the thylakoid membranes. My work suggests that this is accomplished in part by the capacity of Min proteins to distinguish and minimize interactions with the thylakoid membranes while maintaining the capacity to transiently self-organize selectively on the plasma membrane.

Since the oscillation of Min proteins defines the division plane by spatially regulating the assembly of the protein FtsZ, and thus, the site of cytokinesis, my next study explored how FtsZ interacts with the plasma membrane. I show that the protein Ftn2 in cyanobacteria and ARC6 in algae and plant chloroplasts are homologs that tether FtsZ to the inner membrane through an evolutionarily conserved domain. In the

absence of Ftn2, FtsZ assembles primarily as filaments throughout *S. elongatus* cells. In contrast, upon overexpression of Ftn2, numerous FtsZ filaments assemble as zig-zag patterns. These results suggest that Ftn2 stoichiometry is important for properly defining the cell division plane.

Lastly, I explored how oscillation of a ParA-like protein, McdA, contributes to the organization of carboxysomes, cyanobacterial carbon-fixing microcompartments. I found that McdA binds to the nucleoid as a biological surface for self-organization of oscillatory patterns. A novel factor, McdB, was found to be required for McdA dynamics on nucleoids. McdB colocalizes with carboxysomes through interaction with carboxysome shell components, and stimulates the inherent ATPase activity of nearby McdA that is bound to the DNA. This effect is similar to the effect of ParB proteins on ParA ATPase activity even though McdB shares no similarity with known ParB proteins. Computational modeling and *in vivo* microscopy also suggested that McdB-bound carboxysomes produce zones of McdA depletion on nucleoids and that carboxysome movement is directed towards the highest local McdA concentration. Together, this work substantially improves our understanding of how MinD/ParA family proteins self-organize in cyanobacteria and has broader implications for understanding self-organization in other diverse microbes.

Copyright by
JOSHUA SCOTT MACCREADY
2018

ACKNOWLEDGMENTS

I wish to thank my advisors, Daniel Ducat and Katherine Osteryoung, for helping me become a better scientist and for providing me the freedom to fail and succeed on my own. I wish to also thank the members of my guidance committee for their encouragement and support: Lee Kroos, Beronda Montgomery, Claire Vieille and Chris Adami.

TABLE OF CONTENTS

LIST OF FIGURES	viii
KEY TO ABBREVIATIONS	ix
CHAPTER 1	1
A REVIEW OF MIN AND PAR SYSTEM FUNCTION	1
Summary	2
Introduction to Cyanobacteria.....	3
The Min System	5
Introduction.....	5
Conserved features of the Min system across canonical model bacteria.....	6
Differences between model systems	6
In vitro and in silico Min system dynamics	7
The Cyanobacterial Min System.....	9
The Par System	12
Introduction.....	12
Plasmid partitioning by the ParABS System	12
Model for ParA-mediated plasmid partitioning	13
The cyanobacterial McdAB system	14
Conclusion	16
REFERENCES	17
CHAPTER 2	25
ROBUST MIN-SYSTEM OSCILLATION IN THE PRESENCE OF INTERNAL PHOTOSYNTHETIC MEMBRANES IN CYANOBACTERIA	25
Summary	26
Source	26
CHAPTER 3	27
AN EVOLUTIONARILY CONSERVED DOMAIN IN CYANOBACTERIAL FTN2 AND CHLOROPLAST ARC6 INTERACTS WITH FTSZ/FTSZ2.....	27
Summary	28
Introduction	29
Results and Discussion	33
Ftn2 is an Essential Regulator of Z ring formation in <i>S. elongatus</i>	33
A Conserved FtsZ-binding domain in Ftn2 and ARC6	38
A C-terminal Domain of FtsZ is Required for Ftn2 Interaction	41
An Evolutionarily Conserved Mechanism for FtsZ Membrane-Anchoring in the Green Photosynthetic Lineage.....	44
Methods.....	45
Construct Designs	45
Culture Conditions and Transformations	46
Fluorescence microscopy	47
Phylogenetic analysis	47
REFERENCES	48
CHAPTER 4	54
PROTEIN GRADIENTS ON THE NUCLEOID POSITION THE CARBON-FIXING ORGANELLES OF CYANOBACTERIA.....	54

Summary	55
Introduction	56
Results.....	59
McdA Dynamically Patterns Along the Nucleoid	59
A Previously Uncharacterized Protein Localizes to Carboxysomes and is Essential for Emergent McdA Dynamics.....	63
McdB Interacts with Major and Minor Shell Components	66
Carboxysome Formation is Required for the Emergent Oscillations of McdA.....	69
Carboxysome Positioning is Disrupted in McdA/McdB Mutants	71
Carboxysome Ultrastructure is Disrupted in McdA/McdB Mutants.....	75
Carboxysomes Locally Deplete McdA on the Nucleoid and are Required for McdA Oscillation.....	78
Carboxysomes are Hexagonally Arranged when Crowded on a Nucleoid	81
The Brownian-ratchet model is Sufficient to Explain Carboxysome Distributions.....	85
The McdAB System is Evolutionarily Wide-spread in Cyanobacteria	86
Discussion	87
McdA is Not Cytoskeletal and Utilizes the Nucleoid to Position Carboxysomes.....	87
A Unique System for Distributing Protein-based Bacterial Organelles.....	87
McdA Oscillations are a Consequence of Multiple Carboxysomes Sharing the Same Nucleoid in a Rod-shaped Cell.....	89
A Brownian-Ratchet Mechanism Ensures Carboxysome Distributions Required for both Inheritance and Homeostasis.....	90
McdA and McdB may Facilitate Biogenesis and Regulate Carboxysome Size	91
The McdAB System in other Organisms.....	92
Methods.....	93
Construct Designs	93
Culture Conditions and Transformations	94
Bacterial-two-hybrid Analysis	94
Induction Strains.....	95
Fluorescence Microscopy	95
Transmission Electron Microscopy.....	96
MicrobeJ Quantification	96
McdA-GFP-His Expression and Purification	97
His-MBP-McdA Expression and Purification.....	98
ATPase Assay.....	99
DNA Binding Assay	99
TIRFM of McdA-GFP binding to a DNA-carpeted Flowcell.....	99
Theoretical model and computational method	100
REFERENCES	103
CHAPTER 5	111
PERSPECTIVES AND FUTURE DIRECTIONS	111
Cyanobacteria as model systems for studying Min and Par dynamics.....	112
Circadian Rhythms	112
Thylakoid Membranes.....	117
Nucleoid Topology.....	118
Future Directions.....	120
Identification & Diversity of BMC Trafficking Systems Across Bacteria.....	123
REFERENCES	124

LIST OF FIGURES

Figure 1.1: Diverse Min and Par system function.....	11
Figure 3.1: Altered Ftn2 expression disrupts FtsZ patterning	32
Figure 3.2: Identification of the FtsZ2 interacting domain of ARC6 via yeast two-hybrid	36
Figure 3.3: Alignment of Ftn2 and ARC6 FtsZ binding domains across photosynthetic organisms	37
Figure 3.4: Colocalization of Ftn2/ARC6 with FtsZ/FtsZ2 in <i>S. pombe</i> is dependent upon the ZBD domain	40
Figure 3.5: The c-terminus of <i>S. elongatus</i> FtsZ interacts with Ftn2.....	42
Figure 3.6: Cross-interaction between Ftn2/ARC6 and FtsZ2/FtsZ	43
Figure 4.1: The <i>S. elongatus</i> ParA-like protein, McdA, binds nonspecifically to nucleoid DNA with ATP..	61
Figure 4.2: mNG-McdA oscillates and mNG-McdB is recruited to carboxysomes.....	62
Figure 4.3: A small, carboxysome-localized protein is required for McdA oscillatory dynamics	65
Figure 4.4: McdB interacts with the carboxysome shell.....	67
Figure 4.5: McdA/B bacterial two-hybrid against carboxysome shell proteins.....	68
Figure 4.6: McdA and McdB are essential for distributing carboxysomes	70
Figure 4.7: McdAB physically separate and regulate carboxysome ultrastructure	73
Figure 4.8: Quantification of carboxysome size from TEM	74
Figure 4.9: Carboxysomes locally deplete McdA from the nucleoid and cause McdA oscillation at high-copy number	77
Figure 4.10: McdAB account for linear and hexagonal packing of carboxysomes.....	80
Figure 4.11: Carboxysomes fall between nucleoids in elongated cells lacking McdA or McdB.....	83
Figure 4.12: Evolutionary conservation of McdAB	84
Figure 5.1: Cyanobacterial features possibly influencing Min and Par system function.....	116
Figure 5.2: Diversity of bacterial microcompartments	122

KEY TO ABBREVIATIONS

Δ	Deletion
AA	Amino Acid
ARC3	Accumulation and Replication of Chloroplasts protein 3
ARC6	Accumulation and Replication of Chloroplasts protein 6
ATP	Adenosine-5'-Triphosphate
B2H	Bacterial Two-Hybrid
BG-11	Blue-Green Medium
BLAST	Basic Local Alignment Search Tool
BMC	Bacterial Microcompartment
C-terminal	Carboxy terminal
Cdv3	Cell Division protein 3
CL	Cardiolipin
DGDG	Digalactosyldiacylglycerol
DNA	Deoxyribonucleic acid
FRAP	Fluorescence Recovery After Photobleaching
Ftn2	Filamentation protein 2
FtsZ	Filamentous Temperature Sensitive protein Z
GTP	Guanosine-5'-triphosphate
IPTG	Isopropyl-beta-D-thiogalactopyranoside
McdA	Maintenance of Carboxysome Distribution A
McdB	Maintenance of Carboxysome Distribution B
MinC	Minicell phenotype C
MinD	Minicell phenotype D
MinE	Minicell phenotype E
MGDG	Monogalactosyldiacylglycerol

msfGFP	Monomeric Superfolder Green Fluorescent Protein
mNG	mNeonGreen
mTQ	mTurquoise2
N-terminal	Amino terminal
OE	Overexpression
OM	Outer Membrane
ParA	Partitioning protein A
ParB	Partitioning protein B
PARC6	Paralog of Accumulation and Replication of Chloroplasts protein 6
PBS	Phosphate-buffered saline
PCC	Pearson's Correlation Coefficient
PE	Phosphatidylethanolamine
PG	Phosphatidylglycerol
PM	Plasma Membrane
SopA	Segregation of Plasmids Protein A
SopB	Segregation of Plasmids Protein B
SopC	Segregation of Plasmids Protein C
SQDG	Sulfoquinovosyl Diacylglycerol
TEM	Transmission Electron Microscopy
TIRFM	Total Internal Reflection Fluorescence Microscopy
TM	Thylakoid Membrane
Y2H	Yeast Two-Hybrid
ZBD	FtsZ Binding Domain

CHAPTER 1

A REVIEW OF MIN AND PAR SYSTEM FUNCTION

Summary

Biological pattern formation is a fundamental feature found throughout nature. Across a wide range of scales, complex patterns can emerge as a consequence of simple rules of interaction between biological agents. This includes ripples in bird flocks or schools of fish, spirals of sunflower seeds, and zig-zag patterns on sea shells. These patterns can also occur at the protein level, and are referred to as protein self-organization. In bacteria, proteins from the ParA/MinD family of ATPases have been studied for their ability to spontaneously self-organize along biological surfaces, such as membranes and DNA, and display robust and dynamic spatio-temporal oscillation within cells. These emergent patterns are responsible for a variety of processes ranging from the spatial regulation of cytokinesis (Min system) to the partitioning (Par system) of cellular material such as chromosomes, plasmids and other low-copy-number macromolecular complexes. Herein, I review both the Min and Par systems and discuss how these systems may have been adapted for the unique metabolic and architectural features of the cyanobacterial cell.

Introduction to Cyanobacteria

Cyanobacteria are an ancient (~3.5-Billion-year-old) and diverse phylum of prokaryotes that possess many unique cellular features that distinguish them from classic prokaryotic model organisms, such as *Escherichia coli* and *Bacillus subtilis* (Schopf, 2011). For example, cyanobacteria come in a wide range of morphologies, including, unicellular, baeocytous, filamentous, heterocytous and ramified (Shih et al., 2013). Cyanobacteria are also the only prokaryotes that perform oxygenic photosynthesis, estimated to account for between 20 and 30 percent of global photosynthesis (Partensky et al., 1999), so their ecological impact cannot be understated. The molecular machinery required to convert light energy into chemical energy is localized to specialized membranes called thylakoid membranes (Vothknecht and Westhoff, 2001). Thylakoid membranes are positioned interior to the plasma membrane, separate the cytoplasm from the lumen, and dramatically increase the surface area available for light capture and ATP / NADPH production by arranging into extensive networks with complex geometries (Liberton et al., 2013).

The chemical energy produced by photosynthesis (i.e. ATP and NADPH) is then used in combination with ribulose 1,5-bisphosphate and CO₂ to make glyceraldehyde 3-phosphate, the first step of which occurs within protein-based organelles called carboxysomes (Kerfeld et al., 2010). Carboxysomes are large macromolecular structures that help start the Calvin-Benson-Bassham cycle by encapsulating the enzyme Ribulose-1,5-bisphosphate carboxylase / oxygenase with carbonic anhydrase to create a high CO₂ environment, ultimately contributing to nearly 30% of global CO₂ fixation (Field et al., 1998; Liu et al., 1999).

Consistent with their photosynthetic lifestyle, cyanobacteria are also the only known prokaryotes to possess a precise circadian clock that operates on a 24-hour periodicity. This unique cellular feature allows cyanobacteria to change the expression of genes regulating critical processes, such as metabolism, growth and cell division in anticipation of global light / dark cycles (Cohen and Golden, 2013). One of the best examples of this process is with the filamentous cyanobacterium *Lyngbya aestuarii*, where the biological clock temporally separates nitrogen-fixation, which is oxygen sensitive, and photosynthesis (Stal and Krumbein, 1985; Mitsui et al., 1986). This method of nitrogen fixation regulation is not universal among nitrogen-fixing cyanobacteria, however. Some species, such as *Anabaena sp.* PCC 7120, undergo cellular

differentiation to produce heterocysts, specialized cells that lack key components of the oxygen-evolving complex of photosystem II, thereby creating a microoxic environment (Wolk, 1994).

Since cyanobacteria possess diverse biochemical abilities, are genetically tractable and have simple nutrient requirements, they have become the target for numerous biotechnological applications. Emphasis has been placed on metabolic engineering of cyanobacteria for the light-driven production of a variety of commodity, and high-value biologics, including ethanol, ethylene, hydrogen, isobutanol, isoprene, and squalene (Sakai et al., 1997; Atsumi et al., 2009; Lindberg et al., 2010; Ducat et al., 2011; Ruffing, 2011; Zhou et al., 2012; Berla et al., 2013). Cyanobacteria have also been explored as possible alternative bioindustrial feedstocks, either for raw biomass or for their capacity to secrete extracellular sugars that can be converted to other bioproducts through microbial fermentation (Hays and Ducat, 2015). For example, one study demonstrated that stable synthetic consortia could support the growth of *Bacillus subtilis* and *Escherichia coli* and their production of alpha-amylase and polyhydroxybutyrate, respectively, solely from the photosynthate of an engineered sucrose-exporting cyanobacterium (Hays et al., 2017). Using this same sucrose-exporting cyanobacterial strain, another study demonstrated that a high-level of polyhydroxybutyrate production was possible from co-cultures of sugar-secreting cyanobacteria with the heterotrophic microbe *Halomonas boliviensis* (Weiss et al., 2017). A better understanding of cyanobacterial cell biology will ultimately be important moving forward as biotechnological interests increase.

Finally, most cyanobacteria possess multiple copies of their genome. Indeed, while some cyanobacteria, such as *Synechococcus elongatus* PCC 7942, are oligoploid and possess 3-4 copies of their chromosome on average, other species, such as *Synechocystis* sp. PCC 6803, are polyploid, possessing well over 200 copies (Griese et al., 2011). Although genome copy number varies over the cell cycle, protein production surprisingly remains constant (Zheng et al., 2017). Interestingly, while most bacteria possess a nucleoid occlusion system, mechanisms that prevent formation of cell division machinery overtop of a chromosome, cyanobacteria lack homologs of all known nucleoid occlusion systems. Therefore, how cyanobacteria segregate and maintain genome integrity remains an outstanding question. Collectively, these features distinguish cyanobacteria from other well-studied microbes and have broader implications for understanding cell-cycle regulation and biological pattern formation.

The Min System

Introduction

Most bacteria divide at midcell to form two equivalently sized daughter cells (binary fission). Establishment of the division plane at the cell center involves controlled polymerization of the GTPase FtsZ, the prokaryotic homolog of eukaryotic tubulin, into a ring-like structure (Z ring) (Bi et al., 1991). Initially, FtsZ polymerizes into numerous protofilaments by binding GTP (Mukherjee and Lutkenhaus, 1998; Romberg et al., 2001). However, these protofilaments remain relatively short -- roughly 30 subunits long for *E. coli* FtsZ due to its relatively high intrinsic GTPase activity, which promotes subunit exchange from protofilaments (Scheffers et al., 2002; Chen and Erickson, 2005). Therefore, lateral interactions between protofilaments and stabilization along the plasma membrane via interactions with peripheral and/or integral proteins are needed to facilitate Z-ring formation (Huang et al., 2013). This mature Z ring then functions as a scaffold for the recruitment of numerous additional divisome factors required for cell wall synthesis / remodeling and membrane constriction (Lutkenhaus, 2007; Rowlett and Margolin, 2015).

Since cell division will ensue wherever Z rings are assembled, correct positioning of FtsZ filaments near the center of the cell is critical to ensure both daughter cells inherit equal quantities of cellular material. The Min system, coined for the minicell phenotype observed in mutant lines, is mainly responsible for positioning FtsZ at midcell (reviewed in: Lutkenhaus, 2007; Rowlett and Margolin, 2013). Primarily studied in the model gram-negative bacterium *E. coli* and model gram-positive bacterium *B. subtilis*, the Min system functions to inhibit assembly of FtsZ toward polar regions of the cell, confining FtsZ assembly to midcell. While both systems possess nearly the same complement of Min-system proteins, the underlying mechanisms for spatially regulating FtsZ differ greatly.

Conserved features of the Min system across canonical model bacteria

A negative regulator of FtsZ assembly must be positioned in close proximity to FtsZ to prevent Z-ring assembly away from midcell. MinC and MinD fulfill this role in *E. coli* and *B. subtilis* (de Boer et al., 1989; Varley and Stewart, 1992), where the primary FtsZ antagonist, MinC, inhibits FtsZ assembly (de Boer et al., 1990). The N-terminal domain of MinC is responsible for weakening the bonds between FtsZ subunits, whereas the C-terminal domain inhibits lateral interaction between FtsZ polymers and promotes MinC dimerization (Hu and Lutkenhaus, 2000). Therefore, regions within the cell where MinC is concentrated are also areas where FtsZ cannot polymerize into higher-order structures. Since FtsZ assembles along the plasma membrane, the activity of MinC needs to be concentrated to this area. In both organisms, MinD, a Walker A-type cytoskeletal ATPase, dimerizes and cooperatively binds to membranes via a short C-terminal amphipathic helix that transiently inserts into the apolar interior of the lipid bilayer in the presence of ATP (Szeto et al., 2002; Hu and Lutkenhaus, 2003). Membrane-bound MinD then recruits MinC via conserved switch I and switch II domains to form the MinCD anti-FtsZ complex (Zhou and Lutkenhaus, 2004). However, the MinCD complex inherently lacks site specificity within cells, and will form a homogeneous distribution of FtsZ depolymerization activity across the entire plasma membrane in the absence of other positional cues. Therefore, an additional factor is required to concentrate MinCD activity primarily towards polar regions of the cell to confine FtsZ assembly to the cell center.

Differences between model systems

The additional factor that provides site specificity to the MinCD complex differs between the two model bacteria where the Min system has been most intensively studied. In *B. subtilis*, the protein DivIVA recruits the MinCD complex to the membrane via the accessory protein MinJ. Mechanistically, DivIVA possesses a highly conserved N-terminal crossed-loop geometry-sensing domain that binds to regions of the plasma membrane that are negatively curved (Edwards and Errington, 1997; Marston et al., 1998; Marston et al., 1999; Lenarcic et al., 2009; Ramamurthi and Losick, 2009; Oliva et al., 2010; Eswaramoorthy

et al., 2011; Bach et al., 2014). Since membrane curvature is highest towards polar regions of the cell, this topological feature is used as a positional cue for DivIVA to concentrate MinCD at both poles, thereby inhibiting FtsZ assembly. Moreover, once FtsZ assembly is established at midcell and binary fission is initiated, new regions of highly curved membranes emerge adjacent to the division site. A pool of DivIVA, MinJ and MinCD then localizes to this newly formed curvature region where it is proposed to prevent lateral FtsZ filament assembly (Eswaramoorthy et al., 2011) (Figure 1.1A). Thus, in *B. subtilis*, the inherent geometry of the plasma membrane upon which Min proteins assemble is utilized as a positional scaffold to restrict FtsZ polymerization to midcell.

E. coli lacks DivIVA and MinJ; instead it possesses a small protein called MinE (de Boer et al. 1989). Unlike the *B. subtilis* Min system, the *E. coli* Min system proteins do not directly sense the geometry of the membrane. Instead, MinE positions the MinCD complex via a dynamic spatiotemporal mechanism (Raskin and de Boer, 1999). MinE exists as a dimer that binds the plasma membrane via an N-terminal amphipathic helix in the presence of MinD (King et al., 2000; Park et al., 2011). The binding of MinE to MinD stimulates the inherent ATPase activity of MinD (Hu and Lutkenhaus, 2001). Since MinD needs to be bound to ATP to dimerize and bind the membrane, the hydrolysis of its nucleotide promotes the release of MinD, and subsequently MinC, from the plasma membrane. The local MinD-to-MinE ratio is key to emergent protein dynamics, since MinD is stabilized on the membrane when the ratio is high and is released when the ratio is low (Vecchiarelli et al., 2016). This “toggle switch” drives an emergent pole-to-pole oscillation of these proteins, with MinC as a passenger, resulting in a time-averaged gradient of MinC anti-FtsZ activity that is highest at the polar regions of the cell, preventing FtsZ assembly, and lowest at midcell, allowing FtsZ to establish the division plane (Raskin and de Boer, 1999; Lutkenhaus, 2007) (Figure 1.1A).

In vitro and *in silico* Min system dynamics

The *E. coli* MinCDE pole-to-pole oscillation is a remarkable example of protein self-organization. Following the identification of the minimal components required for emergent patterning of the Min system, which include: (i) diffusion, (ii) ATP, (iii) MinD and MinE, and (iv) a lipid membrane, these patterns could be

reconstituted *in vitro* (Meinhardt and de Boer, 2001). One such experiment explored the behavior of Min proteins on a flat lipid surface, where Min proteins form spiraling patterns across the entire surface (Loose et al., 2008; Loose et al., 2011). More recent studies have explored the robust nature of these emergent patterns by altering the geometry of membranes accessible to MinDE. In fabricated lipid-lined micro-compartments, MinDE formed standing-wave patterns in long compartments created to represent filamentous cells (Zieske and Schwille, 2014). In wider compartments, MinDE patterns became erratic, forming swirl-like patterns (Zieske and Schwille, 2014). Additional work has explored how Min patterning behaves in fabricated square, round and triangle-shaped compartments. Although Min proteins oscillated within these unique geometries, oscillations were occasionally observed to spiral around the perimeter of the compartment (Wu et al., 2015). Together, these *in vitro* reconstitution studies highlighted that emergent Min patterning can differ among topologically equivalent compartments, and is thus a consequence of the surface-to-volume ratio of the cell.

The *E. coli* Min system has also been extensively modeled *in silico*. Using reaction-diffusion simulations, based on known protein diffusion coefficients and reaction rates, several studies explored the robust nature of the Min system in more detail; including the influence of a closing septum (Tostevin and Howard, 2006), effect of varying Min-system stoichiometries (Kruse et al., 2007), and how symmetry between MinD and MinE initially emerges (Petrášek and Schwille, 2015). Moreover, these simulations were able to suggest possible Min-system behavior in diverse organisms that are not genetically tractable. For example, one group modeled MinDE patterning in 3-dimensional sinusoidal and helix-shaped cells, morphologies which can be generated using mutant strains of *E. coli* or found natively in bacteria such as spirochaetes and cyanobacteria, and found that striped patterning of Min proteins emerges as a consequence of membrane geometry (Hoffmann and Schwarz, 2013). The combination of *in vitro* and *in silico* techniques has yielded a much better understanding of Min-system behavior that would otherwise be difficult to explore *in vivo*.

The Cyanobacterial Min System

The above studies indicated that the cellular surface-to-volume ratio was a main factor responsible for emergent Min patterning. However, at the outset of my dissertation work, Min dynamics within topologically non-equivalent cells had not been truly explored. Indeed, while fluorescent fusions of mitochondrial MinCDE from the amoebozoia *Dictyostelium purpureum* were heterologously expressed in *Saccharomyces cerevisiae* to determine their localization (Leger et al., 2015), this study did not explore Min protein dynamics. Moreover, cristae are folds of the mitochondrial inner membrane, and are thus, topologically equivalent to basic rod- or spherical-shaped bacteria. Likewise, while MinDE are critical for spatially regulating cytokinesis in algae and plant chloroplasts, and while chloroplasts exhibit a unique membrane topology of multiple stacked grana interconnected by lamellae – both features modified from their cyanobacterial ancestors – Min dynamics have not been explored in chloroplasts. Therefore, since thylakoid membranes do not make contact with the plasma membrane in the model rod-shaped cyanobacterium *Synechococcus elongatus* PCC 7942, these cells represent a new topology where emergent Min-system dynamics had not been explored. It seemed possible that thylakoid membranes might preclude emergent Min system patterning by presenting as a diffusion barrier or by acting as a secondary binding site for MinDE (Figure 1.1B). Moreover, cyanobacteria also appeared to possess a complement of both model systems, encoding *minCDE* and a *divIVA*-like gene called Cdv3 (Miyagishima et al, 2005). To address Min-system functioning in cyanobacteria, we explored the localization and dynamic properties of MinC, MinD, MinE and Cdv3 in the model rod-shaped cyanobacterium *Synechococcus elongatus* PCC 7942 (hereafter *S. elongatus*) (MacCready et al. 2017). We found that Min proteins oscillated from pole to pole despite the presence of thylakoid membranes (Figure 1.1C).

How Min patterns were able to emerge in the presence of thylakoid membranes was not obvious however. Using reaction-diffusion simulations, we tested if previously identified perforations within thylakoid layers were sufficient to allow bulk diffusion of Min proteins throughout the cell. To simulate this, we modeled a typical 3 μm by 1 μm *S. elongatus* cell, incorporated an additional internal membrane layer that represented a thylakoid membrane, and varied the permeability of this layer across simulations. In addition,

we ran simulations to test the resulting patterns of Min proteins if they could bind to both the plasma and thylakoid membranes with equal affinity. Our results showed that thylakoid membranes must possess permeability, though the level need not be large ($> 0.7\%$ permeable), consistent with previous studies detailing the existence of perforations across thylakoid layers (Nevo et al., 2007; Nevo et al., 2009). Moreover, Min proteins must possess features that allow them to distinguish plasma and thylakoid membranes; otherwise, our simulations predicted that Min proteins would be mostly sequestered to the large surface area of thylakoid membranes. Our study showed for the first time that native Min oscillations were possible in bacteria other than *E. coli* and that biologically relevant Min protein patterns could emerge despite complex internal membrane topologies (MacCready et al., 2017). Interestingly, we show that in addition to oscillating, MinC was also recruited to mid-cell in a MinD- and Cdv3-dependent manner. Since Cdv3 shares weak homology with *B. subtilis* DivIVA, this result suggests that the *S. elongatus* Min system might be hybrid, displaying both an *E. coli*-like pole-to-pole oscillation of MinCDE and a *B. subtilis*-like mid-cell recruitment of MinCD and Cdv3 (Figure 1.1D). These results have broad implications for understanding FtsZ spatial regulation in other organisms with unique internal membrane architectures, such as chloroplasts and FtsZ-bearing mitochondria.

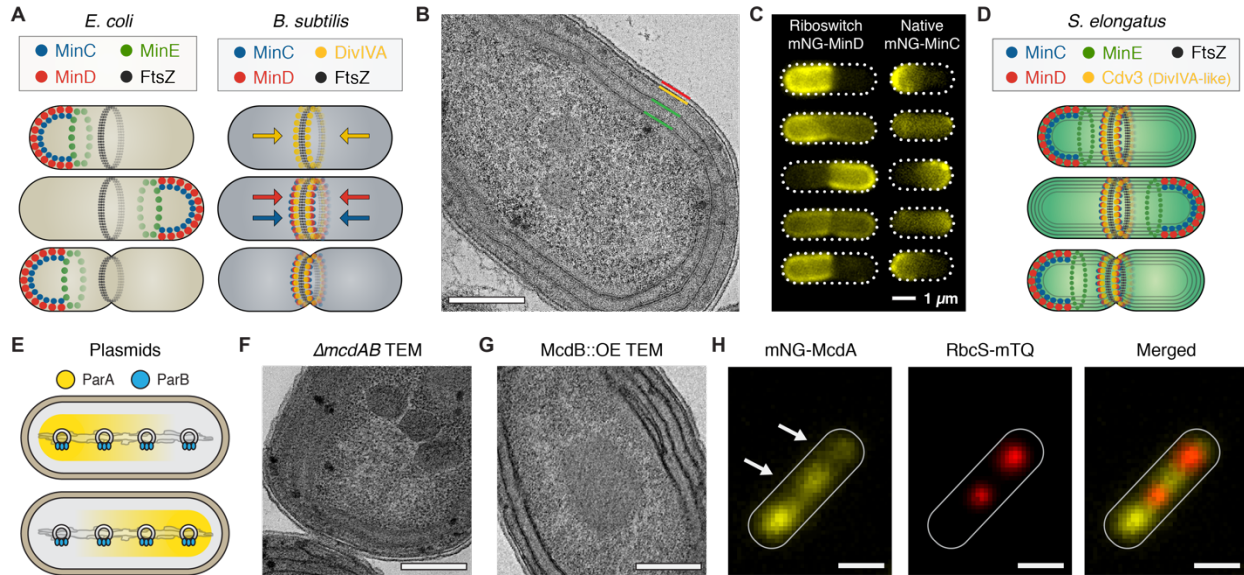


Figure 1.1: Diverse Min and Par system function

(A) Cartoon depiction of Min-system dynamics in *E. coli* and *B. subtilis*. **(B)** Transmission electron micrograph of *S. elongatus* membrane systems. Green = thylakoid membranes, yellow = plasma membrane, red = outer membrane. Scale bar = 200 nm. **(C)** mNG-MinD and mNG-MinC oscillate in *S. elongatus*. Adapted from MacCready et al, 2017. Scale bar = 1 μm . **(D)** Cartoon depiction of Min-system function in *S. elongatus*. **(E)** Cartoon depiction of P1 plasmid segregation in *E. coli*. **(F)** Carboxysomes cluster in *mcdAB* deletions. Scale bar = 200 nm. **(G)** Carboxysome ultrastructure is altered when McdB is overexpressed. Scale bar = 200 nm. **(H)** Depletion zones of McdA (yellow) in the vicinity of carboxysomes (red). Scale bar = 1 μm .

The Par System

Introduction

Prior to cytokinesis, bacteria must segregate cellular cargos, such as chromosomes and low-copy-number plasmids, to ensure faithful inheritance by daughter cells. While eukaryotic cells modify their internal architecture via self-assembling cytoskeletal proteins (reviewed in: Fletcher and Mullins, 2010), it has recently been hypothesized that bacteria primarily utilize ATP-hydrolyzing proteins (ATPases) from the ParA/MinD family to arrange intracellular cargos via self-organization of these proteins into gradients along the nucleoid (reviewed in: Hu et al., 2017). Despite the prevalence and crucial functions of ParA-mediated segregation systems in bacteria, how dynamic gradients of ParA-type ATPases emerge and provide force to arrange intracellular cargo has remained an outstanding question.

Plasmid partitioning by the ParABS System

The best characterized partitioning system is the *E. coli* ParABS system of P1 plasmids (reviewed in: Hayes and Barilla, 2006). ParA shares many similarities with MinD, including an N-terminal Walker A motif, the ability to dimerize upon binding ATP, and ATPase activity (Davis et al., 1992; Lutkenhaus, 2012). However, the biological surfaces upon which MinD and ParA assemble greatly differ: membranes and non-specific DNA, respectively (Vecchiarelli et al., 2012). Nevertheless, additional parallels between the Min system and Par system can be drawn. Similar to how MinD requires a partner protein, MinE or DivIVA, to provide site-specificity, ParA requires ParB. Indeed, ParB is an ATPase-activating protein that dimerizes, binds a sequence-specific region of DNA, and interacts with ParA to stimulate its inherent ATPase activity, resulting in the removal of ParA from the nucleoid (Funnell and Gagnier, 1993).

While MinE alternates between membrane-bound and diffuse states as a component of the Min system, ParB loads onto and around a centromere-like site on P1 plasmids, *parS*, and remains largely static (Davis et al., 1990). Initially, the *E. coli* integration host factor (IHF) binds to the cis-acting *parS* sequence,

which causes a bend in the DNA that facilitates ParB binding (Funnell, 1988). The binding of dimerized ParB nucleates the binding of additional dimers of ParB to form a nucleo-protein complex. The removal of ParA from the nucleoid in the vicinity of ParB-bound plasmids creates a break in ParA symmetry along the nucleoid, resulting in the formation of local depletion zones around individual plasmids (Hwang et al., 2013; Vecchiarelli et al., 2013; Vecchiarelli and Neuman et al., 2014). ParA oscillatory dynamics emerge as plasmids move, or surf, along the nucleoid towards polar regions of the cell. Thus, ParA dynamics and plasmid motion are a recursive phenomenon.

Model for ParA-mediated plasmid partitioning

Several early studies of ParA function described ParA as being cytoskeletal, forming a dynamic helical-like filament that could pull plasmids within the cell (Ebersbach and Gerdes, 2004; Adachi et al., 2006; Ebersbach et al., 2006; Fogel and Waldor, 2006; Hatano et al., 2007; Pratto et al., 2008; Ringgaard et al., 2009). This model proposed that upon binding ATP, ParA would polymerize into helical filaments until coming into contact with ParB-bound plasmids, upon which disassembly of the ParA filament would occur and pull plasmids. This model was largely based on epifluorescence microscopy studies of fluorescently labeled ParA proteins and the tendency for some ParA proteins to form linear filaments *in vitro*.

However, more recent studies have proposed that the ParA-mediated plasmid segregation system is not filament-based, but instead functions as a self-organizing system (Hwang et al., 2013; Vecchiarelli et al., 2013; Vecchiarelli and Neuman et al., 2014; Surovtsev et al., 2016; Hu et al., 2017). These studies used the F plasmid SopABC system, which only significantly differs from the ParABS system in the centromere-like site on the plasmid (Vecchiarelli et al., 2013; Vecchiarelli and Neuman et al., 2014). Initially, magnetic beads, representing plasmids, were coated with *sopC* DNA and preincubated with fluorescently labeled SopB. Likewise, fluorescently labeled SopA was preincubated with ATP. Both solutions were then introduced to a DNA-carpeted flow-cell and the artificial ParB-bound cargos were confined to the DNA carpet surface using a magnetic field perpendicular to the slide. The resulting *in vitro* system was then imaged using Total Internal Reflection Fluorescence Microscopy (TIRFM). Interestingly, depletion zones of

SopA formed around the vicinity of the magnetic bead. Subsequently, the magnetic beads then started traveling across the DNA carpet in a directed and persistent manner. However, not every magnetic bead displayed this movement; some displayed a more random diffusion pattern. This observation was determined to be the result of the number of interactions between DNA carpet-bound SopA and magnetic bead bound SopB. Additionally, directed and persistent motion of the cargo required surface confinement, as SopA-SopB interaction alone was insufficient to tether cargos to the DNA-carpet. Importantly, no SopA filaments were observed during cargo movement and SopA distributed homogenously across the DNA-carpet.

The absence of SopA filament formation led to the hypothesis that ParA-mediated plasmid segregation was driven by a Min-system-like self-organizing protein gradient. This mechanism was termed a burnt-bridge Brownian-Ratchet, due to the inability of cargos to reverse course and move towards SopA depletion zones (Hu et al., 2017). As with all self-organizing protein systems, an input of energy, usually in the form of ATP, is required to maintain protein patterning. However, for directed and persistent motion of plasmids, it's hypothesized that ATP is required to establish the ratchet mechanism itself and bias diffusion, not necessarily functioning to pull the cargo by means of SopA and SopB interaction alone (Hu et al., 2017). Collectively, these experiments have demonstrated that asymmetric distributions of ParA can drive directed and persistent movement of DNA cargos towards increased concentrations of ParA via a Brownian-ratchet mechanism.

The cyanobacterial McdAB system

Whether the Brownian-ratchet model could account for segregation of cellular materials, such as the protein-based carboxysomes of cyanobacteria, was an outstanding question. These large (~ 150 nm diameter) microcompartments are essential to cyanobacteria, as they encapsulate the enzymes RuBisCO and carbonic anhydrase to create a high internal CO₂ environment to drive reactions towards the Calvin-Benson-Bassham cycle and suppress the oxygenase activity of RuBisCO that leads to photorespiration (Kerfeld and Melnicki, 2016).

In 2010, a landmark study using fluorescently labeled RuBisCO showed that carboxysomes are linearly arranged across the longitudinal axis of *S. elongatus* (Savage et al., 2010). This arrangement depended on a ParA-type ATPase, which was observed oscillating within the cell. However, how oscillation of this ParA-like protein emerged, what biological surface was being utilized, and how the ParA-like protein contributed to carboxysome arrangements remained unclear. Moreover, whether the mechanism by which carboxysomes are positioned was similar to that utilized by plasmids was an intriguing question (Figure 1.1E). Interestingly, the *S. elongatus* genome does not encode a ParB homolog. Instead, in work described in Chapter 4 of this thesis, we found that oscillation of the ParA-like protein, termed McdA, utilized the nucleoid as a biological surface and depended on a completely unique protein, termed McdB. McdB shares no similarity with ParB, yet displays many ParB-like features including: (i) McdA interaction, (ii) stimulation of McdA ATPase activity, and (iii) site-specific localization to cargos. In this case, McdB loaded onto carboxysomes through interaction with shell proteins, similar to ParB loading onto and around the centromere-like site of plasmids.

In the absence of McdA and/or McdB, we found that carboxysomes clustered together, either from a natural tendency to interact or from incomplete segregation following biogenesis (Figure 1.1F). Moreover, we found that upon overexpressing McdA, carboxysome ultrastructure was modified, resulting in carboxysomes with rounded or misshaped edges. Likewise, upon overexpressing McdB, carboxysomes became much larger and often formed bar-shaped structures that traversed half of the cell length (Figure 1.1G). This was a surprising result, as the SopABC system does not regulate plasmids in this manner. To our knowledge, this is the first evidence of a ParA-type ATPase system regulating the size of the target cargo.

Since we found that McdA did not form filaments *in vitro*, we also explored whether the Brownian-ratchet model could account for carboxysome distributions. Using reaction-diffusion simulations created for the SopABC system, we showed that carboxysomes could be linearly arranged. Moreover, modeling of an overabundant quantity of carboxysomes on an equivalently-sized nucleoid resulted in carboxysomes that would pack hexagonally, a phenomenon observed *in vivo*. To better test the Brownian-ratchet model, we varied the quantity of carboxysomes *in vivo* and monitored McdA dynamics. Confirming our hypothesis,

depletion zones of McdA on the nucleoid formed in the vicinity of carboxysomes and carboxysome motion was frequently in the direction of increased McdA concentrations (Figure 1.1H). This strongly suggested that the McdAB system uses a Brownian-ratchet mechanism to equidistantly space carboxysomes along the nucleoid to ensure equal inheritance following cell division.

Conclusion

Since the discovery of emergent Min- and Par-system patterning in bacteria, our understanding of the molecular mechanisms responsible for protein self-organization has increased dramatically. Surveys into how these systems operate across evolutionary distances and within diverse organisms is now warranted to further our understanding of the robust nature of these remarkable systems. Moreover, these surveys are likely to identify new classes of self-organizing systems, much like the McdAB system for carboxysome positioning. These novel systems raise new and exciting questions as they are studied in the biological context of the host organisms and challenge long-held views into how cells modify their internal architecture. Many new bacterial systems, like cyanobacteria, are now positioned to become model systems for studying biological pattern formation.

REFERENCES

REFERENCES

- Adachi, S., Hori, K., and Hiraga, S. (2006). Subcellular positioning of F plasmid mediated by dynamic localization of SopA and SopB. *J. Mol. Biol.* 356: 850–863.
- Atsumi, S., Higashide, W., and Liao, JC. (2009). Direct photosynthetic recycling of carbon dioxide to isobutyraldehyde. *Nat. Biotechnol.* 27(12):1177-80.
- Bach, J., Albrecht, N., and Bramkamp, M. (2014). Imaging DivIVA dynamics using photo-convertible and activatable fluorophores in *Bacillus subtilis*. *Front. Microbiol.* 5:59.
- Berla, BM., Saha, R., Immethun, CM., Maranas, CD., Moon, TS., and Pakrasi, HB. (2013). Synthetic biology of cyanobacteria: unique challenges and opportunities. *Front. Microbiol.* 4:246.
- Bi, EF., and Lutkenhaus, J. (1991). FtsZ ring structure associated with division in *Escherichia coli*. *Nature.* 354, 161–164.
- Chen, Y., and Erickson, HP. (2005). Rapid in vitro assembly dynamics and subunit turnover of FtsZ demonstrated by fluorescence resonance energy transfer. *J. Biol. Chem.* 280(23):22549-54.
- Davis, MA., Martin, KA., and Austin, SJ. (1990). Specificity switching of the P1 plasmid centromere-like site. *EMBO J.* 9(4):991-8.
- Davis, MA., Martin, KA., and Austin, SJ. (1992). Biochemical activities of the ParA partition protein of the P1 plasmid. *Mol. Microbiol.* 6, 1141–1147.
- de Boer, P., Crossley, R and Rothfield, L. (1989). A division inhibitor and a topological specificity factor coded for by the minicell locus determine proper placement of the division septum in *E. coli*. *Cell.* 56, 641–649.
- de Boer, P., Crossley, R and Rothfield, L. (1990). Central role for the *Escherichia coli* minC gene product in two different cell division-inhibition systems. *Proc. Natl. Acad. Sci.* 87, 1129–1133.
- Ducat, DC., Way, JC., Silver, PA. (2011). Engineering cyanobacteria to generate high-value products. *Trends Biotechnol.* 29(2):95-103.
- Ebersbach, G., and Gerdes, K. (2004). Bacterial mitosis: partitioning protein ParA oscillates in spiral-shaped structures and positions plasmids at mid-cell. *Mol. Microbiol.* 52: 385-398.

- Ebersbach, G., Ringgaard, S., Moller-Jensen, J., Wang, Q., Sherratt, D.J., and Gerdes, K. (2006). Regular cellular distribution of plasmids by oscillating and filament-forming ParA ATPase of plasmid pB171. *Mol. Microbiol.* 61: 1428-1442.
- Edwards, D., and Errington, J. (1997). The *Bacillus subtilis* DivIVA protein targets to the division septum and controls the site specificity of cell division. *Mol. Microbiol.* 24, 905–915.
- Eswaramoorthy, P., Erb, M., Gregory, J., Silverman, J., Pogliano, K., Pogliano, J., and Ramamurthi, K. (2011). Cellular Architecture Mediates DivIVA Ultrastructure and Regulates Min Activity in *Bacillus subtilis*. *Mbio.* 2, e00257–11.
- Field, CB., Behrenfeld, MJ., Randerson, JT., and Falkowski, P. (1998). Primary production of the biosphere: integrating terrestrial and oceanic components. *Science.* 281(5374):237-40.
- Fletcher, DA, and Mullins, DR. (2010). Cell mechanics and the cytoskeleton. *Nature.* 463(7280): 485–492.
- Fogel, MA., and Waldor, MK. (2006). A dynamic, mitotic-like mechanism for bacterial chromosome segregation. *Genes Dev.* 20: 3269-3282.
- Funnell, BE. (1988). Participation of *Escherichia coli* integration host factor in the P1 plasmid partition system. *Proc. Natl. Acad. Sci.* 85(18):6657-61.
- Funnell, BE., and Gagnier, L. (1993). The P1 plasmid partition complex at parS. II. Analysis of ParB protein binding activity and specificity. *J. Biol. Chem.* 268(5):3616-24.
- Hatano, T., Yamaichi, Y., and Niki, H. (2007). Oscillating focus of SopA associated with filamentous structure guides partitioning of F plasmid. *Mol. Microbiol.* 64: 1198–1213.
- Hayes, F., and Barilla, D. (2006). The bacterial segrosome: a dynamic nucleoprotein machine for DNA trafficking and segregation. *Nat. Rev. Microbiol.* 4, 133–143.
- Hays, SG., and Ducat, DC. (2015). Engineering cyanobacteria as photosynthetic feedstock factories. *Photosynth. Res.* 123(3):285-95.
- Hays, SG, Yan, LLW., Silver PA, and Ducat DC. (2017). Synthetic photosynthetic consortia define interactions leading to robustness and photoproduction. *J. Biol. Eng.* 11:4.
- Hoffmann, M., and Schwarz, U. (2013). Oscillations of Min-proteins in micropatterned environments: a three-dimensional particle-based stochastic simulation approach. *Soft Matter.* 10, 2388–2396.

- Hu, L., Vecchiarelli, AG., Mizuuchi, K., Neuman, KC., and Liu, J. (2017). Brownian ratchet mechanisms of ParA-mediated partitioning. *Plasmid*. 92:12-16.
- Hu, Z., and Lutkenhaus, J. (2000). Analysis of MinC reveals two independent domains involved in interaction with MinD and FtsZ. *J. Bacteriol.* 182, 3965–3971.
- Hu, Z., and Lutkenhaus, J. (2001). Topological regulation of cell division in *E. coli*. *Mol. Cell*. 7, 1337–1343.
- Hu, Z., and Lutkenhaus, J. (2003). A conserved sequence at the C-terminus of MinD is required for binding to the membrane and targeting MinC to the septum. *Mol. Microbiol.* 47, 345–355.
- Huang, KH., Durand-Heredia, J., and Janakiraman, A. (2013). FtsZ ring stability: of bundles, tubules, crosslinks, and curves. *J. Bacteriol.* 195(9): 1859–1868.
- Hwang, L., Vecchiarelli, AG., Han, Y., Mizuuchi, M., Harada, Y., Funnell, B., and Mizuuchi, K. (2013). ParA-mediated plasmid partition driven by protein pattern self-organization. *EMBO J.* 32, 1238–1249.
- Kerfeld, CA., Heinhorst, S., and Cannon, GC. (2010). Bacterial microcompartments. *Annu. Rev. Microbiol.* 64:391-408.
- Kerfeld, C., and Melnicki, M. (2016). Assembly, function and evolution of cyanobacterial carboxysomes. *Curr. Opin. Plant Biol.* 31, 66–75.
- King, G., Shih, YL., Maciejewski, M., Bains, N., Pan, B., Rowland, S., Mullen, G., and Rothfield, L. (2000). Structural basis for the topological specificity function of MinE. *Nat. Struct. Mol. Biology*. 7, 1013–1017.
- Kruse, K., Howard, M., and Margolin, W. (2007). An experimentalist's guide to computational modelling of the Min system. *Mol. Microbiol.* 63, 1279–1284.
- Mitsui, A., Kumazawa, S., Takahashi, A., Ikemoto, S., Cao, S., and Arai, T. (1986). Strategy by which nitrogen-fixing unicellular cyanobacteria grow photoautotrophically. *Nature*. 323, 720-722.
- Leger, MM., Petrů, M., Žárský, V., Eme, L., Viček, Č., Harding, T., Lang, BF., Eliáš, M., Doležal, P., and Roger, AJ. (2015). An ancestral bacterial division system is widespread in eukaryotic mitochondria. *Proc. Natl. Acad. Sci.* 112(33):10239-46.
- Lenarcic, R., Halbedel, S., Visser, L., Shaw, M., Wu, L., Errington, J., Marenduzzo, D., and Hamoen, L. (2009). Localisation of DivIVA by targeting to negatively curved membranes. *EMBO J.* 28, 2272–2282.

- Liberton, M., Page, L.E., O'Dell, W.B., O'Neill, H., Mamontov, E., Urban, V.S., and Pakrasi, H.B. (2013). Organization and flexibility of cyanobacterial thylakoid membranes examined by neutron scattering. *J. Biol. Chem.* 288(5):3632-40.
- Lindberg, P., Park, S., and Melis, A. (2010). Engineering a platform for photosynthetic isoprene production in cyanobacteria, using *Synechocystis* as the model organism. *Metab. Eng.* 12(1):70-9.
- Liu, H., Landry, M.R., Vault, D., and Campbell, L. (1999). *Prochlorococcus* growth rates in the central equatorial Pacific: An application of the f_{max} approach. *J. Geophys. Res.* 104, 3391–3399.
- Loose, M., Fischer-Friedrich, E., Ries, J., Kruse, K., and Schwille, P. (2008). Spatial regulators for bacterial cell division self-organize into surface waves in vitro. *Science.* 320, 789–792.
- Loose, M., Fischer-Friedrich, E., Herold, C., Kruse, K., and Schwille, P. (2011). Min protein patterns emerge from rapid rebinding and membrane interaction of MinE. *Nat. Struct. Mol. Biology.* 18, 577–583.
- Lutkenhaus, J. (2007). Assembly dynamics of the bacterial MinCDE system and spatial regulation of the Z ring. *Annu. Rev. Biochem.* 76, 539–562.
- Lutkenhaus, J. (2012). The ParA/MinD family puts things in their place. *Trends Microbiol.* 20, 411–418.
- MacCready, J.S., Schossau, J., Osteryoung, K.W., and Ducat, D.C. (2017). Robust Min-system oscillation in the presence of internal photosynthetic membranes in cyanobacteria. *Mol. Microbiol.* 103, 483–503.
- Marston, A., Thomaidis, H., Edwards, D., Sharpe, M., and Errington, J. (1998). Polar localization of the MinD protein of *Bacillus subtilis* and its role in selection of the mid-cell division site. *Genes Dev.* 12, 3419-3430.
- Marston, A., and Errington, J. (1999). Selection of the midcell division site in *Bacillus subtilis* through MinD-dependent polar localization and activation of MinC. *Mol. Microbiol.* 33, 84–96.
- Meinhardt, H., and de Boer, P. (2001). Pattern formation in *Escherichia coli*: A model for the pole-to-pole oscillations of Min proteins and the localization of the division site. *Proc. Natl. Acad. Sci.* 98, 14202-14207.
- Miyagishima, S.Y., Wolk, C.P., and Osteryoung, K.W. (2005). Identification of cyanobacterial cell division genes by comparative and mutational analyses. *Mol. Microbiol.* 56(1):126-43.
- Mukherjee, A., and Lutkenhaus, J. (1998). Dynamic assembly of FtsZ regulated by GTP hydrolysis. *EMBO J.* 17(2):462-9.

Nevo, R., Charuvi, D., Shimoni, E., Schwarz, R., Kaplan, A., Ohad, I., and Reich, Z. (2007). Thylakoid membrane perforations and connectivity enable intracellular traffic in cyanobacteria. *EMBO J.* 26, 1467–1473.

Nevo, R., Charuvi, D., Chuartzman, S.G., Shimoni, E., Tsabari, O. and Reich, Z. (2009) Architecture and plasticity of thylakoid membrane networks. *In Lipids in Photosynthesis* (Wada, H. and Murata, N., eds). Dordrecht Springer-Verlag, pp. 295–328.

Oliva, M., Halbedel, S., Freund, S., Dutow, P., Leonard, T., Veprintsev, D., Hamoen, L., and Löwe, J. (2010). Features critical for membrane binding revealed by DivIVA crystal structure. *EMBO J.* 29, 1988–2001.

Park, K.T., Wu, W., Battaile, K.P., Lovell, S., Holyoak, T., and Lutkenhaus, J. (2011). The Min Oscillator Uses MinD-Dependent Conformational Changes in MinE to Spatially Regulate Cytokinesis. *Cell.* 146, 396–407.

Partensky, F., Hess, W.R., and Vaulot, D. (1999). Prochlorococcus, a marine photosynthetic prokaryote of global significance. *Microbiol. Mol. Biol. Rev.* 63(1):106-27.

Petrášek, Z., and Schwille, P. (2015). Simple membrane-based model of the Min oscillator. *New J. Phys.* 17, 043023.

Pratto, F., Cicek, A., Weihofen, W.A., Lurz, R., Saenger, W., and Alonso, J.C. (2008). Streptococcus pyogenes pSM19035 requires dynamic assembly of ATP-bound ParA and ParB on parS DNA during plasmid segregation. *Nucleic. Acids Res.* 36: 3676–3689.

Ramamurthi, K., and Losick, R. (2009). Negative membrane curvature as a cue for subcellular localization of a bacterial protein. *Proc. Natl. Acad. Sci.* 106, 13541–13545.

Raskin, D., and de Boer, P. (1999). Rapid pole-to-pole oscillation of a protein required for directing division to the middle of Escherichia coli. *Proc. Natl. Acad. Sci.* 96, 4971–4976.

Ringgaard, S., Van Zon, J., Howard, M., and Gerdes, K. (2009). Movement and equipositioning of plasmids by ParA filament disassembly. *Proc. Natl. Acad. Sci.* 106: 19369–19374.

Romberg, L., Simon, M., and Erickson, H.P. (2001). Polymerization of Ftsz, a bacterial homolog of tubulin. is assembly cooperative? *J. Biol. Chem.* 276(15):11743-53.

Rowlett, V., and Margolin, W. (2013). The bacterial Min system. *Curr. Biol.* 23, R553–R556.

Rowlett, V., and Margolin, W. (2015). The bacterial divisome: ready for its close-up. *Philos. Trans. R. Soc. Lond. B. Biol. Sci.* 370(1679).

- Ruffing, AM. (2011). Engineered cyanobacteria: Teaching an old bug new tricks. *Bioeng. Bugs.* 2(3):136-49.
- Sakai, M., Ogawa, T., Matsuoka, M., and Fukuda, H. (1997). Photosynthetic conversion of carbon dioxide to ethylene by the recombinant cyanobacterium, *Synechococcus* sp. PCC 7942, which harbors a gene for the ethylene-forming enzyme of *Pseudomonas syringae*. *J. Ferment. Bioeng.* 84, 434–443.
- Savage, D., Afonso, B., Chen, A., and Silver, P. (2010). Spatially Ordered Dynamics of the Bacterial Carbon Fixation Machinery. *Science.* 327, 1258–1261.
- Scheffers, DJ., de Wit, JG., den Blaauwen, T., and Driessen, AJ. (2002). GTP hydrolysis of cell division protein FtsZ: evidence that the active site is formed by the association of monomers. *Biochemistry.* 41(2):521-9.
- Schopf, WJ. (2011). The paleobiological record of photosynthesis. *Photosynth. Res.* 107(1):87-101.
- Shih, PM., Wu, D., Latifi, A., Axen, SD., Fewer, DP., Talla, E., Calteau, A., Cai, F., Tandeau de Marsac, N., Rippka, R. et al. (2013). Improving the coverage of the cyanobacterial phylum using diversity-driven genome sequencing. *Proc. Natl. Acad. Sci.* 110(3):1053-8.
- Stal, JL., and Wolfgang, KE. (1985). Nitrogenase activity in the non-heterocystous cyanobacterium *Oscillatoria* sp. grown under alternating light-dark cycles. *Arch. Microbiol.* 143: 67.
- Surovtsev, I., Campos, M., and Jacobs-Wagner, C. (2016). DNA-relay mechanism is sufficient to explain ParA-dependent intracellular transport and patterning of single and multiple cargos. *Proc. Natl. Acad. Sci.* 113, E7268–E7276.
- Szeto, T., Rowland, S., Rothfield, L., and King, G. (2002). Membrane localization of MinD is mediated by a C-terminal motif that is conserved across eubacteria, archaea, and chloroplasts. *Proc. Natl. Acad. Sci.* 99, 15693–15698.
- Tostevin, F., and Howard, M. (2006). A stochastic model of Min oscillations in *Escherichia coli* and Min protein segregation during cell division. *Phys. Biol.* 3, 1.
- Varley, AW., and Stewart, GC. (1992). The divIVB region of the *Bacillus subtilis* chromosome encodes homologs of *Escherichia coli* septum placement (minCD) and cell shape (mreBCD) determinants. *J. Bacteriol.* 174, 6729–6742.
- Vecchiarelli, AG., Mizuuchi, K., and Funnell, B. (2012). Surfing biological surfaces: exploiting the nucleoid for partition and transport in bacteria. *Mol. Microbiol.* 86, 513–523.

Vecchiarelli, AG., Hwang, L., and Mizuuchi, K. (2013). Cell-free study of F plasmid partition provides evidence for cargo transport by a diffusion-ratchet mechanism. *Proc. Natl. Acad. Sci.* 110, E1390–E1397.

Vecchiarelli, AG., Neuman, K., and Mizuuchi, K. (2014). A propagating ATPase gradient drives transport of surface-confined cellular cargo. *Proc. Natl. Acad. Sci.* 111, 4880–4885.

Vecchiarelli, AG., Li, M., Mizuuchi, M., Hwang, L., Seol, Y., Neuman, K., and Mizuuchi, K. (2016). Membrane-bound MinDE complex acts as a toggle switch that drives Min oscillation coupled to cytoplasmic depletion of MinD. *Proc. Natl. Acad. Sci.* 113, E1479–E1488.

Vothknecht, U., and Westhoff, P. (2001). Biogenesis and origin of thylakoid membranes. *BBA-Mol. Cell Res.* 1541, 91–101.

Weiss, TL., Young, EJ., and Ducat, DC. (2017). A synthetic, light-driven consortium of cyanobacteria and heterotrophic bacteria enables stable polyhydroxybutyrate production. *Metab. Eng.* 44:236-245.

Wolk CP, Ernst A, and Elhai, J. (1994). Heterocyst metabolism and development. In *The Molecular Biology of Cyanobacteria*. Edited by Bryant DA. Dordrecht: Kluwer Academic Publishers. 769-823.

Wu, F., Schie, B., Keymer, J., and Dekker, C. (2015). Symmetry and scale orient Min protein patterns in shaped bacterial sculptures. *Nat. Nanotechnol.* 10, 719–726.

Zhou, H., and Lutkenhaus, J. (2004). The Switch I and II Regions of MinD Are Required for Binding and Activating MinC. *J. Bacteriol.* 186, 1546–1555.

Zhou, J., Zhang, H., Zhang, Y., Li, Y., and Ma, Y. (2012). Designing and creating a modularized synthetic pathway in cyanobacterium *Synechocystis* enables production of acetone from carbon dioxide. *Metab. Eng.* 14(4):394-400.

Zheng, XY., and O'Shea, EK. (2017). Cyanobacteria Maintain Constant Protein Concentration despite Genome Copy-Number Variation. *Cell Rep.* 19(3):497-504.

Zieske, K., and Schwille, P. (2014). Reconstitution of self-organizing protein gradients as spatial cues in cell-free systems. *Elife* 3.

CHAPTER 2

ROBUST MIN-SYSTEM OSCILLATION IN THE PRESENCE OF INTERNAL PHOTOSYNTHETIC MEMBRANES IN CYANOBACTERIA

Summary

The oscillatory Min system of *Escherichia coli* defines the cell division plane by regulating the site of FtsZ-ring formation and represents one of the best-understood examples of emergent protein self-organization in nature. The oscillatory patterns of the Min-system proteins MinC, MinD and MinE (MinCDE) are strongly dependent on the geometry of membranes they bind. Complex internal membranes within cyanobacteria could disrupt this self-organization by sterically occluding or sequestering MinCDE from the plasma membrane. Here, it was shown that the Min system in the cyanobacterium *Synechococcus elongatus* PCC 7942 oscillates from pole-to-pole despite the potential spatial constraints imposed by their extensive thylakoid network. Moreover, reaction-diffusion simulations predict robust oscillations in modeled cyanobacterial cells provided that thylakoid network permeability is maintained to facilitate diffusion, and suggest that Min proteins require preferential affinity for the plasma membrane over thylakoids to correctly position the FtsZ ring. Interestingly, in addition to oscillating, MinC exhibits a midcell localization dependent on MinD and the DivIVA-like protein Cdv3, indicating that two distinct pools of MinC are coordinated in *S. elongatus*. Our results provide the first direct evidence for Min oscillation outside of *E. coli* and have broader implications for Min-system function in bacteria and organelles with internal membrane systems.

Source

For a full text of this work go to: MacCready, JS., Schossau, J., Osteryoung, KW., and Ducat, DC. (2017). Robust Min-system oscillation in the presence of internal photosynthetic membranes in cyanobacteria. *Mol Microbiol.* 103(3):483-503. <http://onlinelibrary.wiley.com/doi/10.1111/mmi.13571/abstract>

CHAPTER 3

AN EVOLUTIONARILY CONSERVED DOMAIN IN CYANOBACTERIAL FTN2 AND CHLOROPLAST

ARC6 INTERACTS WITH FTSZ/FTSZ2

Summary

In most bacteria, establishment of the division plane requires polymerization of the tubulin-like protein FtsZ. Following spatial regulation by the Min system, FtsZ establishes a ring-like structure (Z ring) at mid-cell through interaction with membrane-bound accessory proteins, termed membrane tethers or anchors. Across most of the bacterial world, the protein FtsA is the dominant membrane-tethering protein for FtsZ. However, cyanobacteria represent a phylum of photosynthetic bacteria that lack FtsA. How FtsZ is stabilized along the plasma membrane to promote Z-ring formation in cyanobacteria is unclear. Consistent with the theory that chloroplasts are descended from cyanobacteria, chloroplasts possess a transmembrane protein, termed ARC6, that functions as a membrane tether for FtsZ proteins. Here, we show that the protein Ftn2 in cyanobacteria and ARC6 in chloroplasts share a common origin. Moreover, both proteins possess a single highly conserved domain required for FtsZ interaction. Ftn2 levels in the model rod-shaped cyanobacterium *Synechococcus elongatus* PCC 7942 were found to be critical for cell division, as either deletion of *ftn2* or overexpression of Ftn2 resulted in aberrant FtsZ staining and hyperelongation of cells due to inefficient division. Lastly, we found that the last 17 amino acids of *S. elongatus* FtsZ were required for interaction with Ftn2. Together, these results suggest that Ftn2 and ARC6 are the dominant FtsZ membrane-tethering proteins in the green photosynthetic lineage and have broader impacts for understanding the evolution of diverse FtsZ membrane anchoring proteins.

Introduction

In most bacteria, the cytoskeletal GTPase FtsZ assembles into short protofilaments, which further self-assemble into a ring-like structure (Z ring) at midcell through interaction with a membrane-bound FtsZ anchoring protein; the Z ring then functions as a scaffold for the recruitment of numerous additional division-related factors required for septation (Bi and Lutkenhaus, 1991; Löwe, 1998; Lutkenhaus, 2007; Osawa et al., 2008; Adams and Errington, 2009). Across bacterial phyla, different FtsZ membrane anchors have been identified. These proteins can either be integral or interact with the plasma membrane peripherally via an amphipathic α -helix. The primary FtsZ anchoring factor is FtsA, a broadly conserved actin-like protein that polymerizes from head-to-tail in the presence of ATP and associates with lipids via a C-terminal amphipathic helix (Bork et al., 1992; Sánchez et al., 1994; van den Ent and Löwe, 2000; Feucht et al., 2001; Pichoff and Lutkenhaus, 2005). FtsA is proposed to recruit FtsZ filaments to the plasma membrane, but also to promote destabilization of the FtsZ filament network in a concentration-dependent manner (Loose and Mitchison, 2014). FtsA is essential for Z-ring formation in *E. coli*, but dispensable in *B. subtilis*, although *B. subtilis* cells lacking FtsA are filamentous (Kemp et al., 2002; Rico et al., 2004).

In *E. coli*, additional factors beyond FtsA regulate FtsZ assembly. For example, ZipA is a transmembrane protein that promotes bundling of FtsZ protofilaments and protects FtsZ from the ClpXP protease (Hale and de Boer, 1997; RayChaudhuri, 1999; Pazos et al., 2013). Unlike FtsA, which primarily interacts with FtsZ polymers, ZipA has the ability to recruit individual FtsZ monomers to the plasma membrane (Loose and Mitchison, 2014). Beyond FtsA and ZipA, the FtsZ-associating proteins (Zap) ZapA, ZapB, ZapC and ZapD are completely cytosolic and interact with FtsZ during the early stages of assembly. ZapA and ZapC promote FtsZ assembly and stabilization by strengthening lateral protofilament association (Gueiros-Filho and Losick, 2002; Durand-Heredia et al., 2011; Hale et al., 2011), the coiled-coil protein ZapB interacts with FtsZ via ZapA (Ebersbach et al., 2008), and ZapD has a potential role in stabilizing FtsZ by promoting bundling through enhancement of lateral protofilament associations (Durand-Heredia et al., 2012).

In *B. subtilis*, EzrA and SepF partially substitute for the loss of FtsA. EzrA is a transmembrane protein that lowers the critical concentration of Z-ring assembly by interacting with the C-terminus of FtsZ via a coiled-coil C-terminal domain (Levin et al., 1999; Singh et al., 2007; Land et al., 2014). SepF interacts with the plasma membrane peripherally through an N-terminal amphipathic helix and self-assembles into rings *in vitro* via a C-terminal globular domain that promotes FtsZ assembly (Hamoen et al., 2006; Duman et al., 2013). Lastly, in *Caulobacter crescentus*, FtsA is essential, yet the recently discovered protein FzIC also functions as a membrane anchor that links Z rings to cell wall hydrolysis (Meier et al., 2016). Despite the fact that FzIC has no regions of similarity to other anchoring proteins, the same C-terminal region of FtsZ that interacts with FtsA, SepF and ZipA also interacts with *C. crescentus* FzIC (Pichoff and Lutkenhaus, 2005; Hale et al., 2000; Król et al., 2012; Sundararajan and Goley, 2017).

Consistent with the theory of endosymbiosis, cyanobacteria and chloroplasts share some features related to division regulation, such as FtsZ (Osteryoung and Pyke, 2014). In chloroplasts of *Arabidopsis thaliana*, FtsZ serves a similar function in coordinating chloroplast fission, yet unlike bacteria, chloroplasts possess two distinct FtsZ homologs (FtsZ1 and FtsZ2) that co-assemble to establish a mature Z ring. Whereas FtsZ2 is believed to be more ancestral and promote mature Z-ring formation (Osteryoung et al., 1998; Strepp et al., 1998; Chen et al., 2018), FtsZ1 is believed to have arisen from a duplication event of FtsZ2 (Miyagishima et al., 2004; TerBush et al., 2013b) and functions to increase the rate of FtsZ2 turnover, possibly by destabilizing the interface between subunits (TerBush and Osteryoung, 2012). This feature appears to be widely conserved across the green photosynthetic lineage (TerBush et al., 2017). Interestingly, both cyanobacteria and chloroplasts conspicuously lack the common FtsZ-tethering proteins FtsA, EzrA and ZipA. Instead, in chloroplasts, the C-terminal domain of FtsZ2 anchors the Z ring to the inner envelope membrane through an interaction with ARC6 (Accumulation and Replication of Chloroplasts protein 6) (Robertson et al., 1995; Glynn et al., 2008; McAndrew et al., 2008; Irieda and Shiomi, 2017). ARC6 is a transmembrane inner envelope protein, with its N-terminus, which interacts with FtsZ2 via the C-terminus of FtsZ2, facing the stroma and its C-terminus facing the intermembrane space (Chen et al., 2018). By contrast, the membrane tether of FtsZ in cyanobacteria is less clear: while cyanobacteria possess a protein with similarity to SepF that can stabilize FtsZ polymers *in vitro*, functional Z-rings are still formed

in *sepF* mutants (Marbouty et al., 2009a), indicating the presence of additional tethering factors. Interestingly, ARC6 shares similarity with a cyanobacterial protein predicted to be a transmembrane protein, Ftn2 (also called ZipN) (Koksharova and Wolk, 2002; Vitha et al., 2003). Ftn2 which has been previously shown to be important for cyanobacterial division, localizes near mid-cell in *Synechocystis sp.* PCC 6803, and binds FtsZ *in vitro* (Mazouni et al., 2004; Miyagishima et al., 2005; Marbouty et al., 2009b; Gorelova et al., 2013). Yet how ARC6 and Ftn2 interact with FtsZ2 and FtsZ, respectively, remains an open question.

Here we show that a conserved domain within *S. elongatus* PCC 7942 Ftn2 and *A. thaliana* ARC6 interacts with FtsZ and FtsZ2, respectively. In *S. elongatus*, deletion of Ftn2 resulted in filamentous cells with aberrant Z ring formations and numerous lateral FtsZ filament-like structures. Consistent with a role in promoting Z-ring formation, fluorescent mNeonGreen (mNG) fusions to Ftn2 (mNG-Ftn2) revealed a mid-cell localization. When overexpressed, mNG-Ftn2 was distributed homogeneously along the plasma membrane, resulting in helical-like formations of FtsZ throughout filamentous cells. Using an established heterologous system and fluorescence microscopy, we found that a conserved domain within Ftn2 and ARC6 was responsible for their colocalization with FtsZ and FtsZ2, respectively, suggesting this domain mediates these interactions. Likewise, we also found that the C-terminus of *S. elongatus* FtsZ is required for its interaction with Ftn2, consistent with the role of this region of FtsZ in interacting with other well-known FtsZ membrane anchors. These results suggest that Ftn2 is a major factor in Z-ring formation in cyanobacteria and have broader implications for understanding the evolution of binary fission in the green photosynthetic lineage.

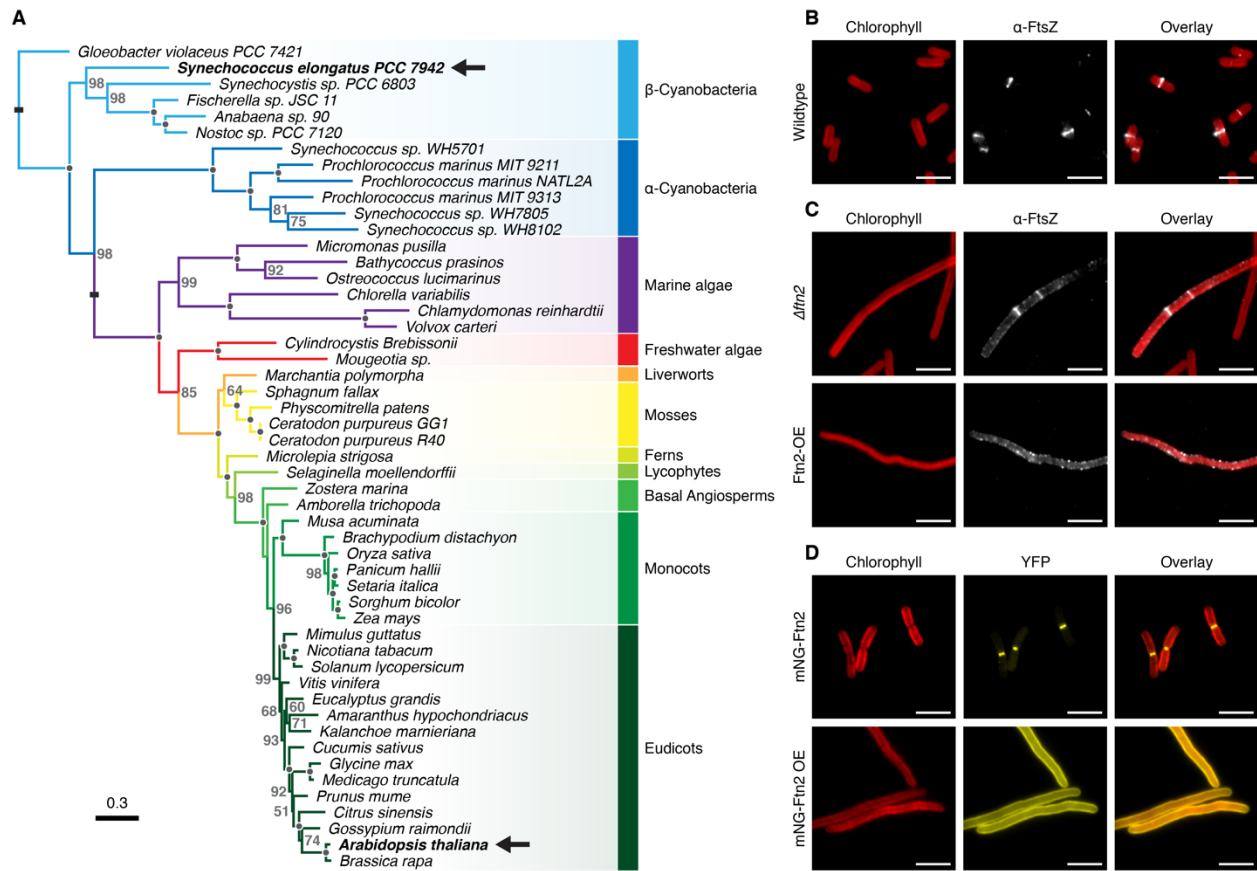


Figure 3.1: Altered Ftn2 expression disrupts FtsZ patterning

(A) Phylogenetic inference from Ftn2 and ARC6 sequences across the green photosynthetic lineage. Bootstrap values <100 are reported near nodes while grey circles on nodes represent 100%. Arrows denote organisms analyzed in this study. **(B)** Immunostaining of wild-type cells reveals FtsZ (white) strongly concentrates to the midcell Z-ring in *S. elongatus*. Chlorophyll a autofluorescence in red. **(C)** FtsZ staining (white) in $\Delta ft n 2$ (top) and Ftn2 overexpression (bottom) lines. **(D)** mNG-Ftn2 (yellow) localizes to the midcell (top) and distributes homogenously when overexpressed (bottom). Scale bars = 5 μ m.

Results and Discussion

Ftn2 is an Essential Regulator of Z-ring formation in S. elongatus

Ftn2 and ARC6 have been identified throughout the green photosynthetic lineage (Vitha et al., 2003). To better understand the evolution of these proteins, we performed a rigorous Bayesian analysis using Ftn2 and ARC6 sequences from α - and β -cyanobacteria, fresh water and marine algae, liverworts, mosses, ferns, lycophytes, basal angiosperms, monocots and eudicots. Our analysis revealed that Ftn2 shares a common origin with ARC6, most likely descending from α -cyanobacterial Ftn2 (Figure 3.1A). This result is consistent with the hypothesis that a *Prochlorococcus*-like species was the ancestor of chloroplasts (Tomitani et al., 1999), though this is still under heavy debate (Sánchez-Baracaldo et al., 2017). Our analysis also revealed that Ftn2 and ARC6 are good overall markers for studying the evolution of photosynthetic species from the green lineage, as both large proteins possess several highly conserved domains with minimal gaps and no observable polytomies.

We next sought to determine the influence of Ftn2 on Z-ring formation in cyanobacteria by genetically ablating *ftn2*, or upregulating Ftn2 protein levels via an inducible expression system. Prior research in the spherical cyanobacterium *Synechocystis* sp. PCC 6803 has shown that Ftn2 and FtsZ interact *in vitro*, and that Ftn2 localizes to the septum (Mazouni et al., 2004). However, the influence of Ftn2 expression on Z-ring formation has not been explored in detail. As expected, immunofluorescence analysis with an anti-FtsZ antibody revealed that FtsZ localizes to a well-defined Z ring at the midcell of wild-type *S. elongatus* cells (Figure 3.1B) (Miyagishima et al., 2005; MacCready et al., 2017). By contrast, in Δ *ftn2* mutants, we observed extreme cell filamentation, as previously reported (Koksharova and Wolk, 2002), and several mislocalized Z rings with interspersed FtsZ polymers (Figure 3.1C). This result is in contrast to a previous study where no Z rings were observed in Δ *ftn2* mutants (Miyagishima et al., 2005), most likely due to our use in the current study of an improved immunostaining protocol for FtsZ in *S. elongatus* (MacCready et al., 2017). In cells overexpressing Ftn2 by IPTG induction, we observed severe cell elongation and no clearly defined Z rings were detected (Figure 3.1C). Instead, FtsZ formed more of a punctate or zig-zag-

like patterning throughout the length of the cell (Figure 3.1C). These results are also reminiscent of phenotypes in chloroplasts with altered ARC6 activity, as inactivation of *arc6* in chloroplasts results in the formation of giant chloroplasts with numerous aberrant FtsZ2 filaments and overexpression of ARC6 results in giant chloroplasts with multiple, mispositioned, Z rings and spirals (Vitha et al., 2003).

To determine if Ftn2 localizes to midcell in *S. elongatus*, we generated an Ftn2 fluorescent reporter by inserting a second copy of Ftn2 tagged at the N-terminus with mNeonGreen and expressed it from an IPTG-inducible Ptrc promoter. In the absence of IPTG induction, the Ptrc promoter is leaky in *S. elongatus*, and we observed mNG-Ftn2 localized solely at midcell (Figure 3.1D). Upon overexpression of mNG-Ftn2 with IPTG, cell filamentation was observed and mNG-Ftn2 localized throughout the entire plasma membrane (Figure 3.1D). This result explains FtsZ patterning in our non-fluorescently tagged Ftn2 overexpression lines, as Ftn2 is known to stabilize FtsZ polymers *in vitro* (Marbouty et al., 2009a) and overexpression of Ftn2 would present an overabundant quantity of binding sites for FtsZ, resulting in a zig-zag-like patterning of FtsZ throughout the length of the cell (Figure 3.1CD).

It is intriguing to speculate why cyanobacteria and chloroplasts lack FtsA and instead possess a completely unique FtsZ membrane-anchoring protein. One possibility could be the mechanism by which proteins such as FtsA interact with the membrane. Indeed, FtsA possesses a C-terminal amphipathic helix that non-discriminately binds lipids along the inner membrane face (Pichoff and Lutkenhaus, 2005). However, unlike canonical bacterial systems such as *E. coli* or *B. subtilis*, cyanobacteria and chloroplasts possess an additional system of internal membranes, thylakoid membranes. These membrane systems might otherwise complicate FtsA localization to the plasma membrane by also recruiting FtsA to the thylakoid membranes. In this way, a geometric complexity would be present due to FtsA orientation on the outer surface of the thylakoid membranes facing both towards cell center and towards the plasma membrane, complicating FtsZ assembly. Indeed, as discussed in detail in Chapter 2, a similar problem exists with the Min system of *S. elongatus*. Like FtsA, MinD possesses a C-terminal amphipathic helix that allows for indiscriminate binding of the plasma membrane in *E. coli* (Szeto et al., 2002). While this feature is sufficient for *E. coli* MinD, this helix poses a problem in cyanobacteria due to the presence of thylakoid membranes. We have shown previously that *S. elongatus* MinD must possess a mechanism to differentiate

plasma and thylakoid membranes, otherwise, the ability for the Min system to spatially regulate FtsZ assembly along the plasma membrane would be insufficient. Therefore, it's possible that cyanobacteria lost FtsA, and gained Ftn2, during the evolution of thylakoid membranes, though this remains highly speculative.

A second hypothesis for the evolution of Ftn2 could be the importance of the periplasmic region. Indeed, although we haven't completely determined whether Ftn2 is indeed an integral membrane protein, Ftn2 possesses a predicted transmembrane region that corresponds to the ARC6 transmembrane region, which spans the inner membrane of chloroplasts (Vitha et al., 2003). The large C-terminal intermembrane space domain of ARC6 (DUF4101) has recently been crystallized (Kumar et al., 2016) and shown to be critical for communication between the chloroplast Z ring within the stroma and the dynamin (DRP5B) ring that assembles on the cytosolic surface of the chloroplast's outer membrane (Chen et al., 2018). The coordination between FtsZ1/2 and DRP5B is crucial for binary fission, given that the vast majority of chloroplasts lack peptidoglycan (Chen et al., 2018). While cyanobacteria lack DRP5B, we can't rule out the possibility that communication between the plasma and outer membrane is required for cytokinesis. Further molecular and biochemical analyses are now needed to determine why the green photosynthetic lineage has evolved a unique FtsZ membrane-anchoring protein.

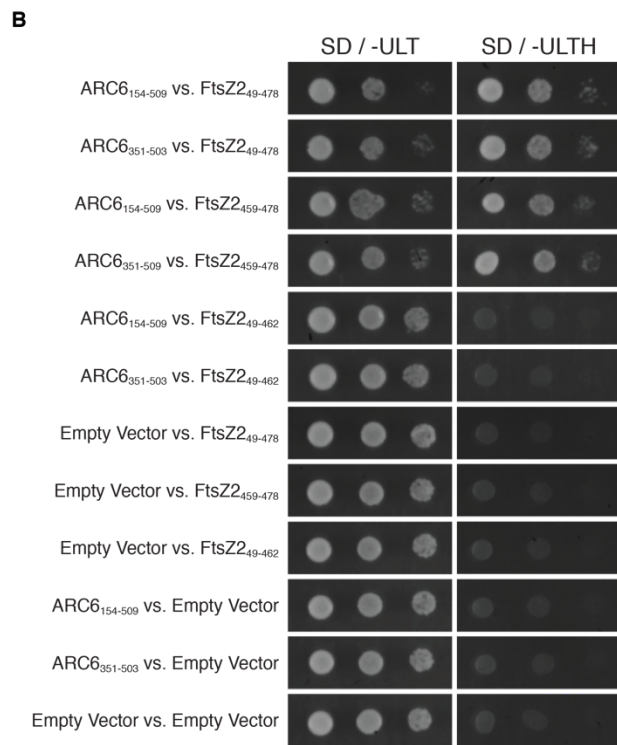
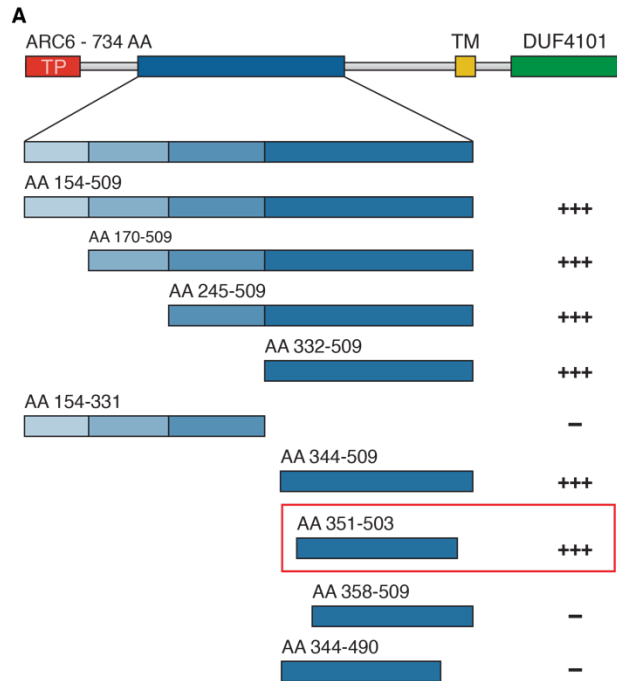


Figure 3.2: Identification of the FtsZ2 interacting domain of ARC6 via yeast two-hybrid

(A) Cartoon schematic of the fragments of ARC6 used for a yeast two-hybrid interaction assay. Red box denotes smallest fragment allowing for interaction. (B) Yeast two-hybrid results between FtsZ2 and ARC6 fragments. Figure adapted from Glynn, 2009.

A conserved FtsZ-binding domain in Ftn2 and ARC6

How Ftn2 and FtsZ interact is an outstanding question. Previous work using yeast-two-hybrid assays has shown that a conserved domain in ARC6 (AA 351-503) is required for interaction with FtsZ2 (Figure 3.2AB; Glynn, 2009). This FtsZ-binding domain (ZBD) is highly conserved across ARC6 sequences from fresh water and marine algae, liverworts, mosses, ferns, lycophytes, basal angiosperms, monocots and eudicots (Figure 3.3). Importantly, the ARC6 ZBD is also highly conserved in α - and β -cyanobacterial Ftn2 (Figure 3.3), suggesting a conserved mechanism of Ftn2 / FtsZ interaction.

To explore in greater detail whether the Ftn2 and ARC6 ZBDs were solely responsible for interaction with *S. elongatus* FtsZ and *A. thaliana* FtsZ2, respectively, we used *Schizosaccharomyces pombe* as a heterologous yeast expression system. This system, which lacks endogenous FtsZ and its numerous assembly regulators, has proven valuable for investigating the dynamic behavior of fluorescent FtsZ filaments from bacteria and chloroplasts in a model cellular environment, and for evaluating the effects of FtsZ assembly regulators on filament assembly patterns and dynamics (Srinivasan et al., 2008; TerBush and Osteryoung, 2012; TerBush et al., 2017). Therefore, we generated *S. pombe* expression constructs for three variants of the regions of Ftn2 and ARC6 that are predicted to face the cytosol and stroma, respectively. The protein fragments included: (i) full cytosolic/stromal regions (Ftn2 AA 1-451 and ARC6 AA 66-614), (ii) Δ ZBD (Ftn2 AA 1-260/396-451 and ARC6 AA 66-350/504-614), and (iii) ZBD only (Ftn2 AA 261-395 and ARC6 AA 351-503) (Figure 3.4AB). The C-terminal transmembrane domain and periplasmic/intermembrane space regions of Ftn2 (AA 452-631) and ARC6 (AA 615-801) were removed (Δ TM). For ARC6, the predicted N-terminal chloroplast transit peptide (AA 1-65) was also removed (Figure 3.4B). The fluorescent protein mRuby3 was appended to the N-terminus of each Ftn2 and ARC6 variant in order to monitor its intracellular localization. To generate our FtsZ reporters, we inserted the fluorescent protein msfGFP with an N-terminal GSGSGS linker at a conserved loop region in the middle of *S. elongatus* FtsZ (FtsZ-msfGFP-FtsZ) and *A. thaliana* FtsZ2 (FtsZ2-msfGFP-FtsZ2). An FtsZ fusion protein bearing the YFP variant mVenus in this loop region has previously been shown to be fully functional for cell division in

E. coli (Moore et al., 2016), and we recently showed that an *S. elongatus* FtsZ fusion protein tagged with msGFP at the equivalent site assembles dynamic filaments in *S. pombe* (TerBush et al., 2017).

Since some fluorescent proteins have a natural tendency to dimerize which can lead to localization artifacts (Landgraf et al., 2012), we verified that the signal was diffuse upon expression of only our fluorescent proteins (Figure 3.4C). We then ensured that our mRuby3-Ftn2 and mRuby3-ARC6 variants did not possess the ability to self-assemble by expressing them alone. All mRuby3-Ftn2 and mRuby3-ARC6 variants were diffuse with no evidence of self-assembly, similar to the mRuby3 control (Figure 3.4C). However, *A. thaliana* mRuby3-ZBD did not express (not shown), potentially due to misfolding (Figure 3.4C). We also note that fluorescent signal is increased around the *S. pombe* nucleus, a phenotype also observed in our mRuby3 and msfGFP control lines and consistent with previous studies of heterologous fluorescent protein expression in *S. pombe* (Srinivasan et al., 2008; TerBush et al., 2012; Zhang et al., 2016).

Upon expression of FtsZ-msfGFP-FtsZ and FtsZ2-msfGFP-FtsZ2, we observed filament formation throughout the cells (Figure 3.4DE). While we have previously reported on *S. elongatus* FtsZ-msfGFP-FtsZ assembly and dynamics (TerBush et al., 2017), this is the first evidence that *A. thaliana* FtsZ2 can also self-assemble when the msfGFP tag is inserted in the loop region. The FtsZ2-msfGFP-FtsZ2 filaments wrapped around *S. pombe* cells and frequently had smaller polymers flaring out from the main polymer (Figure 3.4E), resembling previous phenotypes from FtsZ2 C-terminal fluorescent fusions (TerBush et al., 2012; TerBush et al., 2017). Upon co-expressing *S. elongatus* FtsZ-msfGFP-FtsZ with mRuby3-Ftn2 Δ TM or mRuby3-Ftn2(ZBD), we observed strong colocalization of signal based on Pearson Correlation Coefficients (PCCs) of 0.66 ± 0.08 and 0.62 ± 0.20 , respectively (Figure 3.4F). However, we did not see colocalization in our mRuby3-Ftn2 Δ ZBD lines (PCC = 0.24 ± 0.14), suggesting that the ZBD is the only region of Ftn2 required for FtsZ interaction. Likewise, we observed strong colocalization of signal when co-expressing *A. thaliana* FtsZ2-msfGFP-FtsZ2 and mRuby3-ARC6 full stromal (PCC = 0.72 ± 0.22), but not our ARC6 Δ ZBD strains (0.38 ± 0.24) (Figure 3.4G). No obvious differences in FtsZ-msfGFP-FtsZ or FtsZ2-msfGFP-FtsZ2 polymers were observed in the presence and absence of mRuby3-Ftn2 or mRuby3-ARC6, respectively. Together, these results suggest that the highly conserved ZBD region in both Ftn2 and ARC6 is both required and sufficient for interaction with *S. elongatus* FtsZ and *A. thaliana* FtsZ2, respectively.

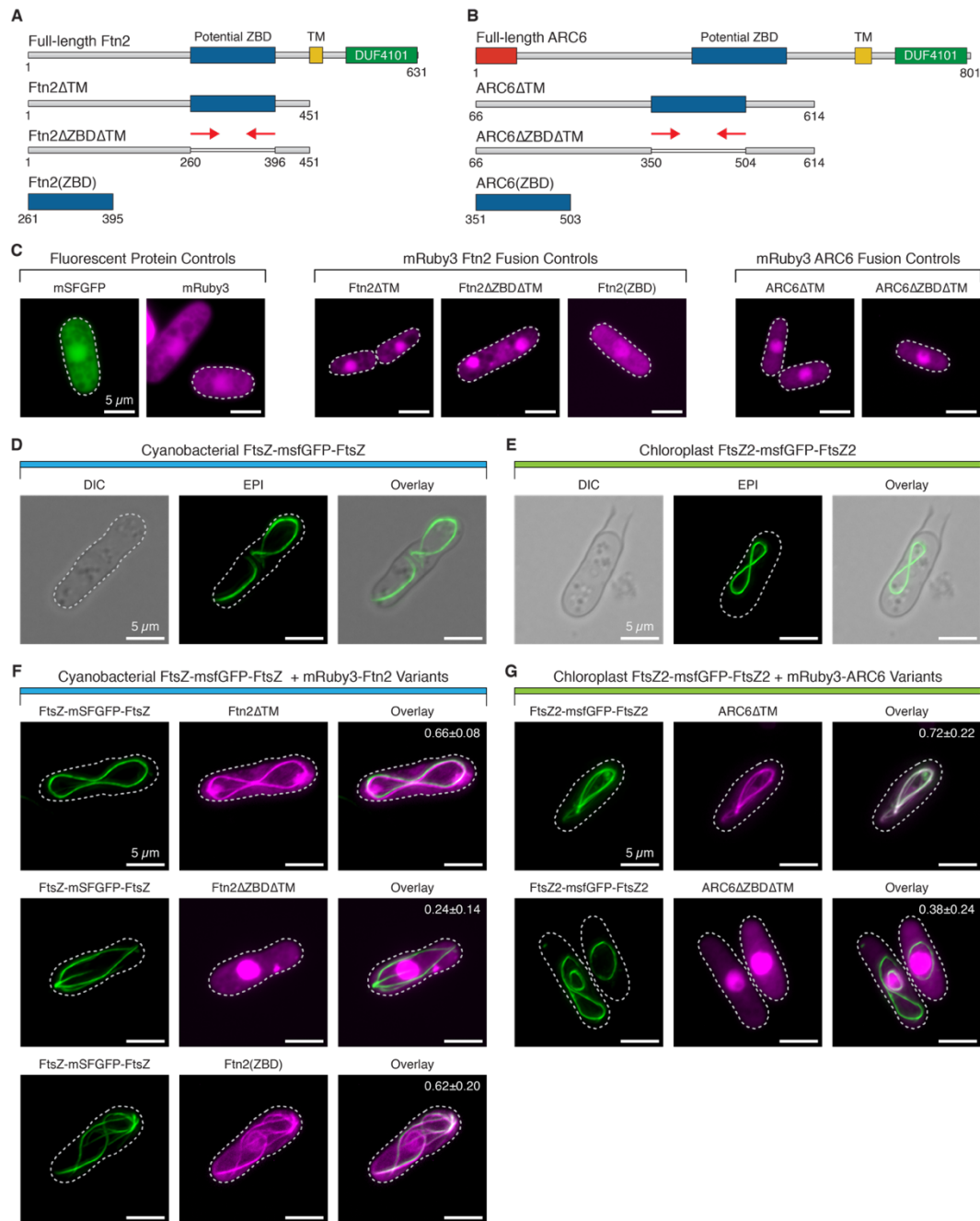


Figure 3.4: Colocalization of Ftn2/ARC6 with FtsZ/FtsZ2 in *S. pombe* is dependent upon the ZBD domain

(A) Truncations of Ftn2 and (B) ARC6 were cloned into inducible expression vectors in *S. pombe*. TM = transmembrane region. Red box = chloroplast transit peptide. Red arrows denote removal of the ZBD and fusion of the two halves. (C) Unfused fluorophores display a diffuse localization pattern (left). N-terminally tagged Ftn2 (middle) and ARC6 (right) fluorescent fusions display a predominantly diffuse patterning when expressed without FtsZ, although the reporters were observed to occasionally concentrate within the *S. pombe* nucleus. When (D) *S. elongatus* FtsZ or (E) *A. thaliana* FtsZ2 are expressed alone in *S. pombe*, filamentous structures are formed in the cytosol. (F) No FtsZ localization is detected in the absence of the Ftn2 ZBD (G) No FtsZ2 localization is detected in the absence of the ARC6 ZBD. PCC in top right corner (n = 15). Scale bars = 5 μ m.

A C-terminal Domain of FtsZ is Required for Ftn2 Interaction

Similar to FtsZ interaction with FtsA, ZipA, EzrA and SepF in *E. coli* and *B. subtilis*, the extreme C-terminus of *A. thaliana* FtsZ2 has been shown to mediate FtsZ2 interaction with ARC6 (Maple et al., 2005). To test whether this same region in *S. elongatus* FtsZ was responsible for interaction with Ftn2, we generated a variant of FtsZ-msfGFP-FtsZ (FtsZ Δ CTP) with the last 17 AA's removed (Figure 3.5A). Similar to FtsZ-msfGFP-FtsZ, FtsZ-msfGFP-FtsZ Δ CTP assembled into polymers when expressed in *S. pombe* (Figure 3.5B). However, unlike the full-length FtsZ (Figure 3.4F), neither the full cytosolic (mRuby3-Ftn2: 0.38 ± 0.16) nor ZBD-only Ftn2 variants (mRuby3-ZBD: 0.32 ± 0.11) co-localized with FtsZ Δ CTP (Figure 3.5C). These results confirm that the C-terminus of *S. elongatus* FtsZ is required for Ftn2 interaction, a common mechanism for FtsZ interaction with other membrane anchoring proteins.

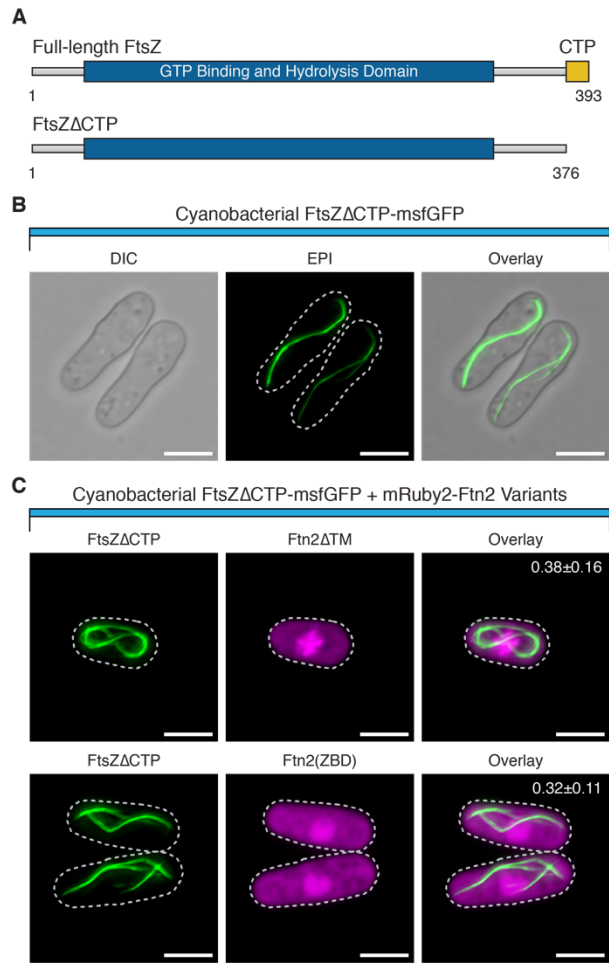


Figure 3.5: The c-terminus of *S. elongatus* FtsZ interacts with Ftn2

(A) Cartoon illustration of full-length and truncated (FtsZ Δ CTP) *S. elongatus* FtsZ. **(B)** C-terminally truncated FtsZ forms filaments in *S. pombe*. **(C)** Truncated FtsZ is no longer able to interact with cytosolic Ftn2 or Ftn2 ZBD, as evidenced by a lack of co-localization of these proteins. PCC in top right corner (n = 15). Scale bars = 5 μ m.

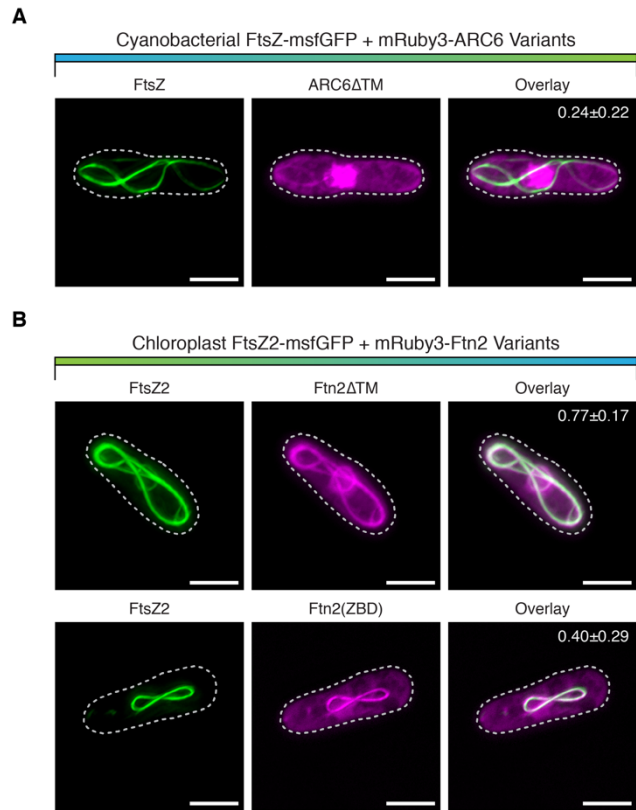


Figure 3.6: Cross-interaction between Ftn2/ARC6 and FtsZ2/FtsZ

(A) *S. elongatus* FtsZ colocalizes with cytosolic *A. thaliana* ARC6. **(B)** *A. thaliana* FtsZ2 colocalizes with *S. elongatus* cytosolic Ftn2 and Ftn2 ZBD-only. PCC in top right corner (n = 15). Scale bars = 5 μ m.

An Evolutionarily Conserved Mechanism for FtsZ Membrane-Anchoring in Cyanobacteria and Plants

Since the ZBDs of Ftn2 and ARC6 are highly conserved (Figure 3.3), we next sought to determine if FtsZ / ARC6 and FtsZ2 / Ftn2 could cross-interact. To test this, we coexpressed *S. elongatus* FtsZ-msfGFP-FtsZ and full cytosolic mRuby3-ARC6 in *S. pombe*. Co-localization of these reporters was clearly visible (Figure 3.6A), although a higher background signal of diffuse mRuby3-ARC6 resulted in a fairly low correlation score (0.24 ± 0.22). It is possible that the binding of mRuby3-ARC6 to cyanobacterial FtsZ was weaker than binding to chloroplast FtsZ2, leading to a greater fraction of unbound reporter. Alternatively, high expression of full cytosolic mRuby3-ARC6 relative to *S. elongatus* FtsZ-msfGFP-FtsZ, may have resulted in complete saturation of possible binding sites on FtsZ and elevated full cytosolic mRuby3-ARC6 background. Coexpression of *A. thaliana* FtsZ2-msfGFP-FtsZ2 and full cytosolic mRuby3-Ftn2 and mRuby3-Ftn2 ZBD resulted in strong correlation, 0.77 ± 0.17 and 0.40 ± 0.29 , respectively (Figure 3.6A). These results confirm that Ftn2 and ARC6 share an evolutionarily conserved domain for the recruitment of *S. elongatus* FtsZ and Arabidopsis FtsZ2 to the membrane.

This was a surprising result given the large evolutionary distance between *S. elongatus* Ftn2 and *A. thaliana* ARC6. Future work should now be targeted towards understanding the biochemical influence Ftn2 and ARC6 have on FtsZ dynamics, such as the rate of polymer turnover and/or GTPase activity. One recent study used Fluorescence Recovery After Photobleaching to show that the rate of FtsZ2 polymer turnover was somewhat reduced when FtsZ2 was co-expressed with the full stromal region of ARC6 in *S. pombe* (Terbush et al., 2013a). It is also interesting to speculate why chloroplasts and cyanobacteria recruit FtsZ assembly inhibitors, ARC3 and MinC respectively, in close proximity to membrane-anchoring proteins. In cyanobacteria, Ftn2 interacts with the protein Cdv3, which is known to recruit MinC in a MinD-dependent manner to midcell (Marbouty et al., 2009b; MacCready et al., 2017). Similarly, in chloroplasts, a paralog of ARC6, PARC6 (Glynn et al 2009; Zhang et al 2009), recruits ARC3 to the midplastid (Zhang et al., 2016; Chen et al., 2018), although whether ARC6 directly interacts with ARC3 remains unclear. It's possible that both Ftn2 and ARC6 initially stabilize FtsZ polymers along the membrane, promoting maturation of the divisome complex, and that subsequently these anti-FtsZ factors are recruited near Z rings to control the

rate of division or facilitate remodeling of the Z ring during constriction. In support of this idea, a recent study demonstrated that ARC3 prevents bundling of FtsZ2 polymers and stimulates FtsZ2 GTPase activity (Shaik et al., 2018). Moreover, FtsZ staining in our *S. elongatus* Ftn2 overexpression lines closely resembled that of our previous $\Delta minE$ lines (MacCready et al., 2017), suggesting that Ftn2 might have a role in stabilizing FtsZ filaments and protecting FtsZ from MinC. Therefore, exploration of why these anti-FtsZ factors are in such close proximity to the Z ring in the green photosynthetic lineage is crucial for understanding how cyanobacteria and chloroplasts divide. Taken together, our results provide strong evidence for how FtsZ is recruited to membranes and have broader implications for understanding the evolution and function of cyanobacterial- and chloroplast-derived division factors.

Methods

Construct Designs

All constructs in this study were generated using Gibson Assembly (Gibson et. al., 2009) from synthesized dsDNA. The construct for the deletion of *ftn2* was generated by amplification of 1000 bp upstream and downstream of *ftn2* by PCR, followed by replacement of *ftn2* with spectinomycin. The construct for the overexpression of Ftn2 was generated by PCR amplification of *ftn2* and insertion into *S. elongatus* neutral site 3; driven by a Ptrc promoter (Clerico et. al., 2007). Likewise, generation of an inducible mNG-Ftn2 fluorescent fusion was performed by insertion of mNG with a C-terminal GSGSGS linker following the Ptrc promoter and prior to the *ftn2* gene within NS3. Synthesized DNA for *S. elongatus* FtsZ-msfGFP-FtsZ and *A. thaliana* FtsZ2-msfGFP-FtsZ2 were cloned into *S. pombe* vector pREP41 at cut sites NdeI and BamHI. Likewise, synthesized DNA for *S. elongatus* mRuby3-Ftn2 Δ TM, mRuby3-Ftn2 Δ ZBD Δ TM, mRuby3-Ftn2(ZBD), and *A. thaliana* mRuby3-ARC6 Δ TM, mRuby3-ARC6 Δ ZBD Δ TM, mRuby3-ARC6(ZBD), were cloned into *S. pombe* vector pREP42 at cut sites NdeI and BamHI.

Culture Conditions and Transformations

All *S. elongatus* cultures were grown in 125 mL baffled flasks (Corning) containing 50 ml BG-11 medium (SIGMA) buffered with 1 g L⁻¹ HEPES to pH 8.3. Flasks were cultured in a Multitron II (atrbiotech.com) incubation system with settings: 80 $\mu\text{mol m}^{-2} \text{s}^{-1}$ light intensity, 32°C, 2% CO₂, shaking at 130 RPM. Transformation of plasmids was performed in *E. coli* DH5 α chemically competent cells (Invitrogen). All *S. elongatus* transformations were performed as previously described (Clerico et. al., 2007). Cells were plated on BG-11 agar with either 25 mg ml⁻¹ spectinomycin or 30 mg ml⁻¹ chloramphenicol. Single colonies were picked into 96-well plates containing 300 μl of BG-11 with identical antibiotic concentrations. Cultures were removed from antibiotics prior to imaging.

Cultures of wildtype *S. pombe* were grown in 50mL Yeast Extract with Supplements (YES) growth medium at 32°C to OD 0.5. Cells were then centrifuged at 4000 x g at room temperature. Resulting cell pellet was then washed with 1x TE buffer pH 7.5, centrifuged, and resuspended in 1 mL 1x TE buffer pH 7.5 / 0.1 M lithium acetate. Cells were incubated for 30 minutes at 32°C shaking at 200 RPM. 200 μl of cells were then placed within a 2 mL Eppendorf tube and 200 μg of carrier DNA and 1 μg of plasmid DNA were added and mixed. 1.2 mL of polyethylene glycol solution (40% PEG11, 1x TE buffer pH 7.5, 0.1 M lithium acetate) was then added, vortexed, and incubated for 30 minutes at 32°C shaking at 200 RPM. Cells were then heat shocked for 15 minutes at 42°C and centrifuged at 7000 x g for 30 seconds. Supernatant was discarded and cells resuspended in 300 μl of 1x TE buffer pH 7.5. Cells were then plated (200 μl and 50 μl) on PMG (Pombe Minimal Glutamate) dropout medium. For pREP41 transformants, leucine was excluded from the PMG. For pREP42 transformants, uracil was excluded from the PMG. For pREP41 and pREP42 double transformants, both leucine and uracil was excluded from the PMG. Cells were incubated at 32°C for 4-5 days.

Fluorescence microscopy

Roughly 30 hours prior to imaging, a single colony of *S. pombe* was transferred to 3 mL of PMG dropout medium. 7 μ l of cell culture was then transferred to poly-L-lysine coated glass slides. Epifluorescence imaging was performed as described in TerBush et al. 2016. Image analysis and Pearson's Correlation Coefficient calculations were performed with FIJI (<https://fiji.sc>).

Phylogenetic analysis

Phylogenetic analysis was performed as described in TerBush et al. 2016. Alignment of Ftn2 and ARC6 protein sequences was performed using MAFFT E-INS-i algorithm (BLOSUM62). Gblocks v. 0.91b was used to eliminate poorly conserved columns and/or amino acids. Bayesian analysis was then performed using MrBayes v. 3.2.6 with the LG model (lset nst=6 rates=invgamma); run occurred until the convergence value (the standard deviation of split frequencies) reached 0.01. The resulting tree was ordered and bootstrap values added by FigTree v. 1.4.3.

REFERENCES

REFERENCES

- Adams, DW., and Errington, J. (2009). Bacterial cell division: assembly, maintenance and disassembly of the Z ring. *Nat. Rev. Microbiol.* 7(9):642-53.
- Bi, EF., and Lutkenhaus, J. (1991). FtsZ ring structure associated with division in Escherichia coli. *Nature.* 354(6349):161-4.
- Bork, P., Sander, C., and Valencia, A. (1992). An ATPase domain common to prokaryotic cell cycle proteins, sugar kinases, actin, and hsp70 heat shock proteins. *Proc. Natl. Acad. Sci.* 89(16):7290-4.
- Chen, C., MacCready, JS., Ducat, DC., Osteryoung, KW. (2018). The Molecular Machinery of Chloroplast Division. *Plant Physiol.* 176(1):138-151.
- Clerico, EM., Ditty, JL., and Golden, SS. (2007). Specialized techniques for site-directed mutagenesis in cyanobacteria. *Methods Mol. Biol.* 362:155-71.
- Duman, R., Ishikawa, S., Celik, I., Strahl, H., Ogasawara, N., Troc, P., Löwe, J., and Hamoen, LW. (2013). Structural and genetic analyses reveal the protein SepF as a new membrane anchor for the Z ring. *Proc. Natl. Acad. Sci.* 110(48):E4601-10.
- Durand-Heredia, JM., Yu, HH., De Carlo, S., Lesser, CF., and Janakiraman A. (2011). Identification and characterization of ZapC, a stabilizer of the FtsZ ring in Escherichia coli. *J. Bacteriol.* 193(6):1405-13.
- Durand-Heredia, JM, Rivkin, E., Fan, G., Morales, J., and Janakiraman, A. (2012). Identification of ZapD as a cell division factor that promotes the assembly of FtsZ in Escherichia coli. *J. Bacteriol.* 194(12):3189-98.
- Ebersbach, G., Galli, E., Møller-Jensen, J., Löwe, J., and Gerdes, K. (2008). Novel coiled-coil cell division factor ZapB stimulates Z ring assembly and cell division. *Mol. Microbiol.* 68(3):720-35.
- Feucht, A., I. Lucet, M. D. Yudkin, and J. Errington. (2001). Cytological and biochemical characterization of the FtsA cell division protein of Bacillus subtilis. *Mol. Microbiol.* 40:115-125.
- Glynn, JM., Froehlich, JE., and Osteryoung, KW. (2008). Arabidopsis ARC6 coordinates the division machineries of the inner and outer chloroplast membranes through interaction with PDV2 in the intermembrane space. *Plant Cell.* 20(9):2460-70.
- Glynn, JM. (2009). Coordination of division complexes across the plastid envelope membranes. Michigan State University, East Lansing.

- Gorelova, OA., Baulina, OI., Rasmussen, U., and Koksharova, OA. (2013). The pleiotropic effects of *ftn2* and *ftn6* mutations in cyanobacterium *Synechococcus* sp. PCC 7942: an ultrastructural study. *Protoplasma*. 250(4):931-42.
- Gueiros-Filho, FJ., and Losick, R. (2002). A widely conserved bacterial cell division protein that promotes assembly of the tubulin-like protein FtsZ. *Genes Dev*. 16(19):2544-56.
- Hale, CA., and de Boer, PA. (1997). Direct binding of FtsZ to ZipA, an essential component of the septal ring structure that mediates cell division in *E. coli*. *Cell*. 88(2):175-85.
- Hale, CA., Rhee, AC., and de Boer, PA. (2000). ZipA-induced bundling of FtsZ polymers mediated by an interaction between C-terminal domains. *J. Bacteriol*. 182(18):5153-66.
- Hale, CA., Shiomi, D., Liu, B., Bernhardt, TG., Margolin, W., Niki, H., and de Boer, PA. (2011). Identification of *Escherichia coli* ZapC (YcbW) as a component of the division apparatus that binds and bundles FtsZ polymers. *J. Bacteriol*. 193(6):1393-404.
- Hamoen, LW., Meile, JC., de Jong, W., Noirot, P., and Errington, J. (2006). SepF, a novel FtsZ-interacting protein required for a late step in cell division. *Mol. Microbiol*. 59(3):989-99.
- Irieda, H., and Shiomi, D. (2017). ARC6-mediated Z ring-like structure formation of prokaryote-descended chloroplast FtsZ in *Escherichia coli*. *Sci. Rep*. 7(1):3492.
- Kemp, JT., Driks, A., and Losick, R. (2002). FtsA mutants of *Bacillus subtilis* impaired in sporulation. *J. Bacteriol*. 184(14):3856-63.
- Koksharova, OA., and Wolk, CP. (2002). A novel gene that bears a DnaJ motif influences cyanobacterial cell division. *J. Bacteriol*. 184(19):5524-8.
- Kumar, N., Radhakrishnan, A., Su, CC., Osteryoung, KW., and Yu, EW. (2016). Crystal structure of a conserved domain in the intermembrane space region of the plastid division protein ARC6. *Protein Sci*. 25(2):523-9.
- Król, E., van Kessel, SP., van Bezouwen, LS., Kumar, N., Boekema, EJ., and Scheffers, DJ. (2012). *Bacillus subtilis* SepF binds to the C-terminus of FtsZ. *PLoS One*. 7(8):e43293.
- Land, AD., Luo, Q., and Levin, PA. (2014). Functional domain analysis of the cell division inhibitor EzrA. *PLoS One*. 9(7):e102616.

Landgraf, D., Okumus, B., Chien, P., Baker, TA., and Paulsson, J. (2012). Segregation of molecules at cell division reveals native protein localization. *Nat. Methods*. 9(5):480-2.

Levin, PA., Kurtser, IG., and Grossman, AD. (1999). Identification and characterization of a negative regulator of FtsZ ring formation in *Bacillus subtilis*. *Proc. Natl. Acad. Sci.* 96(17):9642-7.

Loose, M., and Mitchison, TJ. (2014). The bacterial cell division proteins FtsA and FtsZ self-organize into dynamic cytoskeletal patterns. *Nat. Cell Biol.* 16(1):38-46.

Löwe, J. (1998). Crystal structure determination of FtsZ from *Methanococcus jannaschii*. *J. Struct. Biol.* 124(2-3):235-43.

Lutkenhaus, J. (2007). Assembly dynamics of the bacterial MinCDE system and spatial regulation of the Z ring. *Annu. Rev. Biochem.* 76:539-62.

Maple, J., Aldridge, C., and Møller, SG. (2005). Plastid division is mediated by combinatorial assembly of plastid division proteins. *Plant J.* 43(6):811-23.

Marbouty, M., Saguez, C., Cassier-Chauvat, C., and Chauvat, F. (2009). Characterization of the FtsZ-interacting septal proteins SepF and Ftn6 in the spherical-celled cyanobacterium *Synechocystis* strain PCC 6803. *J. Bacteriol.* 191(19):6178-85.

Marbouty, M., Saguez, C., Cassier-Chauvat, C., and Chauvat, F. (2009). ZipN, an FtsA-like orchestrator of divisome assembly in the model cyanobacterium *Synechocystis* PCC6803. *Mol. Microbiol.* 74(2):409-20.

Mazouni, K., Domain, F., Cassier-Chauvat, C., and Chauvat, F. (2004). Molecular analysis of the key cytokinetic components of cyanobacteria: FtsZ, ZipN and MinCDE. *Mol. Microbiol.* 52(4):1145-58.

McAndrew, RS., Olson, BJ., Kadirjan-Kalbach, DK., Chi-Ham, CL., Vitha, S., Froehlich, JE., and Osteryoung, KW. (2008). In vivo quantitative relationship between plastid division proteins FtsZ1 and FtsZ2 and identification of ARC6 and ARC3 in a native FtsZ complex. *Biochem. J.* 412(2):367-78.

Meier, EL., Razavi, S., Inoue, T., and Goley, ED. (2016). A novel membrane anchor for FtsZ is linked to cell wall hydrolysis in *Caulobacter crescentus*. *Mol. Microbiol.* 101(2):265-80.

Miyagishima, SY., Nozaki, H., Nishida, K., Nishida, K., Matsuzaki, M., and Kuroiwa, T. (2004). Two types of FtsZ proteins in mitochondria and red-lineage chloroplasts: the duplication of FtsZ is implicated in endosymbiosis. *J. Mol. Evol.* 58(3):291-303.

Miyagishima, SY., Wolk, CP., and Osteryoung, KW. (2005). Identification of cyanobacterial cell division genes by comparative and mutational analyses. *Mol. Microbiol.* 56(1):126-43.

Moore, DA., Whatley, ZN., Joshi, CP., Osawa, M., and Erickson, HP. (2016). Probing for Binding Regions of the FtsZ Protein Surface through Site-Directed Insertions: Discovery of Fully Functional FtsZ-Fluorescent Proteins. *J. Bacteriol.* 199(1). pii: e00553-16.

Osawa, M., Anderson, DE., and Erickson, HP. (2008). Reconstitution of contractile FtsZ rings in liposomes. *Science.* 320(5877):792-4.

Osteryoung, KW., Stokes, KD., Rutherford, SM., Percival, AL., and Lee, WY. (1998). Chloroplast division in higher plants requires members of two functionally divergent gene families with homology to bacterial ftsZ. *Plant Cell.* 10(12):1991-2004.

Osteryoung, KW., and Pyke, KA. (2014). Division and dynamic morphology of plastids. *Annu. Rev. Plant Biol.* 65:443-72.

Pazos, M., Natale, P., and Vicente, M. (2013). A specific role for the ZipA protein in cell division: stabilization of the FtsZ protein. *J. Biol. Chem.* 288(5):3219-26.

Pichoff, S., and Lutkenhaus, J. (2005). Tethering the Z ring to the membrane through a conserved membrane targeting sequence in FtsA. *Mol. Microbiol.* 55(6):1722-34.

RayChaudhuri, D. (1999). ZipA is a MAP-Tau homolog and is essential for structural integrity of the cytokinetic FtsZ ring during bacterial cell division. *EMBO J.* 18(9): 2372–2383.

Robertson, EJ., Pyke, KA., and Leech, RM. (1995). arc6, an extreme chloroplast division mutant of Arabidopsis also alters proplastid proliferation and morphology in shoot and root apices. *J. Cell Sci.* 108 (Pt 9):2937-44.

Sánchez, M., Valencia, A., Ferrándiz, MJ., Sander, C., and Vicente, M. (1994). Correlation between the structure and biochemical activities of FtsA, an essential cell division protein of the actin family. *EMBO J.* 13(20):4919-25.

Sánchez-Baracaldo, P., Raven, JA., Pisani, D., and Knoll, AH. (2017). Early photosynthetic eukaryotes inhabited low-salinity habitats. *Proc. Natl. Acad. Sci.* 114(37):E7737-E7745.

Shaik, RS., Sung, MW., Vitha, S., and Holzenburg, A. Chloroplast division protein ARC3 acts on FtsZ2 by preventing filament bundling and enhancing GTPase activity. *Biochem. J.* 475(1):99-115.

Singh, JK., Makde, RD., Kumar, V., and Panda, D. (2007). A membrane protein, EzrA, regulates assembly dynamics of FtsZ by interacting with the C-terminal tail of FtsZ. *Biochemistry.* 46(38):11013-22.

Srinivasan, R., Mishra, M., Wu, L., Yin, Z., and Balasubramanian, MK. (2008). The bacterial cell division protein FtsZ assembles into cytoplasmic rings in fission yeast. *Genes Dev.* 22(13):1741-6.

Strepp, R., Scholz, S., Kruse, S., Speth, V., and Reski, R. (1998). Plant nuclear gene knockout reveals a role in plastid division for the homolog of the bacterial cell division protein FtsZ, an ancestral tubulin. *Proc. Natl. Acad. Sci.* 95(8):4368-73.

Sundararajan, K., and Goley, ED. (2017). The intrinsically disordered C-terminal linker of FtsZ regulates protofilament dynamics and superstructure in vitro. *J. Biol. Chem.* 292(50):20509-20527.

Szeto, T., Rowland, S., Rothfield, L., and King, G. (2002). Membrane localization of MinD is mediated by a C-terminal motif that is conserved across eubacteria, archaea, and chloroplasts. *Proc. Natl. Acad. Sci.* 99, 15693–15698.

TerBush, AD., and Osteryoung, KW. (2012). Distinct functions of chloroplast FtsZ1 and FtsZ2 in Z-ring structure and remodeling. *J. Cell Biol.* 199(4):623-37.

TerBush, AD., Porzondek, CA., and Osteryoung, KW. (2013). Functional Analysis of the Chloroplast Division Complex Using *Schizosaccharomyces pombe* as a Heterologous Expression System. *Microsc. Microanal.* 22(2):275-89.

TerBush, AD., Yoshida, Y., and Osteryoung, KW. (2013). FtsZ in chloroplast division: structure, function and evolution. *Curr. Opin. Cell Biol.* 25(4):461-70.

TerBush, AD., MacCready, JS., Chen, C., Ducat, DC., and Osteryoung, KW. (2017). Conserved Dynamics of Chloroplast Cytoskeletal FtsZ Proteins Across Photosynthetic Lineages. *Plant Physiol.* 176(1):295-306.

Tomitani, A., Okada, K., Miyashita, H., Matthijs, HC., Ohno, T., and Tanaka, A. (1999). Chlorophyll b and phycobilins in the common ancestor of cyanobacteria and chloroplasts. *Nature.* 400(6740):159-62.

van den Ent, F., and Löwe, J. (2000). Crystal structure of the cell division protein FtsA from *Thermotoga maritima*. *EMBO J.* 19(20):5300-7.

Vitha, S., Froehlich, JE., Koksharova, O., Pyke, KA., van Erp, H., and Osteryoung, KW. (2003). ARC6 is a J-domain plastid division protein and an evolutionary descendant of the cyanobacterial cell division protein Ftn2. *Plant Cell.* 15(8):1918-33.

Zhang, M., Chen, C., Froehlich, JE., TerBush, AD., and Osteryoung, KW. (2016). Roles of Arabidopsis PARC6 in Coordination of the Chloroplast Division Complex and Negative Regulation of FtsZ Assembly. *Plant Physiol.* 170(1):250-62.

CHAPTER 4

PROTEIN GRADIENTS ON THE NUCLEOID POSITION THE CARBON-FIXING ORGANELLES OF CYANOBACTERIA

Summary

Carboxysomes are protein-based bacterial organelles that encapsulate a key enzyme of the Calvin-Benson-Bassham cycle. Previous work has implicated a ParA-like protein (hereafter McdA) as important for spatially organizing carboxysomes along the longitudinal axis of the model cyanobacterium *Synechococcus elongatus* PCC 7942. Yet, how self-organization of McdA emerges and contributes to carboxysome positioning is unknown. Here, we show that a small protein, termed McdB, localizes to carboxysomes through interactions with carboxysome shell proteins to drive emergent oscillatory patterning of McdA on the nucleoid. Our results demonstrate that carboxysome-dependent McdA depletion zone formation on the nucleoid is required for directed motion of McdB-bound carboxysomes towards increased concentrations of McdA. We propose that McdA and McdB are a new class of self-organizing proteins that follow a Brownian-ratchet mechanism for equidistant positioning of carboxysomes in cyanobacteria and have broader implications for understanding the spatial organization of protein mega-complexes and organelles in other bacteria.

Introduction

Many bacteria possess specialized protein-based organelles that compartmentalize sensitive metabolic processes (Axen et al., 2014). Among those identified, the best characterized are the large (~175 nm) carbon-fixing organelles of all cyanobacteria, called carboxysomes, which are required for growth under atmospheric CO₂ concentrations (reviewed here: Rae et al., 2013; Kerfeld et al., 2016). Carboxysomes encapsulate the key Calvin-Benson-Bassham cycle enzyme, ribulose-1,5-bisphosphate carboxylase/oxygenase (RuBisCO) and are thought to enhance the carbon fixation efficiency of this enzyme by creating a microenvironment that is enriched for CO₂. Specifically, carboxysomes consist of an outer “shell” layer that encapsulates both RuBisCO and carbonic anhydrase: the localized conversion of bicarbonate to CO₂ near RuBisCO is thought to greatly reduce its oxygenase activity, thereby suppressing the energetically-costly process of photorespiration. Since cyanobacteria contribute to greater than 25% of global carbon fixation, the function of carboxysomes is of considerable ecological, evolutionary and biotechnological interest. In the model rod-shaped cyanobacterium *Synechococcus elongatus* PCC 7942 (hereafter *S. elongatus*), it has been shown that carboxysomes align along the longitudinal axis of the cell (Savage et al., 2010). This distinct positioning is thought to promote equal inheritance of carboxysomes to both daughters of a dividing cell. However, despite their importance, the mechanism by which carboxysomes are positioned within *S. elongatus* has remained elusive.

While the mechanism is not understood, a prior study has shown that oscillation of a ParA-type ATPase (hereafter McdA - Maintenance of carboxysome distribution A) was required for proper positioning of carboxysomes (Savage et al., 2010), suggesting that McdA might use similar mechanisms to traditional ParA proteins for distributing carboxysomes along the length of the cell. ParA is a family of proteins that have been most comprehensively studied as factors important for the segregation of genetic material; bacterial chromosomes and low-copy plasmids (reviewed here: Baxter and Funnell, 2014). Early hypotheses of ParA function favored a cytoskeletal model in which ParA formed filaments that self-assemble into a larger scaffold that could be used to segregate genetic cargo, analogous to a primitive mitotic spindle (Ringgaard et al., 2009; Ptacin et al., 2010). These models were supported in part by in vitro

observations of fibrous, long bundled filaments of purified members of the ParA/MinD family of proteins (Reviewed here: Vecchiarelli et al., 2012). Recent experiments in reconstituted cell-free systems (Hwang et al., 2013; Vecchiarelli et al., 2013; Vecchiarelli et al., 2014), in parallel with super-resolution microscopy (Le Gall et al., 2016; Lim et al., 2014), crystallography (Zhang et al., 2017), and mathematical modelling approaches (Hu et al., 2015; Hu et al., 2017; Le Gall et al., 2016; Lim et al., 2014; Surovtsev et al., 2016), have converged upon a new hypothesis: asymmetric distributions of ParA dimers on the nucleoid can drive directed and persistent movement of DNA cargos towards increased concentrations of ParA via a Brownian-ratchet mechanism that does not require a cytoskeletal element.

The above experiments suggest a minimalistic ParA-mediated DNA segregation mechanism that requires only three factors: (i) a ParA-type ATPase that dimerizes and non-specifically binds the nucleoid in the presence of ATP (Leonard et al., 2005; Hester and Lutkenhaus, 2007; Castaing et al., 2008; Vecchiarelli et al., 2010), (ii) a partner protein, ParB, that site-specifically binds DNA and stimulates the ATPase activity of ParA to displace it from the nucleoid (Davis et al., 1992; Bouet et al., 1999; Bouet et al., 2000), and (iii) a centromere-like site on the DNA cargo (parS) that ParB loads onto (Davis et al., 1988; Funnell, 1988). In this model, multiple dimers of ParB form a large protein-DNA complex around the parS site, which leads to a break in ParA symmetry across the nucleoid due to the formation of local ParA depletion zones around individual ParB-bound cargos (Adachi et al., 2006; Hatano et al., 2007; Hwang et al., 2013; Vecchiarelli et al., 2014). In turn, transient ParA-ParB interactions could translate the asymmetrical distribution of ParA across the nucleoid into a directional cue for processive motion of cargo towards the highest local concentration of ParA.

Previously, it was proposed that McdA could form a cryptic cytoskeletal network that could be used to partition carboxysomes (Savage et al., 2010), although our changing understanding of ParA-mediated partitioning of DNA suggests that alternative mechanisms could be possible (Hu et al., 2017). Furthermore, because there have been no published reports identifying factors analogous to ParB or parS that act to position carboxysomes, whether McdA acts as part of a ParA-like system or utilizes a unique mechanism has remained an open question. Indeed, several fundamental questions arise in relation to carboxysome positioning: (i) Does McdA form a cytoskeletal structure or follow a Brownian-ratchet mechanism? (ii) What

biological surface does McdA bind? (iii) What factors are responsible for McdA patterning? (iv) How do oscillations of McdA contribute to carboxysome distributions?

Here, we show that a novel factor, we term McdB (Maintenance of carboxysome distribution protein B), localizes to carboxysomes via interaction with carboxysome shell proteins and drives oscillation of McdA along the nucleoid. Changes in McdB expression resulted in loss of McdA oscillatory dynamics, loss of equidistant carboxysome positioning and alteration of carboxysome ultrastructure. Surprisingly, the oscillatory dynamics of McdA also rely upon the cargo itself: disruption of carboxysome assembly disrupted both McdB localization and McdA dynamics. Our results have implications for understanding bacterial microcompartment biogenesis, equidistant positioning of cellular cargos by emergent protein patterning, and the evolution of a new class of self-organizing proteins.

Results

McdA Dynamically Patterns Along the Nucleoid

In the DNA partition process, ParA-type ATPases successively bind ATP, dimerize, and bind non-specifically to DNA (Leonard et al., 2005; Hester et al., 2007; Castaing et al., 2008; Vecchiarelli et al., 2010). *In vivo*, this mechanism establishes the nucleoid as the biological surface upon which directed DNA cargo motion occurs (Hatano et al., 2010; Sengupta et al., 2010; Castaing et al., 2008; Le Gall et al., 2016). In the model rod-shaped cyanobacterium *S. elongatus*, the ParA-like protein we call McdA (Synpcc7942_1833) is required for positioning carboxysomes via an unknown oscillatory mechanism (Savage et al., 2010). However, since this family of ATPases consists of both MinDs and ParAs, which bind membranes or DNA, respectively, it remained unclear what biological surface was being exploited by emergent McdA patterning to position carboxysomes, or if McdA was forming cytoskeletal filaments as has been proposed. We note, that while contaminating DNA is often found following carboxysome purification (Holthuijzen et al., 1986), another study suggested that chromosomes and carboxysomes were spatially mutually exclusive (Jain et al., 2012). Therefore, we first sought to determine if McdA bound to nucleoid DNA, and/or utilized it as a surface upon which to promote directed movement of cargo.

We began by examining endogenous localization and dynamics of McdA by generating mNeonGreen (mNG) fluorescent fusions to McdA using the native *mcdA* promoter and chromosomal location. Our native, N-terminally tagged mNG-McdA strain displayed robust oscillations that traversed the central longitudinal axis of the cell with a periodicity of 15.3 min per 3.3 μm , roughly 5-6x faster than previously reported (Savage et al., 2010) (Figure 4.1AD and Figure 4.2A), while the C-terminally tagged reporter (McdA-mNG) did not show dynamic oscillations (Figure 4.1B and Figure 4.2B). A carboxysome reporter was then generated by insertion of an additional copy of the small subunit of RuBisCO (RbcS) fused at the C-terminus to mTurquoise2 (mTQ) and expressed using a second copy of the native *rbcS* promoter. In this line, an average of 2 carboxysomes per micron of cell length was observed (Figure 4.2C). Cells bearing the mNG-McdA construct maintained normal carboxysome positioning (Figure 4.2D),

indicating the N-terminal fusion could fully complement McdA's known functions. Interestingly, we also observed dim foci in the wake of the mNG-McdA oscillation, suggesting a subpopulation of mNG-McdA might remain in the vicinity of carboxysomes (Figure 4.1C). To assay *in vivo* whether mNG-McdA could be binding the nucleoid, we stained the cyanobacterial nucleoid with 4',6-Diamidino-2'-phenylindole dihydrochloride (DAPI) and recorded the mNG-McdA signal as it traversed the length of the cell. We found that the topology of the mNG-McdA signal closely resembled that of the DAPI stained nucleoid (Figure 4.1E), suggesting the nucleoid could be the surface upon which McdA dynamics were occurring.

To directly assay McdA DNA-binding, we purified McdA and performed an Electrophoretic Mobility Shift Assay (EMSA) using non-specific DNA (nsDNA) (Figure 4.2E). McdA-GFP-6xHis significantly shifted nsDNA in the presence of ATP, confirming that it can bind to DNA and bolstering our *in vivo* observation that McdA appears to localize to the nucleoid (Figure 4.1F). A very subtle shift in nsDNA was also observed in the absence of nucleotide (Figure 4.1F), which we attribute to ATP contamination during purification because the competing substrates ADP and ATP- γ -S (a non-hydrolyzable ATP analog) prevented this shift (Figure 4.1F).

Since it has been proposed that *S. elongatus* McdA is a cytoskeletal protein (Savage et al., 2010), we used Total Internal Reflection Fluorescence Microscopy (TIRFM) to visualize how McdA-GFP interacts with nsDNA *in vitro* to determine if it formed filamentous structures. A nucleoid biomimetic was made by carpeting the surface of a flowcell with sonicated nsDNA fragments (~ 500bp) at high density (~ 1,000 fragments/ μm^2). When infused into the DNA-carpeted flowcell with ATP, McdA-GFP bound the DNA carpet (Figure 4.1G). With no nucleotide and either ADP or ATP- γ -S, McdA-GFP showed no appreciable binding to the DNA carpet (Figure 4.1H). Together, our results demonstrate that ATP-bound McdA uniformly binds DNA and does not display indications of polymer formation at the resolution limits of our microscope.

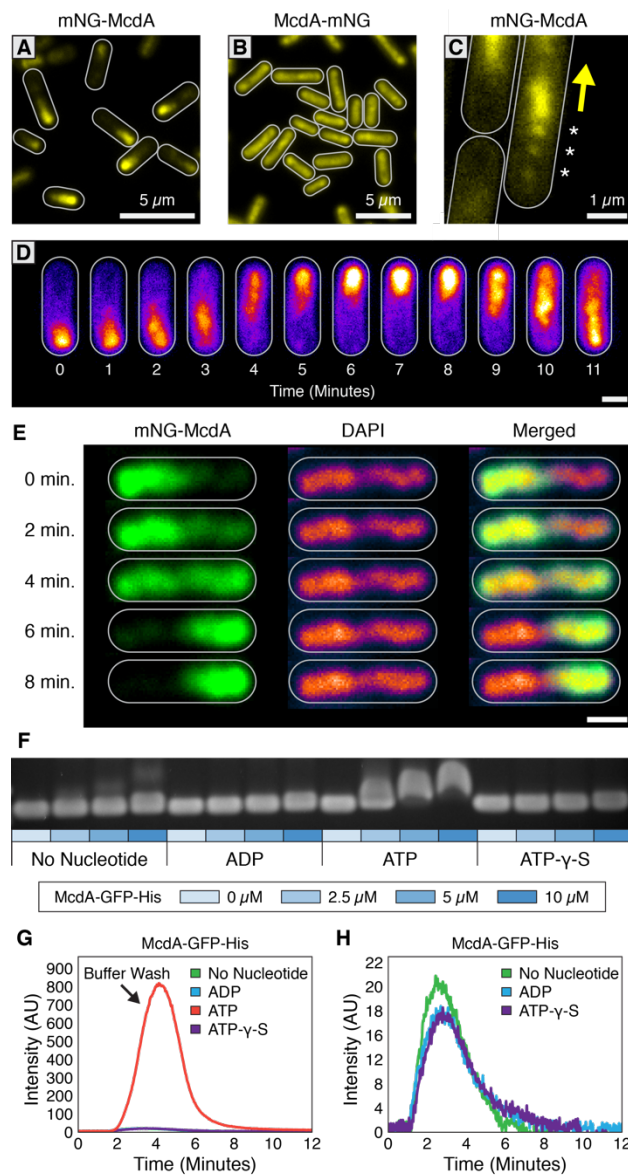


Figure 4.1: The *S. elongatus* ParA-like protein, McdA, binds nonspecifically to nucleoid DNA with ATP

(A) Native mNG-McdA displays robust oscillations, while the C-terminally tagged variant (B) McdA-mNG, does not oscillate. (C) mNG-McdA forms transient foci along the central axis in the wake of the oscillation. (D) mNG-McdA waves concentrate predominantly in the center of the cell, and do not concentrate at the periphery near the cell membrane. Scale bar = 1 μm . (E) Oscillation of mNG-McdA co-localizes with DAPI staining of nucleoid DNA, which is also centrally localized and is excluded from peripheral thylakoid membranes. Scale bar = 1 μm . (F) Purified McdA-GFP-His causes a gel shift in the migration of DNA in an ATP-dependent manner. (G) In flow cell experiments containing a carpet of non-specific DNA, McdA-GFP is preferentially retained by binding the DNA-carpet only in the presence of ATP, and releases when switching to a wash buffer after 3 minutes. (H) Magnified version of Panel G to show no protein binding without ATP.

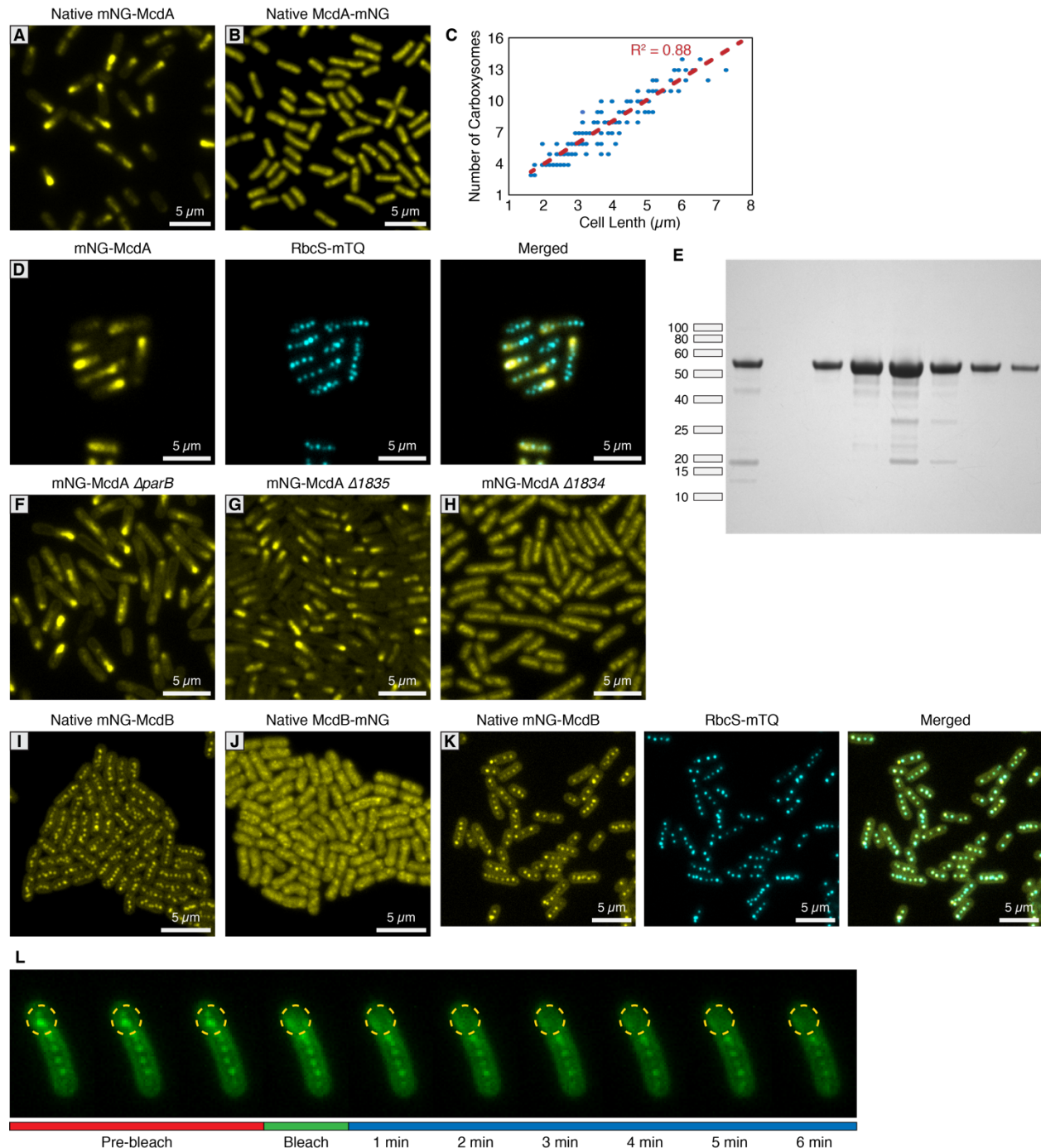


Figure 4.2: mNG-McdA oscillates and mNG-McdB is recruited to carboxysomes

(A) Native mNG-McdA displays robust oscillations. (B) Native McdA-mNG does not oscillate. (C) Carboxysome quantity measured in relation to cell size. (D) Carboxysomes remained positioned in our mNG-McdA strain. (E) SDS-PAGE of purified McdA-GFP-6xHis (~55 kD). First lane MonoQ load, space, peak fractions lanes 3-8. (F) Deletion of ParB does not influence mNG-McdA oscillation. (G) Deletion of *Synpcc7942_1835* does not influence mNG-McdA oscillation. (H) Deletion of *Synpcc7942_1834* collapses mNG-McdA oscillation. (I) Native mNG-McdB forms central foci structures. (J) Native McdB-mNG forms diffuse and punctate-like structures throughout cells. (K) mNG-McdB and RbcS-mTQ colocalize. (L) Recovery of mNG-McdB is not observed following photobleach.

A Previously Uncharacterized Protein Localizes to Carboxysomes and is Essential for Emergent McdA Dynamics

Traditional ParA-family members require cognate ParB proteins to stimulate their ATPase activity and promote oscillatory dynamics. Yet no ParB-like ortholog has been identified for McdA. Although no obvious chromosomally-encoded homolog of *parB* could be detected in *S. elongatus*, we identified a *parB*-like gene (Synpcc7942_B2626) on the large plasmid (pANL) (Figure 4.3A). However, deletion of pANL *parB* did not disrupt oscillation of mNG-McdA (Figure 4.2F and Figure 4.3B). Two additional hypothetical genes were then selected due to their proximity to the *mcdA* gene, Synpcc7942_1834 and Synpcc7942_1835 (Figure 4.3A). While deletion of Synpcc7942_1835 had no observable effect on mNG-McdA oscillation (Figure 4.2G and Figure 4.3C), deletion of Synpcc7942_1834 resulted in complete loss of mNG-McdA dynamics; forming a stochastic signal across the nucleoid (Figure 4.2H and Figure 4.3D). To more descriptively designate the activities we observe for Synpcc7942_1834 in this work, we will hereafter refer to this gene as maintenance of carboxysome distribution B (*mcdB*).

Bioinformatic analysis of the McdB protein by BlastP (protein-protein blast) revealed that McdB lacked similarity to any known protein outside of cyanobacteria, and has no significantly conserved regions with known ParB proteins. Likewise, Phyre2 (Kelley et al., 2015) was unable to generate a reliable protein homology model. McdB is small (17 kD) with a secondary structure, as predicted by jPred4 (Drozdetskiy et al., 2015), to mainly consist of alpha-helices with a highly charged N-terminal α_1 -helix and predicted coiled-coil C-terminal α_8 -helix (Figure 4.3E). We sought to determine if McdA and McdB directly interact by performing a bacterial two-hybrid assay (B2H) between N- and C-terminally tagged McdA and McdB (Figure 4.3F). McdA and McdB were able to self-associate in the B2H analysis (Figure 4.3F). Furthermore, we observed a reciprocal interaction between N-terminally tagged McdA and N-terminally tagged McdB. However, C-terminally tagged McdB failed to show an interaction with McdA, while C-terminally tagged McdA association with McdB was dependent upon expression conditions. These results suggest that N-terminally tagged McdA only interacts with N-terminally tagged McdB, while C-terminal fusions of either of these proteins may partially disrupt their functions, consistent with our *in vivo* observation of mNG-McdA / McdA-mNG dynamics (Figure 4.1AB).

ParB partners stimulate the ATPase activity of their cognate ParA synergistically with nsDNA (Davis et al., 1992; Bouet et al., 1999; Bouet et al., 2000). ParB stimulation is suggested to be coupled to ParA depletion on the nucleoid in the vicinity of ParB-bound cargo, as ADP does not support ParA binding to nsDNA (Leonard et al., 2005; Hester et al., 2007; Castaing et al., 2008; Vecchiarelli et al., 2010). We set out to determine if N- or C-terminally fused McdA variants displayed ATPase activity and if nsDNA and McdB stimulated this activity (Figure 4.3G); to better solubilize McdA for purification, we fused it to Maltose Binding Protein (MBP). His-MBP-McdA displayed strong ATPase activity alone compared to traditional ParA family ATPases. When adding only nsDNA or McdB to this reaction, we observed very mild stimulation of McdA ATPase activity. However, when both nsDNA and McdB were added together, a two-fold stimulation that was statistically-significant was observed. McdA-GFP-6xHis also displayed ATPase activity that was stimulated by nsDNA, but did not respond to the addition of McdB. The findings further confirm that C-terminal fusions of McdA may disrupt its natural functions, as observed in our prior *in vivo* (Figure 4.1B), and *in vitro* assays (Figure 4.3F).

We next sought to elucidate McdB's localization. Similar to our native McdA reporters, we generated N- and C-terminal mNG fusions to McdB using the native *mcdA* promoter and chromosomal location. N-terminal mNG-McdB was observed as multiple discrete fluorescent foci near the central longitudinal axis of the cell, a result that strongly resembles the localization pattern of native carboxysomes (Figure 4.2I and Figure 4.3H). In contrast, C-terminal fusions of McdB displayed a diffuse localization with random punctate-like patterns, again suggestive that C-terminal tags may disrupt some native functions of McdB (Figure 4.2J and Figure 4.3I). We confirmed co-localization of McdB with carboxysomes by co-expression of the carboxysome fluorescent reporter in the mNG-McdB strain. Both the mNG-McdB and RbcS-mTQ signals colocalized as fluorescent foci near the long central axis of the cell (Figure 4.2K and Figure 4.3J). To determine if mNG-McdB interaction with carboxysomes was dynamic, we performed FRAP analysis within our native mNG-McdB strain. We found that mNG-McdB signal did not recover following bleaching (Figure 4.2L), indicating that mNG-McdB has a stable association with the carboxysome. Taken together, the data suggest that McdB drives emergent McdA oscillation dynamics on the nucleoid by locally stimulating McdA ATPase activity and nucleoid release in the vicinity of carboxysomes.

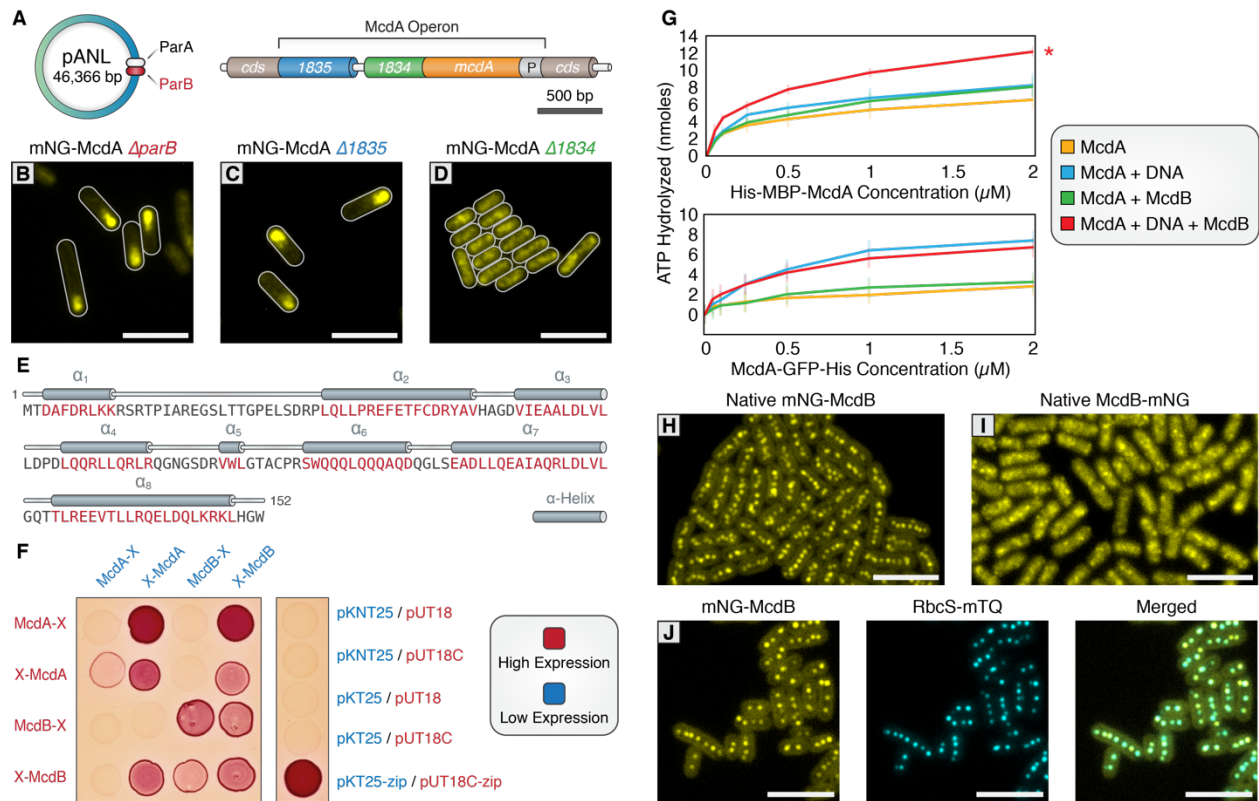


Figure 4.3: A small, carboxysome-localized protein is required for McdA oscillatory dynamics

(A) Candidate genes controlling McdA dynamics on either the native plasmid (left) or within the genomic neighborhood of *mcdA*. **(B)** Deletion of pANL *parB* and **(C)** *Synpcc7942_1835* has no effect on mNG-McdA dynamics. **(D)** Deletion of *Synpcc7942_1834* collapses mNG-McdA oscillatory dynamics. **(E)** *Synpcc7942_1834* secondary structure prediction: residues in red are predicted to form α -helical secondary structures. **(F)** Left - bacterial two-hybrid between McdA and McdB tagged at their N-termini (X-McdA, X-McdB) or C-termini (McdA-X, McdB-X). Right - control plasmids. Red = high expression, blue = low expression. **(G)** ATPase activity assays of His-MBP-McdA and McdA-GFP-His reveal stimulatory roles of DNA and McdB. **(H)** A natively tagged mNG-McdB reporter localizes to centralized foci in live *S. elongatus* cells. **(I)** Native McdB-mNG forms diffuse and punctate-like structures throughout cells. **(J)** mNG-McdB and a carboxysome reporter - RbcS-mTQ - colocalize. All scale bars = 5 μ m.

McdB Interacts with Major and Minor Shell Components

We therefore sought to determine if McdB's interaction with the carboxysome is direct, and if so, what carboxysome components bind McdB. During biogenesis, carboxysomes first form a core structure containing RuBisCO and carbonic anhydrase, which are coordinated into an ordered array through interactions with CcmM (Figure 4.4A) (Long et al., 2007; Cot et al., 2008; Long et al., 2010; Cameron et al., 2013). This core is thought to recruit the shell proteins that coat the carboxysome through the mediating protein CcmN (Fan et al., 2012; Kinney et al., 2012) (Figure 4.4A). CcmK2 is the dominant shell protein that composes the facets of the shell, and which has been shown to directly interact with CcmN (Kinney et al., 2012). Along with CcmK2, proteins CcmO, CcmL, CcmK3, CcmK4, and CcmP are also recruited to complete compartmentalization (Figure 4.4B) (Tanaka et al., 2008; Tanaka et al., 2009; Rae et al., 2012; Cai et al., 2013). We therefore explored if the outer shell proteins of the carboxysome could be involved in recruiting McdB through a bacterial two-hybrid screen. Using N-terminally tagged McdA or McdB as bait, we tested the shell proteins CcmK2, CcmK3, CcmK4, CcmL, CcmO and CcmP. This assay suggested McdB interacts with the shell proteins CcmK2, CcmK3, CcmK4, CcmL, and CcmO (Figure 4.4C). In contrast, we did not find evidence for direct interaction between McdA and carboxysome shell proteins (Figure 4.4C and Figure 4.5ABC), suggesting that residual McdA localization near carboxysomes (Figure 4.1C) is due to an indirect interaction – possibly mediated by McdB.

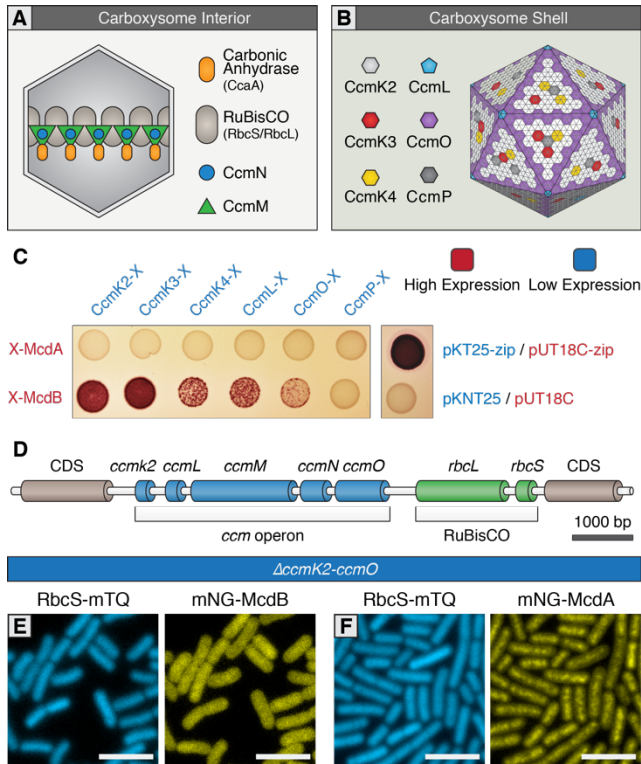


Figure 4.4: McdB interacts with the carboxysome shell

(A) Cartoon depiction of the internal and (B) external shell components of the cyanobacterial carboxysome, adapted from models presented in Rae et al., 2013. Note that the relative geometric arrangement of some shell components to one another remain somewhat speculative. (C) Left - bacterial two-hybrid of McdA and McdB against carboxysome shell proteins. Right –control plasmids. Red = high expression, blue = low expression. (D) Cartoon schematic of the *S. elongatus* carboxysome operon. (E) Without carboxysomes (Δ *ccmK2-ccmO*), mNG-McdB is not localized to central puncta but rather diffuse throughout the cell. (F) mNG-McdA oscillatory dynamics are lost without carboxysomes (Δ *ccmK2-ccmO*). All scale bars = 5 μ m.

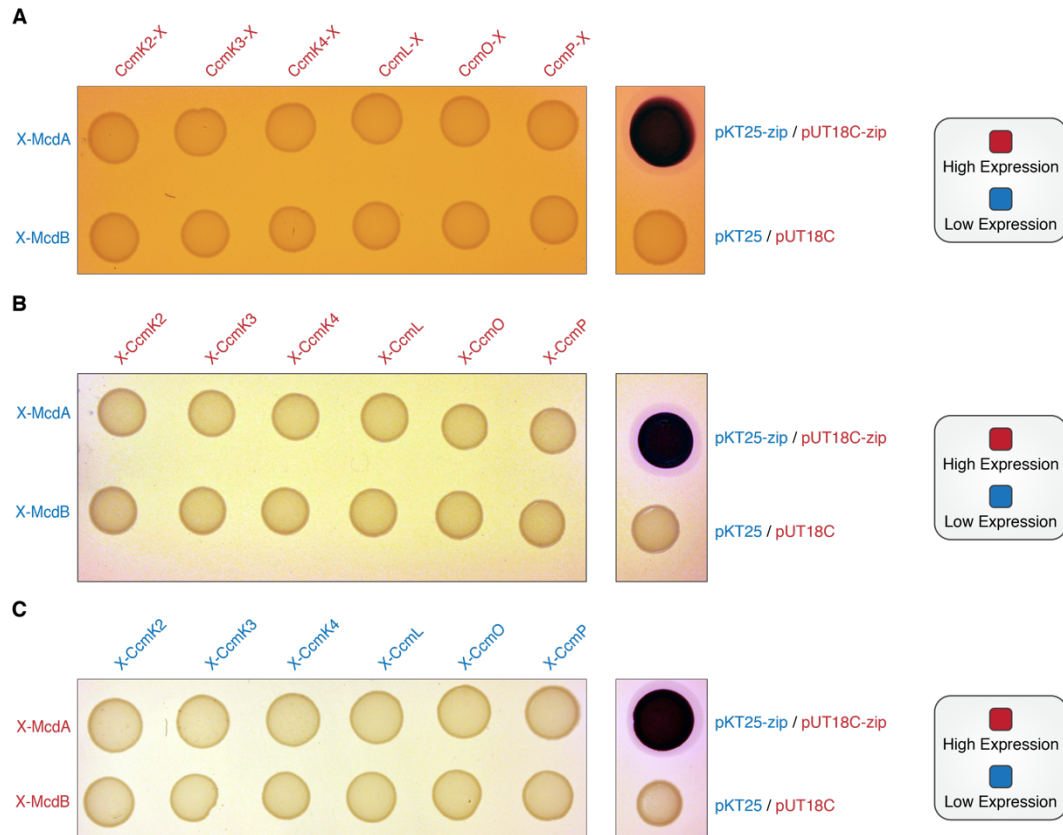


Figure 4.5: McdA/B bacterial two-hybrid against carboxysome shell proteins

(A) Bacterial two-hybrid between McdA and McdB tagged at their N-termini (low expression) against carboxysome shell proteins tagged at their C-termini (high expression). **(B)** Bacterial two-hybrid between McdA and McdB tagged at their N-termini (low expression) against carboxysome shell proteins tagged at their N-termini (high expression). **(C)** Bacterial two-hybrid between McdA and McdB tagged at their N-termini (high expression) against carboxysome shell proteins tagged at their N-termini (low expression).

Carboxysome Formation is Required for the Emergent Oscillations of McdA

To further investigate the association of McdB with the carboxysome, we examined McdB dynamics in a *S. elongatus* background that lacks functional carboxysomes. While carboxysomes are essential for growth under an ambient atmosphere, mutants deleted for the *ccm* operon ($\Delta ccmK2LMNO$; Figure 4.4D) can be recovered in high CO₂ (Price et al., 1993; Cameron et al., 2013). We therefore examined the dynamics of mNG-McdB in a $\Delta ccmK2LMNO$ background, and found that mNG-McdB signal was diffuse and no longer localized to discrete foci (Figure 4.4E). As expected, RbcS-mTQ signal was also diffuse in $\Delta ccmK2LMNO$ cells, confirming the absence of carboxysomes (Figure 4.4E). Interestingly, in the absence of carboxysomes, mNG-McdA did not oscillate and formed a homogenous distribution along the nucleoid similar to that of our mNG-McdA $\Delta mcdB$ strain (Figure 4.4F and Figure 4.3D). This result suggests that the concentration of McdB onto carboxysomes is an important prerequisite of self-organized McdA oscillations.

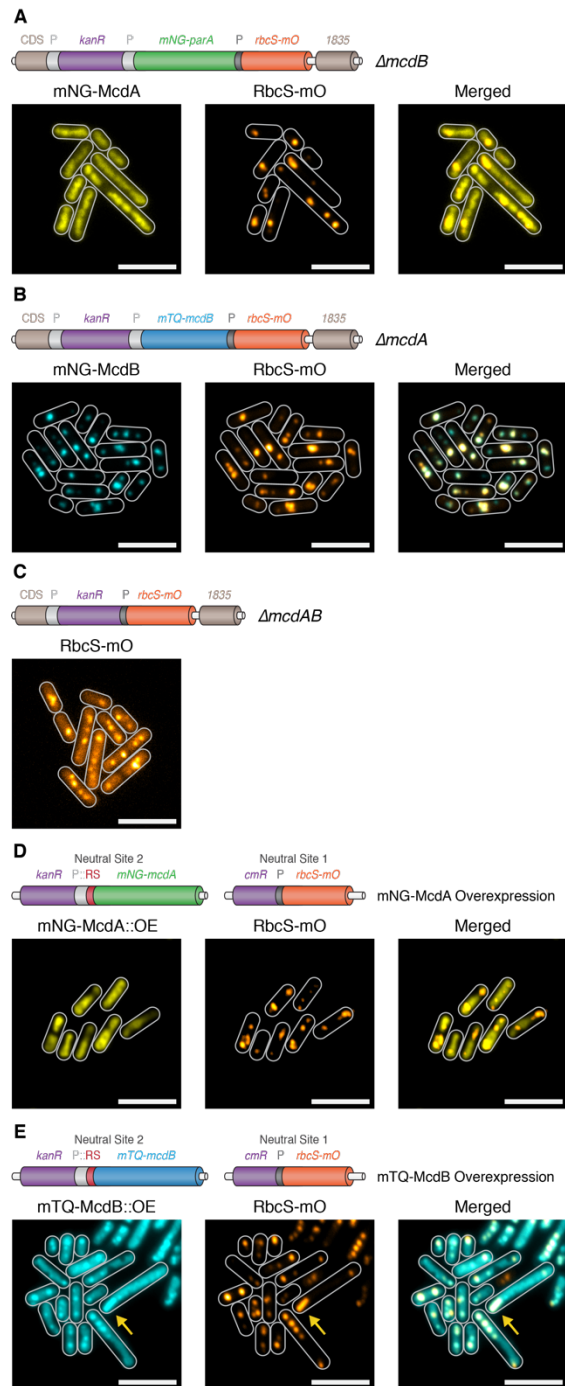


Figure 4.6: McdA and McdB are essential for distributing carboxysomes

(A) Carboxysome (orange; *rbcS-mO*) and mNG-McdA (yellow) distribution in a $\Delta mcdB$ background. Cartoon schematics (top) of the genetic construct are depicted, *mcdA* promoter “P” = light grey, *rbcS* promoter = dark grey. (B) Carboxysome and mTQ-McdB (cyan) distribution in a $\Delta mcdA$ background. (C) Carboxysome distribution with *mcdAB* deleted. (D) Carboxysome positioning is disrupted and oscillation of mNG-McdA does not occur upon mNG-McdA overexpression. Riboswitch = Red RS. (E) Bar carboxysome structures (yellow arrow) and loss of positioning are observed upon overexpression of mTQ-mcdB. All scale bars = 5 μm .

Carboxysome Positioning is Disrupted in McdA/McdB Mutants

Since we found that both McdA and McdB are implicated in the regulation of carboxysome positioning, we next investigated how carboxysomes were distributed in strains lacking these proteins. To reduce potential off-target effects in the $\Delta mcdA$ and $\Delta mcdB$ lines, we generated knockouts in a manner designed to minimize alterations in expression of neighboring genes. This included insertion of the kanamycin resistance cassette outside of the McdA operon, and duplication of the mcdA promoter upstream of the mcdB gene in constructs where interruption of mcdA might be expected to disrupt downstream gene expression (see Figure 4.6AB). We also inserted RbcS fused to mOrange2 (mO) expressed from the native *rbcS* promoter to visualize carboxysomes (Figure 4.6ABC).

In $\Delta mcdB$ lines, mNG-McdA did not oscillate and distributed along the nucleoid, confirming deletion of *mcdB* (Figure 4.6A). Carboxysomes in this line were observed as large irregularly shaped polar fluorescent foci with smaller randomly distributed signals within the cell (Figure 4.6A). In the absence of McdB, McdA was evenly distributed along the nucleoid and was not depleted in the vicinity of carboxysomes. In $\Delta mcdA$ lines, mTQ-McdB still localized to carboxysomes, indicating McdA is not required for the association, but carboxysomes formed large fluorescent foci with adjacent carboxysomes in close proximity, suggesting carboxysomes could be clustering in the absence of McdA (Figure 4.6B). In the absence of both McdA and McdB, carboxysomes appeared as irregular foci of varying sizes (Figure 4.6C). The fluorescence intensity from the RbcS-mO reporter was also ~4-fold weaker in these lines.

We next investigated carboxysome positioning in McdA and McdB overexpression lines. For these experiments, we inserted the RbcS-mO fluorescent reporter in neutral site 1, a genomically neutral locus (Clerico et al., 2007), and overexpressed either mNG-McdA or mTQ-McdB from a synthetic riboswitch (Nakahira et al., 2013) inserted into neutral site 2 (Clerico et al., 2007) (Figure 4.6DE). Upon the overexpression of mNG-McdA, we observed loss of McdA oscillation and the formation of large irregularly-shaped RbcS-mO fluorescent foci reminiscent of $\Delta mcdA$, $\Delta mcdB$ and $\Delta mcdAB$ lines (Figure 4.6D). With endogenous levels of McdB present, the McdA signal was generally depleted in the vicinity of these carboxysome aggregates. Upon the overexpression of mTQ-McdB, we observed mTQ-McdB signal

colocalized at irregularly-shaped RbcS-mO fluorescent foci or diffuse within the cell (Figure 4.6E). Moreover, we also observed much larger RbcS-mO bar-shaped structures within the cell, indicating that McdB levels might influence carboxysome size and ultrastructure (Figure 4.6E).

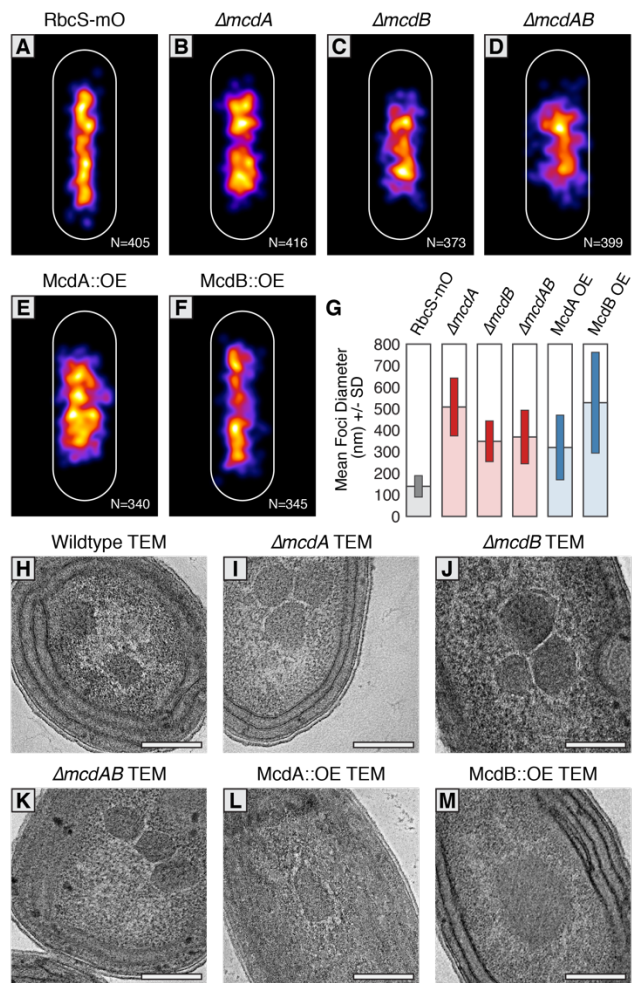


Figure 4.7: McdAB physically separate and regulate carboxysome ultrastructure
(A-F) MicrobeJ average distribution heat-map of carboxysomes in the indicated genetic background strains. Quantity measured in lower right corner. **(G)** Mean RbcS-mO foci area and standard deviation for wildtype and the indicated mutant strains. **(H-M)** Electron micrographs of carboxysomes from wildtype and mutant strains. All scale bars = 250 nm.

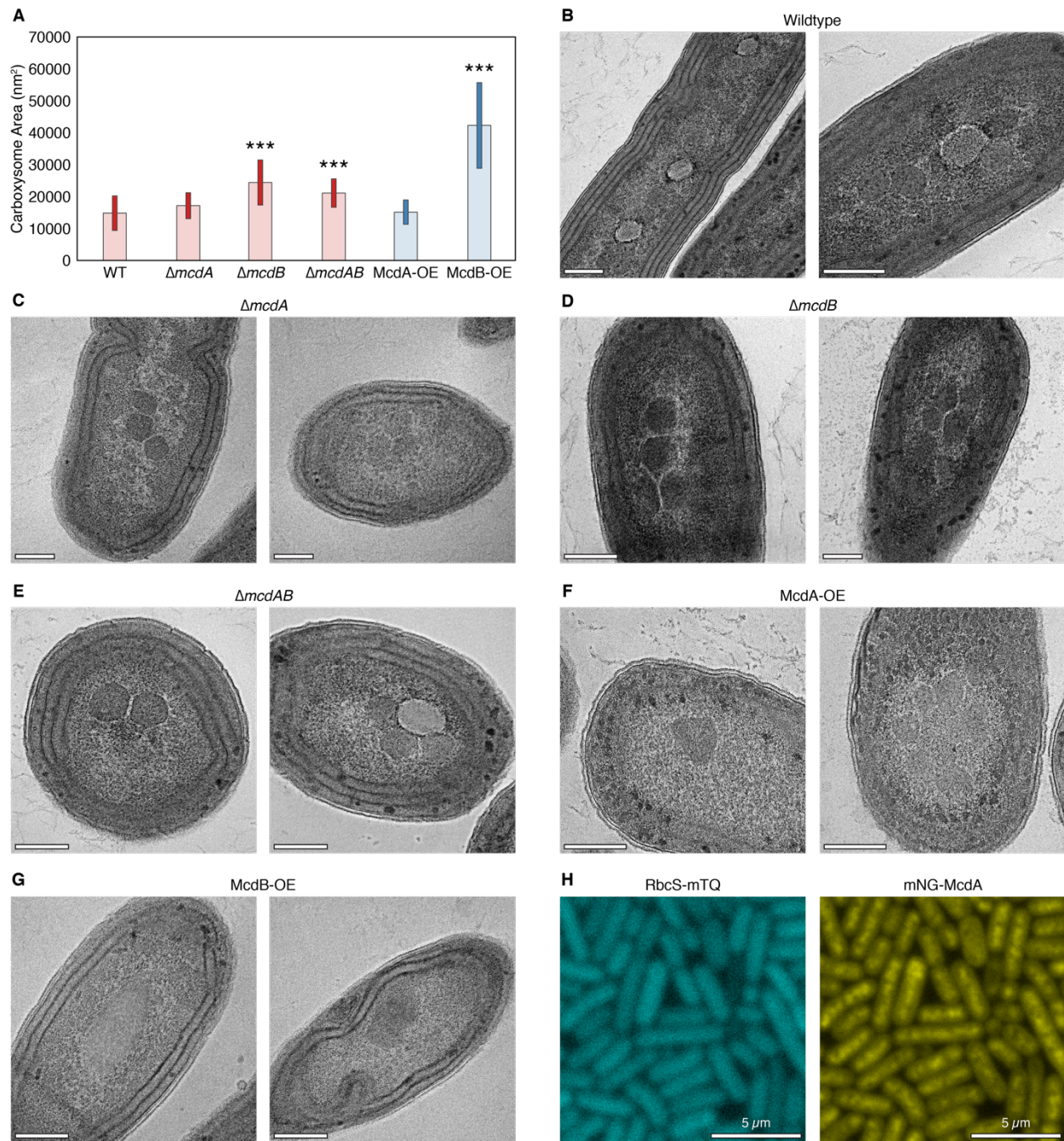


Figure 4.8: Quantification of carboxysome size from TEM

(A) Mean carboxysome area and standard deviation for wildtype and mutant strains. $P < 0.0001$ denoted as (***). Additional representative TEM images for (B) $\Delta mcdA$ (C) $\Delta mcdB$ (D) $\Delta mcdAB$ (E) McdA overexpression and (F) McdB overexpression. (G) RbcS-mTQ signal is diffuse and mNG-McdA does not display oscillatory dynamics in the absence of the theophylline inducer. All scale bars = 250 nm.

Carboxysome Ultrastructure is Disrupted in McdA/McdB Mutants

To quantify carboxysome distributions in our mutant lines, we utilized MicrobeJ to automatically detect and characterize our fluorescent signals (Ducret et al., 2016). In our RbcS-mO only reporter line, fluorescent signal was observed predominantly along the central axis and mean foci diameter was $140 \text{ nm} \pm 100 \text{ nm}$ (Figure 4.7AG). In comparison to this strain, carboxysomes in $\Delta mcdA$ ($510 \text{ nm} \pm 270 \text{ nm}$), $\Delta mcdB$ ($350 \text{ nm} \pm 190 \text{ nm}$), and $\Delta mcdAB$ ($370 \text{ nm} \pm 250 \text{ nm}$) lines had a much broader distribution off the central axis with larger mean foci diameters and deviations (Figure 4.7BCDG). Likewise, overproduction of McdA produced carboxysome distributions off the central axis and a mean foci diameter ($320 \text{ nm} \pm 300 \text{ nm}$) similar to those of deletion lines (Figure 4.7BCDEG). Lastly, McdB overexpression produced carboxysomes that were distributed mostly along the central longitudinal axis, but exhibited the largest mean foci diameter and deviation ($530 \text{ nm} \pm 470 \text{ nm}$) (Figure 4.7FG). These data suggest that in addition to spatially regulating carboxysome distributions, McdA and McdB could influence carboxysome size and/or ultrastructure.

To differentiate whether the changes in size of RbcS-mO foci were due to clustering of multiple carboxysomes or changes in carboxysome ultrastructure, we used Transmission Electron Microscopy (TEM). In contrast to faithfully distributed carboxysomes in our wild type TEM images (Figure 4.7H and Figure 4.8B), we observed multiple carboxysomes tightly clustered in our $\Delta mcdA$, $\Delta mcdB$, and $\Delta mcdAB$ strains (Figure 4.7IJK and Figure 4.8ACDE). This observation suggested McdA and McdB are required to separate neighboring carboxysomes, or that newly synthesized carboxysomes may be incompletely detached from one another during biogenesis (Cameron et al., 2013; Chen et al., 2013) in the absence of McdA or McdB.

Upon overproduction of McdA, we observed irregularly-shaped carboxysomes with “rounded” edges that tightly clustered (Figure 4.7L and Figure 4.8AF). It should be noted however, that this strain displayed severe growth defect and possessed an unusually abundant number of granules which we assume to be polyphosphate bodies throughout the cell. Consistent with this observation, ParA overproduction in many organisms is lethal (Lasocki et al., 2007). Most strikingly, carboxysomes did not cluster in McdB overproduction strains either, instead, carboxysome ultrastructure was dramatically altered.

Unlike the classic icosahedral-shape, carboxysomes were observed as large irregular bar-like structures (Figure 4.7M and Figure 4.8AG). In some instances, these “bar-carboxysomes” extended hundreds of nanometers (Figure 4.6E), resembling previous reports of improperly assembled carboxysomes in cells lacking *ccmL* (Price and Badger, 1989; Cameron et al., 2013). Together, these results highlight the importance of the McdAB system for spatially separating carboxysomes and regulating the underlying size and ultrastructure.

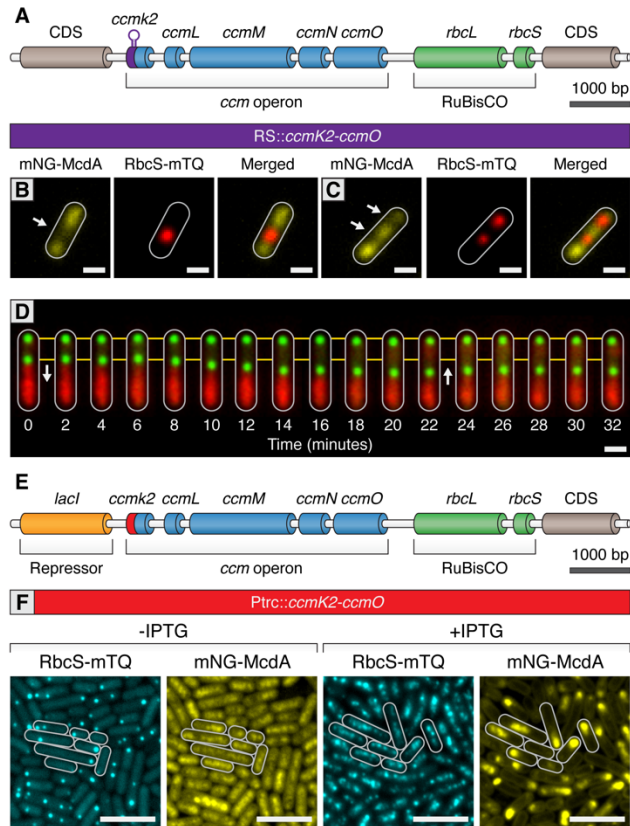


Figure 4.9: Carboxysomes locally deplete McdA from the nucleoid and cause McdA oscillation at high-copy number

(A) Cartoon schematic of the inducible carboxysome operon with the synthetic, theophylline-inducible riboswitch preceding *ccmK2*. Induction of carboxysome biogenesis with either (B) 400 μ M or (C) 600 μ M theophylline leads to the formation of one or two carboxysomes (red; RbcS-mTurq). mNG-McdA (yellow) is depleted from the vicinity of nearby carboxysomes (white arrows). Scale bar = 1 μ m. (D) In a representative timelapse imaging of a newly formed carboxysome (green), the central carboxysome moves towards (white arrow) a cellular location with increased mNG-McdA (red). When sufficient distance is obtained between carboxysomes (~20 min) mNG-McdA begins to be recruited between them. Scale bar = 1 μ m. (E) Cartoon schematic of carboxysome operon with *Ptrc* promoter and *lacI* preceding *ccmK2*. (F) mNG-McdA oscillations are reconstituted following addition of IPTG and the assembly of multiple carboxysomes. Scale bar = 5 μ m.

Carboxysomes Locally Deplete McdA on the Nucleoid and are Required for McdA Oscillation

How multiple carboxysomes are equally spaced along the cell length by an oscillating McdA protein is not intuitively obvious. Through *in vivo* and *in vitro* experimentation, it has been demonstrated that ParB-bound cargos form ParA depletion zones by stimulating release of ParA from the nucleoid in their vicinity (Hatano et al., 2007; Ringgaard et al., 2009; Schofield et al., 2010; Hwang et al., 2013; Vecchiarelli et al., 2013, 2014). Therefore, we wished to determine if McdB-bound carboxysomes also cause similar local depletions of McdA on the nucleoid and whether oscillation of McdA is a requirement for carboxysome motion and equidistant positioning, even at low-copy numbers.

To explore this question, we needed the ability to regulate the initiation of carboxysome formation as well as to modulate the number of carboxysomes per cell. To accomplish this, we replaced the native *ccmK2* promoter with a P_{trc} promoter lacking the *lacI* repressor and attached a 5' synthetic riboswitch preceding *ccmK2* (Figure 4.9A). Expression from this riboswitch has been shown to be tightly off and extremely tunable relative to the concentration of theophylline (Nakahira et al., 2013). Consistent with no expression from the RS::*ccmK2LMNO* operon in the absence of theophylline, we observed that RbcS-mTQ signal was diffuse and mNG-McdA was distributed homogeneously along the nucleoid (Figure 4.8H). When these strains were induced with either 400 μ M or 600 μ M theophylline, we were able to generate on average 1 or 2 carboxysomes per cell, respectively (Figure 4.9BC). In the presence of 1 carboxysome, we observed mNG-McdA signal distributed along the nucleoid with a depletion zone that correlated with the position of the carboxysome (Figure 4.9B). Likewise, with two carboxysomes, mNG-McdA signal again distributed along the nucleoid but was depleted in areas correlating to carboxysomes (Figure 4.9C). In this strain, we performed real-time imaging of mNG-McdA dynamics and RbcS-mTQ motion. In instances where cells contained two, closely spaced carboxysomes, one carboxysome could be clearly observed to move in the direction of the higher McdA concentration (Figure 4.9D). When a sufficient distance was reached between the two carboxysomes, mNG-McdA was re-recruited to the depleted nucleoid region between the two carboxysomes (Figure 4.9D). As mNG-McdA rebound on the nucleoid, movement of the centralized carboxysome halted and moved back in the opposite direction (Figure 4.9D). This result is consistent with

the Brownian-Ratchet mechanism for genetic cargo movement towards increased concentrations of ParA (Vecchiarelli et al., 2010; Vecchiarelli et al., 2014; Hu et al. 2017). Indeed, in separate time-lapse experiments of mNG-McdA and RbcS-mTQ strains, we frequently observed that carboxysomes move towards increased concentration of McdA as it oscillates along the nucleoid.

We next sought to determine if we could reconstitute carboxysome-dependent oscillation of McdA. Even at relatively high concentrations of theophylline inducer, our synthetic riboswitch was unable to generate wildtype quantities of carboxysomes. Therefore, we used a variant of a previously published approach (Cameron et al., 2013) by replacing the *ccmK2* promoter with the P_{trc} promoter and inserted an upstream *lacI* repressor (Figure 4.9E). This promoter is generally capable of driving higher expression levels of gene targets. In the absence of Isopropyl β -D-1-thiogalactopyranoside (IPTG), some carboxysome formation was observed due to leaky expression of the P_{trc} promoter in cyanobacteria (Figure 4.9F). Similarly to prior results, mNG-McdA was depleted in the vicinity of carboxysomes (Figure 4.9F). Following induction with IPTG, multiple carboxysomes formed throughout cells and mNG-McdA oscillations emerged (Figure 4.9F). Altogether, these experiments strongly indicate that McdB is concentrated upon carboxysomes and that this pool of McdB changes the dynamics of McdA bound to neighboring regions of the nucleoid. Under conditions where there are relatively few (1-3) carboxysomes, McdB appears to continuously stimulate the release of nearby McdA. It is only at higher numbers of carboxysomes (4+) when a self-organized oscillation of McdA from end-to-end of the nucleoid emerges. Moreover, our results also strongly suggest that carboxysome motion occurs towards increased McdA concentrations on the nucleoid, consistent with the Brownian-ratchet model of cargo movement.

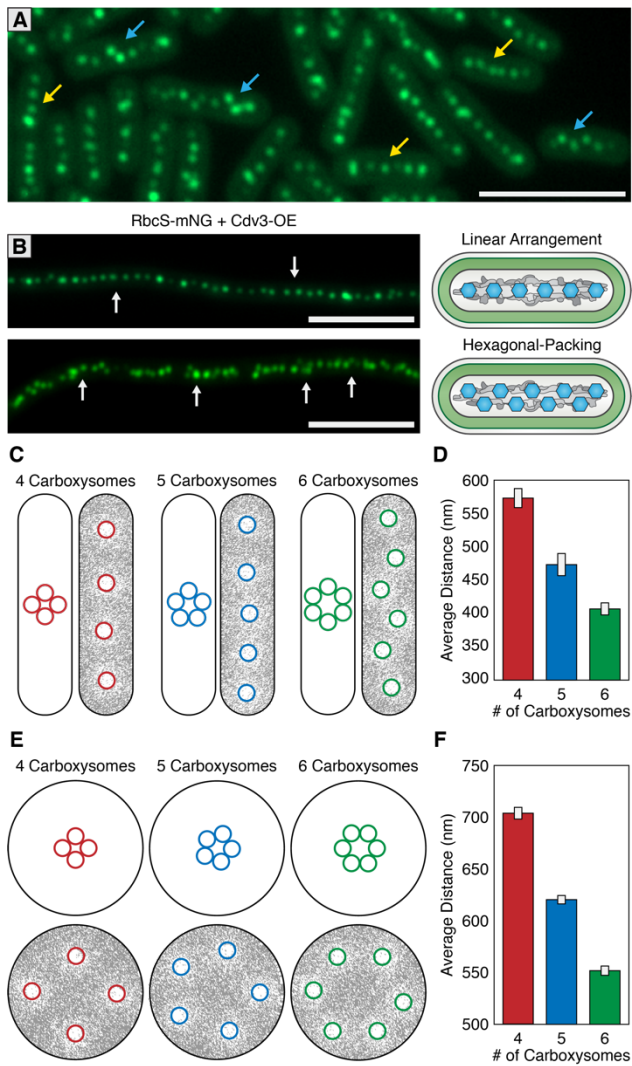


Figure 4.10: McdAB account for linear and hexagonal packing of carboxysomes

(A) In a field of *S. elongatus* cells, carboxysomes are found in either a linear (yellow arrow) or hexagonal (blue arrow) arrangement. Scale bar = 5 μm . **(B)** Linear or hexagonal arrangement of carboxysomes in filamentous cells (white arrows). Scale bar = 5 μm . **(C)** Reaction-diffusion simulations of 4, 5, or 6 carboxysomes on a rounded-rectangle surface. Positions of carboxysomes in representative simulations indicated at the start of the simulation (left) and after the simulation has reached steady state (right). Grey = McdA. White = Nucleoid. **(D)** Average distance between carboxysomes. **(E)** Reaction-diffusion simulations of 4, 5, or 6 carboxysomes upon a round surface. Grey = McdA. White = Nucleoid. **(F)** Average distance between carboxysomes. Error bars = standard deviation.

Carboxysomes are Hexagonally Arranged when Crowded on a Nucleoid

Carboxysomes are frequently described as being linearly arranged along the longitudinal axis of *S. elongatus*. In addition to linear distributions, we also routinely observed carboxysomes that were equidistant to each other, but no longer linearly arranged (Figure 4.10A). Instead, carboxysomes displayed a hexagonal packing phenomenon where the linear arrangement along the longitudinal axis looked kinked or displayed a zig-zag pattern. This arrangement was typically correlated with cells that had a high number of carboxysomes relative to the cell's length. However, it is difficult to ascertain if this different packing arrangement is due solely to carboxysome number, or any number of other factors that could be differentially regulated between distinct cells.

To better understand this hexagonal packing phenomenon, we examined carboxysome positioning in hyperelongated cells. We have previously shown that overexpression of the FtsZ regulatory protein Cdv3 results in division arrest and subsequent cell elongation up to 2 mm (Jordan et al., 2017; MacCready et al., 2017). In this strain, we observed both linear and hexagonal carboxysome packing (Figure 4.10B). Importantly, such hyperelongated *S. elongatus* cells are known to contain nucleoid clusters which are separated by intermittent gaps that physically separate the clusters from one another (Miyagishima et al., 2005). Consistent with this, carboxysomes in these hyperelongated cells always co-localized with a nucleoid cluster, as visualized by DAPI staining (Figure 4.11A), and are never observed in the gaps between clusters. By contrast, in a $\Delta mcdA$ or $\Delta mcdB$ background, when we induced hyperelongation by expressing Cdv3, carboxysomes were frequently observed in these gap regions (Figure 4.11BC). These results further support a model whereby McdA/B tether carboxysomes to the nucleoid.

In individual hyperelongated cells, we frequently observed carboxysomes both in linear and hexagonal-packing arrangements within the same cell but on different nucleoid clusters (Figure 4.11D). Because cells containing both linear and hexagonal packing arrangements share the same cytosol, it is unlikely that the carboxysome packing is regulated by a global change within a cell (such as a diffusible factor). Instead, we found once again that the hexagonal packing was typically observed when the number of carboxysomes were higher on a given nucleoid cluster. These results strengthen the hypothesis that

carboxysome arrangement may be a self-emergent property that is related to the density of carboxysomes on a given nucleoid surface area.

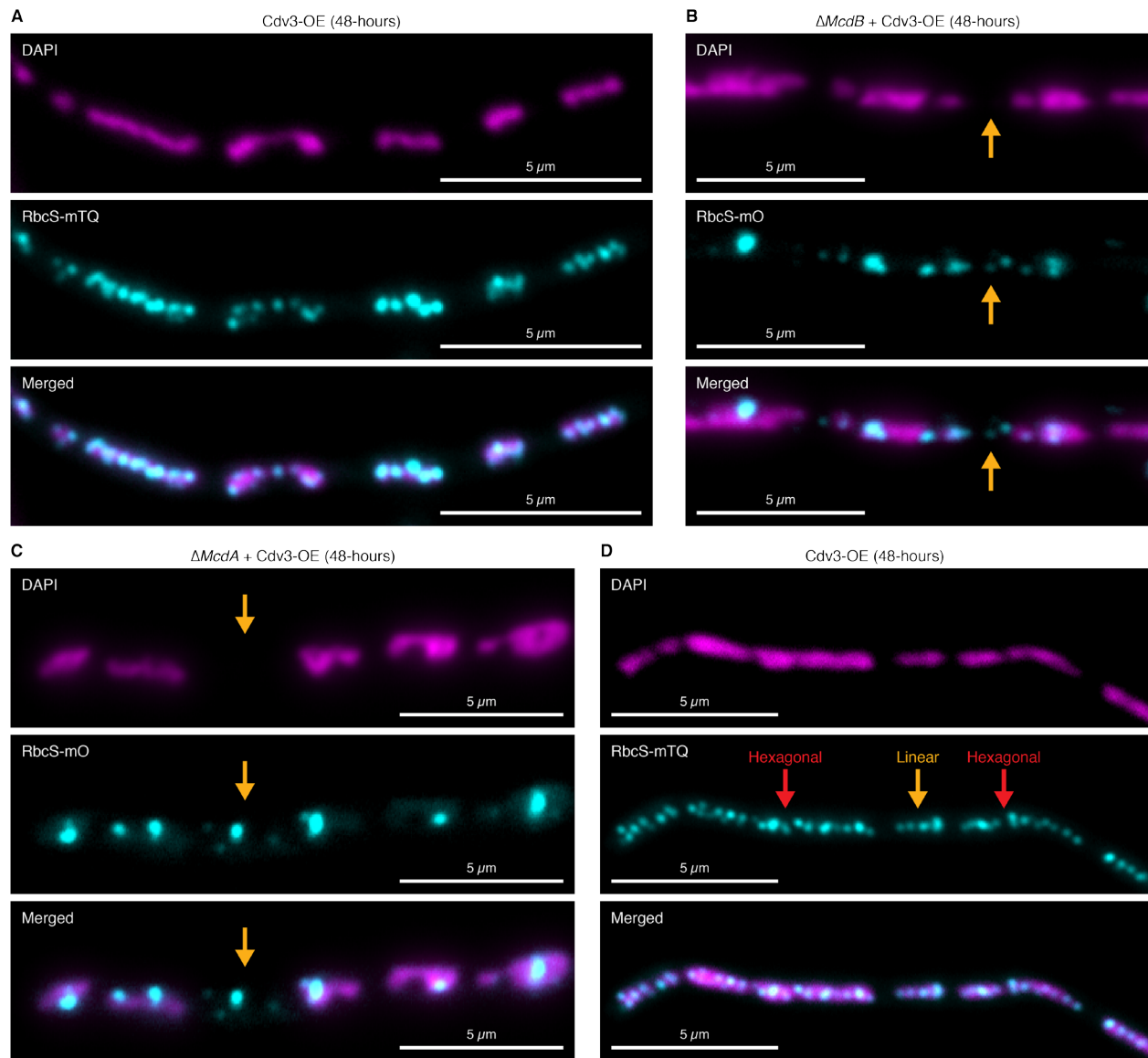


Figure 4.11: Carboxysomes fall between nucleoids in elongated cells lacking McdA or McdB
(A) Carboxysomes are confined to nucleoid “islands”. **(B)** Carboxysomes fall off nucleoids (orange arrow) in the absence of McdB. **(C)** Carboxysomes fall off nucleoids (orange arrow) in the absence of McdA. **(D)** Carboxysomes can display hexagonal-packing (red arrows) or linear arrangements (orange arrow) from nucleoid-to-nucleoid.

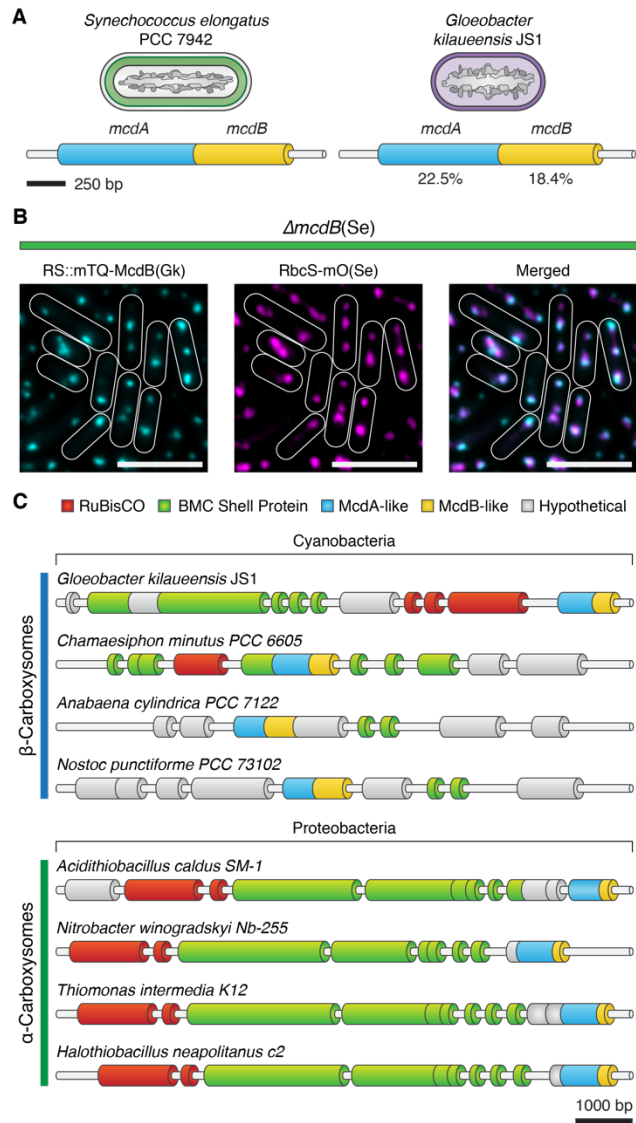


Figure 4.12: Evolutionary conservation of McdAB

(A) Cartoon illustration of McdAB operon structures in *S. elongatus* and *Gloeobacter kilauensis* JS1. (B) *Gloeobacter kilauensis* JS1 McdB is localized to *S. elongatus* carboxysomes (RbcS-mO). Scale bar = 5 μ m. (C) McdA/B-like sequences co-localize in the genome with predicted carboxysome components across diverse microbes.

The Brownian-ratchet Model is Sufficient to Explain Carboxysome Distributions

To assess if the Brownian-Ratchet model of carboxysome positioning could account for both carboxysome spacing and patterning (i.e. linear vs. hexagonal), we turned to an established *in silico* mathematical model that has successfully described several aspects of the Brownian-ratchet mechanism for ParA-mediated partitioning of plasmids (Hu et al., 2017). Since we have yet to determine which biochemical parameters of the Mcd system differ from that of the Par system, in this treatment, we simply increased the number of cargo copies on the nucleoid matrix while keeping all other biochemical parameters as previously described so as to determine if increasing cargo copy number is enough to convert linear positioning into hexagonal packing. We programmed the geometry of the nucleoid surface area (2.5 μm by 0.6 μm rounded rectangle) and carboxysome cargo (175 nm) based off of previously measured values of wildtype *S. elongatus* (Rae et al., 2012; Murata et al., 2016). All simulations are initiated with tightly clustered carboxysomes near the center of the nucleoid (Figure 4.10C; left images), but carboxysomes are allowed to travel towards the highest gradient of McdA using the previously-established parameter values.

With the Brownian-Ratchet model, five or less carboxysomes will linearly distribute on a rectangular surface representative of *S. elongatus*' nucleoid. The mathematical model confirms that with increasing cargo number a linear arrangement is maintained, but with tighter spacing (Figure 4.10CD). When six or more cargos occupy the same simulated nucleoid, carboxysomes arrange even closer together yet display hexagonal packing, reminiscent of the *in vivo* distributions (Figure 4.10ABCD). As many other cyanobacterial species exhibit spherical morphology, including the model *Synechocystis sp. PCC 6803*, we also examined the predicted distribution of carboxysomes upon a 1.7 μm circular nucleoid (Figure 4.10EF). We suggest that the linear arrangement of carboxysomes in rod-shaped cells is largely a byproduct of nucleoid geometry, and thus, cell morphology. In support of this proposition, many spherical (Kerfeld et al., 2005) and filamentous (Montgomery, 2015) cyanobacterial cells also show a hexagonal carboxysome arrangement. Furthermore, *S. elongatus* cells grown under environmental conditions that increase carboxysome synthesis also dominantly display hexagonal packing (e.g. Sun et al., 2016).

The McdAB System is Evolutionarily Wide-spread in Cyanobacteria

Homologs of ParA-type ATPases have been described within extended carboxysome operons of cyanobacteria (Axen et al., 2014). Therefore, we examined other distant cyanobacterial species for possible McdAB homologs. One such case is the primitive thylakoid-less cyanobacterium *Gloeobacter kilaueensis* JS1, which drives expression of an *mcdA*-like gene from the *rbcL* promoter. Interestingly, upon further examination, we found a small coding sequence following this *mcdA*-like gene with weak similarity to *mcdB*. BlastP determined that *S. elongatus* McdA had 22.5% pairwise sequence identity to the *G. kilaueensis* JS1 McdA-like protein, while *S. elongatus* McdB had only 18.4% pairwise identity to the McdB-like protein (Figure 4.12A). To investigate the possibility that the McdB-like protein of *G. kilaueensis* JS1 functions similarly to *S. elongatus* McdB, we expressed a fluorescent fusion of the *G. kilaueensis* JS1 *mcdB*-like gene, mTQ-McdB(Gk), in our *S. elongatus* $\Delta mcdB$ strain. Despite the low primary sequence identity of McdB(Gk), we found that mTQ-McdB(Gk) colocalized with RbcS-mO, indicating that mTQ-McdB(Gk) can interact with *S. elongatus* carboxysomes (Figure 4.12B). These results suggest that carboxysome positioning by McdA and McdB may be widespread among cyanobacteria.

Discussion

McdA is Not Cytoskeletal and Utilizes the Nucleoid to Position Carboxysomes

Carboxysomes are essential components of the photosynthetic metabolism of cyanobacteria, yet the mechanism underlying their strategic positioning within the cells have remained elusive. Prior work in *S. elongatus* led to a widely-adopted hypothesis that McdA may form cytoskeletal-like structures that connect adjacent carboxysomes and coordinate their distribution (Savage et al., 2010; Murat et al., 2010). However, we did not find evidence for filament formation in our *in vivo* imaging studies or *in vitro* assays. Instead, McdA appears to homogeneously bind non-specific DNA in suspension or in a carpeted flowcell (Figure 4.1FGH), and McdA also co-localizes with the nucleoid in living cells (Figure 4.1E). The cytoskeletal hypothesis partially rested upon observations that disruption of MreB also disrupts carboxysome positioning (Savage et al., 2010), although in light of our results we suggest this phenotype may be due to gross alteration in cell morphology and nucleoid topology that are known to accompany $\Delta mreB$ mutations in cyanobacteria (Hu et al., 2007). Overall, our data strongly suggests that carboxysomes are not positioned by an independent bacterial cytoskeletal system involving McdA and MreB, but are instead self-organized along the surface of the cyanobacterial nucleoid. Our work here provides multiple lines of evidence to suggest that this self-organization is dependent upon a carboxysome's capacity to locally detect gradients in nucleoid-bound McdA, and to move towards the direction of the highest concentration.

A Unique System for Distributing Protein-based Bacterial Organelles

Our hypothesis of carboxysome positioning is both informed by the ParA-based mechanisms used to segregate low-copy number plasmids, and provides a novel platform to study the dynamics of ParA-like proteins. Low-copy plasmids often contain DNA regions (e.g. *parS*) that bind ParB, which drives the directed and persistent movement of plasmids towards increased concentrations of ParA on the nucleoid (Vecchiarelli et al., 2010; Le Gall et al., 2016). In this way, it is proposed that ParA can provide a positional

cue allowing plasmid cargo to “surf” along the larger bacterial chromosome without a separate cytoskeletal system (Vecchiarelli et al., 2012).

Beyond the fact that McdA appears to be involved in segregating a large protein complex (carboxysomes), there are other key distinctions between this cyanobacterial protein and classically-characterized ParA family members. Importantly, the specific activity of McdA ATPase activity (~50/min; Figure 4.3G) is roughly two-orders of magnitude greater than that of other well-studied ParA systems (Vecchiarelli et al., 2010; Ah-Seng et al., 2009). Likewise, while we were unable to identify a ParB homolog involved in positioning carboxysomes, we instead identified a small novel protein, McdB, that appeared to function analogously. Indeed, although McdB and ParB share no similarity, we found that McdB interacted with McdA (Figure 4.3F), stimulated its ATPase activity (Figure 4.3G), and was responsible for emergent dynamics of McdA along the nucleoid (Figure 4.3D). Moreover, similar to ParB loading onto and around the *parS* centromere-like sites of plasmids, we found evidence that McdB was recruited to carboxysomes (Figure 4.3J), likely through interactions with both major and minor shell components (Figure 4.4C). We propose that McdB is therefore acting to interface carboxysomes with nucleoid-bound McdA, processively pulling this protein cargo towards whichever local direction has the highest McdA concentrations (Figure 4.9D).

It is curious that McdB is able to associate with a number of different shell proteins in our B2H assay. This observation suggests that the interactions may not be sequence-specific, but could be largely based on electrostatic or hydrophobic interactions. Indeed, evolutionarily distant hexameric shell proteins of the bacterial microcompartment (BMC-H) family share a number of similarities in structural features and key residues at hexamer interfaces that are largely conserved (Cai et al., 2015; Sommer et al., 2017; Young et al., 2017). Further support of this hypothesis can be drawn from our observation that *G. kilaueensis* JS1 McdB was still able to associate with *S. elongatus* carboxysomes despite low sequence similarity between *G. kilaueensis* JS1 McdB and *S. elongatus* McdB (Figure 4.12B). This suggests a common mechanism for McdB interaction with carboxysomes over evolutionary time. We do note that our B2H analysis may indicate that McdB may have a higher affinity to some shell proteins, including CcmK3 (Figure 4.4C). This could explain why carboxysomes cluster in $\Delta ccmK3-4$ mutants (Rae et al., 2012), as this may reduce the amount

of McdB recruited to the carboxysome surface. Another possibility is that McdB could directly integrate within the shell of mature carboxysomes, although we consider the experimental evidence for this to be less robust. Indeed, our $\Delta mcdB$ strain did not possess a high CO₂-requiring phenotype and McdB has not been identified in previously-published carboxysome purification studies (Faulkner et al., 2017), both of which suggest that McdB is not an integral shell component. It will be important for future studies to biochemically characterize both McdA and McdB to determine the mechanistic commonalities and variations for ParA-mediated positioning of genetic versus protein-based cargos as well as to identify how McdB associates with carboxysomes.

McdA Oscillations are a Consequence of Multiple Carboxysomes Sharing the Same Nucleoid in a Rod-shaped Cell

One surprising result of our study was that we observed that both McdB and carboxysomes themselves were required for the emergence of McdA oscillations along the nucleoid (Figure 4.4E). Furthermore, a critical threshold number of carboxysomes were required to be localized on the same nucleoid in order for McdA oscillation to ensue (generally >3; Figure 4.9F). This suggests that it is not sufficient for McdB to be merely present, it must be specifically localized and/or concentrated to promote the oscillation of McdA. Furthermore, we note that McdA oscillation per se is not required to segregate one carboxysome from another. In cells where we induced the formation of only 2 carboxysomes, these carboxysomes reliably separated from one another despite the fact that no McdA oscillations were present (Figure 4.9D). Furthermore, our Brownian-Ratchet simulations were able to recapitulate the separation between carboxysomes *in silico* without any requirement for an oscillating pool of McdA (Figure 4.10CDEF).

These results call the value of McdA oscillations into question, as well as raise other issues related to how McdA oscillations emerge. One possibility is that McdA oscillation itself might be a byproduct of the motion of multiple carboxysomes removing McdA along the nucleoid. Indeed, the dynamics of carboxysome motion are more complex when viewed at rapid time scales. During McdA oscillation, we observed that some carboxysomes at the wave front paused, and in some cases, were observed to get sucked into the approaching wave. While in the wave, carboxysome diffusion was suppressed. As the wave passed,

carboxysome diffusion was anisotropic, drifting in the direction of the wave. An alternative hypothesis is that the global dynamics of McdA oscillation are dependent upon a balanced level of activities between McdA and McdB. In this case, recruitment of soluble McdB to a defined location (the carboxysome) may concurrently act to remove it from the bulk cytosol, reducing the concentration that McdA perceives when not near a carboxysome. There is precedence for this interpretation in the ParA-like family of proteins, including the oscillatory behaviors of MinD and MinE. MinD binds to the plasma membrane when bound to ATP and exhibits an emergent pole-to-pole localization that is driven by the ATPase-stimulating activities of the partner protein MinE (Lutkenhaus, 2007). The ratio of these activities is important for their higher-order behaviors, and if they become severely unbalanced oscillatory patterns can collapse (Fange et al., 2006; Loose et al., 2008; Loose et al., 2011; Zieske et al., 2014; MacCready et al., 2017).

It is intriguing to speculate whether McdA would oscillate in cyanobacteria displaying different morphologies, such as the spherical *Synechocystis sp.* 6803 or the filamentous *Fremyella diplosiphon*. While carboxysomes in these organisms are equidistantly spaced, they display a packing more reminiscent of the hexagonal arrangement rather than a linear distribution (Kerfeld et al., 2005; Montgomery, 2015). Our modeling suggests that this could be a natural outcome of the McdAB system operating on a nucleoid topology that is more spherical, rather than rod-shaped. While McdA oscillation could still be possible, it is unclear what patterns would be expected. Further analysis of McdAB dynamics in other cyanobacteria is required to elucidate the effects of nucleoid morphology on McdA pattern formation.

A Brownian-Ratchet Mechanism Ensures Carboxysome Distributions Required for both Inheritance and Homeostasis

The linear distribution of carboxysomes along the cell length resembles the ParA-mediated distribution of low-copy plasmids (1–3 copies/cell). For plasmids, the linear distribution ensures that at least one copy of the plasmid is inherited after division. But carboxysome copy number can reach as high as 10–20 copies. Under these crowded conditions, carboxysomes still separate from each other, but are often no longer

linearly arranged. Instead, a hexagonal packing phenomenon is observed where carboxysomes are arranged in a zig-zag pattern. Using a mathematical model of the Brownian-ratchet mechanism for ParA-mediated plasmid partitioning (Hu et al., 2015, Hu et al. 2017) we find hexagonal packing is naturally explained by the same model as a linear arrangement when the nucleoid matrix is overcrowded with cargos. Consistent with this finding, under high light conditions, hexagonal packing of carboxysomes occurs in *S. elongatus* at a much higher frequency when carboxysome production increases to compensate for increased light capture (Sun et al., 2016).

Given the equidistant positioning of carboxysomes even at high number, we propose that in addition to ensuring inheritance, McdA and McdB ensure organelle homeostasis. In the absence of positioning, an asymmetric distribution of carboxysomes after cell division would cause a significant growth disadvantage to cells with fewer carboxysomes, particularly in low CO₂ environments. Biogenesis of a single carboxysome requires the ordered assembly of thousands of shell proteins and enzymes (Rae et al., 2012; Cameron et al., 2013). Therefore, as is the case for DNA molecules, uniform positioning ensures that each daughter cell inherits carboxysomes after cell division, but also in the right number. We find here that McdA and McdB position approximately two carboxysomes per micron length of the cell to ensure equal inheritance and maintain homeostasis (Figure 4.2C).

McdA and McdB may Facilitate Biogenesis and Regulate Carboxysome Size

Our analysis provides a number of lines of evidence to suggest that McdA and McdB activities can also influence the ultrastructure of carboxysomes in *S. elongatus*. Cyanobacterial strains that are genetic knockouts of *mcdB* display carboxysomes that are significantly enlarged (Figure 4.8AD). Furthermore, overexpression of McdB resulted in massive carboxysome globules that sometimes spanned the entire short axis of the cell (Figure 4.8AG), while overexpression of McdA resulted in irregularly-shaped carboxysomes with rounded edges (Figure 4.8AF). While we cannot rule out the possibility of indirect effects, it is intriguing to speculate that McdA and McdB may act to directly regulate the size or shape of microcompartments as they are formed. In *S. elongatus*, it has been suggested that new carboxysomes

bud off from existing carboxysomes (Cameron et al., 2013; Chen et al., 2013). Our model for carboxysome positioning requires that the interaction of McdB with McdA provide a pulling force exerted on the carboxysome shell that acts to processively move the protein compartment up an McdA gradient. It is therefore possible that these same molecular forces act during the synthesis of a new carboxysome. The relative ratio between McdA and McdB activities may play a role in the differences in carboxysome sizes observed under different environmental conditions or within different species. Future research will be required to confirm such a model.

The McdAB System in other Organisms

Carboxysomes exist in two distinct forms, α & β , depending on the form of RuBisCO they encapsulate. While both are found in cyanobacteria, α -carboxysomes also exist in many actinobacteria and proteobacteria. In these organisms, the vast majority of carboxysome-related genes tend to form loci with their respective encapsulated enzymes (Axen et al., 2014). We find that *mcdA/B*-like sequences frequently fall in regions near α - & β -carboxysome operons (Figure 4.12C). We propose that the *mcdA/B*-like sequences near the α -carboxysome operon could also function to equidistantly space α -carboxysomes to ensure equal inheritance following cell division. Further study is now needed to determine how widespread the McdAB system is across evolutionary space. Indeed, protein microcompartments that catalyze a range of biochemical activities are widespread in bacteria (Kerfeld et al., 2015). More broadly, these findings aid in understanding the spatial organization of other protein-based mesoscale assemblies that encode ParA family members and are associated with diverse biological processes, including secretion (Perez-Cheeks et al., 2012; Vollmer et al., 2002), conjugation (Atmakuri et al., 2007), chemotaxis (Thompson et al., 2006; Ringgaard et al., 2011; Alvarado et al., 2017), and cell motility (Youderian et al., 2003; Kusumoto et al., 2008).

Methods

Construct Designs

All constructs in this study were generated using Gibson Assembly (Gibson et. al., 2009) from synthesized dsDNA and verified by sequencing. Constructs contained flanking DNA that ranged from 500 to 1500 bp in length upstream and downstream of the targeted insertion site to promote homologous recombination into target genomic loci (Clerico et al., 2007). Native fluorescent fusions: For native McdA fluorescent fusions, the fluorescent protein mNeonGreen (mNG) was attached to either the 5' or 3' region of the native *mcdA* coding sequence, separated by a GSGSGS linker. Since the upstream coding sequence next to *mcdA* is essential and presumably expressed from the same region of DNA as *mcdA*, the kanamycin resistance cassette was inserted upstream of the *mcdA* promoter to prevent operon disruption, and a duplicate *mcdA* promoter was inserted upstream of kanamycin to drive expression of the essential coding sequence. For the native McdB-mNG construct, mNG was inserted at the 3' end of the *mcdB* coding sequence, separated by a GSGSGS linker, followed by the kanamycin resistance cassette. Alternatively, for the native mNG-McdB construct, the *mcdB* sequence was codon optimized to prevent recombination at this site and mNG was inserted at the 5' end. The kanamycin resistance cassette was inserted downstream. To visualize carboxysomes, a second copy of the *rbcS* promoter and gene, attached at the 3' end with either the fluorescent protein mTurquoise2 (mTQ) or mOrange2 (mO) and separated with a GSGSGS linker, were inserted into neutral site 1. Single Deletions: Deletion constructs of plasmid *parB*, *hyp2*, and *mcdB* were created by replacing the respective coding sequences with a spectinomycin resistance cassette. Likewise, deletion of the carboxysome operon was performed by replacing the entire coding sequence, starting with the *ccmK2* promoter and ending with *ccmO*, with a spectinomycin resistance cassette. Native fluorescent fusions with deletion or overexpression: For fluorescent and deletion lines, single plasmids were created that contained 5' fluorescently labeled *mcdA* (mNG) or *mcdB* (mTQ), separated by a GSGSGS linker, that simultaneously deleted *mcdA* or *mcdB* and integrated the *rbcS::rbcS-mO* fluorescent reporter upstream of the *mcdB* coding sequence (Figure 4.6ABC). In these lines, the kanamycin resistance cassette was inserted

upstream similarly to our native mNG-McdA constructs (Figure 4.6ABC). For our $\Delta mcdAB$ strain, a codon optimized *rbcS-mO* sequence was inserted to replace the entire *mcdA* operon while inserting the kanamycin resistance cassette upstream. Overexpression of mNG-McdA or mTQ-McdB were performed by insertion into neutral site 2 and expressed using a P_{trc} promoter with an attached 5' theophylline riboswitch (Nakahira et. al., 2013). Carboxysome induction systems: To generate a tunable carboxysome operon, we replaced the native *ccmK2* promoter with a P_{trc} promoter in the absence of the *lacI* repressor and inserted a theophylline riboswitch (Nakahira et. al., 2013) on the 5' end of *ccmK2*. Alternatively, we also replaced the *ccmK2* promoter with a P_{trc} promoter without a 5' riboswitch on *ccmK2* and inserted the *lacI* repressor upstream. In both constructs, the spectinomycin resistance cassette was inserted upstream of the inserted promoters.

Culture Conditions and Transformations

All *S. elongatus* cultures were grown in 125 mL baffled flasks (Corning) containing 50 ml BG-11 medium (SIGMA) buffered with 1 g L⁻¹ HEPES to pH 8.3. Flasks were cultured in a Multitron II (atrbitech.com) incubation system with settings: 80 $\mu\text{mol m}^{-2} \text{s}^{-1}$ light intensity, 32°C, 2% CO₂, shaking at 130 RPM. Transformation of plasmids was performed in *E. coli* DH5 α chemically competent cells (Invitrogen). All *S. elongatus* transformations were performed as previously described (Clerico et. al., 2007). Cells were plated on BG-11 agar with either 12.5 mg ml⁻¹ kanamycin or 25 mg ml⁻¹ spectinomycin. Single colonies were picked into 96-well plates containing 300 μl of BG-11 with identical antibiotic concentrations. Cultures were verified for complete insertion via PCR and removed from antibiotic pressure.

Bacterial-two-hybrid Analysis

N- and C-terminal T18 and T25 fusions of McdA, McdB and shell proteins CcmK2, CcmK3, CcmK4, CcmL, CcmO and CcmP were constructed using plasmid pKT25, pKNT25, pUT18C and pUT18, sequence-verified and co-transformed into *E. coli* BTH101 in all pairwise combinations (Karimova et al. 1998). Several

colonies of T18/T25 cotransformants were isolated and grown in LB medium with 100 $\mu\text{g/ml}$ ampicillin, 50 $\mu\text{g/ml}$ kanamycin and 0.5 mM IPTG overnight at 30°C with 225 rpm shaking. Due to the self-assembling nature of carboxysome shell proteins, overnight IPTG induction for cotransformants bearing T18/T25 shell protein fusions was carried out at 0.1 mM IPTG. Overnight cultures were spotted on indicator MacConkey plates supplemented with 100 $\mu\text{g/ml}$ ampicillin, 50 $\mu\text{g/ml}$ kanamycin and 0.5 mM IPTG. Plates were incubated at 30°C up to 48 hours before imaging.

Induction Strains

Overproduction of mNG-McdA and mTQ-McdB were accomplished by inducing strains with 1500 μM theophylline for 48 hours. For carboxysome induction under the riboswitch, strains were incubated in 400 μM theophylline (1 carboxysome) or 600 μM theophylline (2 carboxysomes) for 24-hours prior to imaging. Alternatively, for carboxysome induction under the Ptrc promoter and LacI repressor, cells were incubated with 1000 μM IPTG for 16 hours prior to imaging.

Fluorescence Microscopy

All live-cell microscopy was performed using exponentially growing cells. Two mL of culture was spun down at 5000xg for 30 s, resuspended in 200 μl of BG-11 and 2 μl transferred to a square 1.5% agarose + BG-11 pad on glass slides. All images were captured using a Zeiss Axio Observer A1 microscope (100x, 1.46NA) with an Axiocam 503 mono camera except the carboxysome induction experiments. Carboxysome induction experiments were performed using a Nikon Ti2-E motorized inverted microscope with LED-based light sources (100x, 1.45NA) with a Photometrics Prime 95B Back-illuminated sCMOS Camera. Image analysis was performed using Fiji v 1.0.

Transmission Electron Microscopy

Cultures were grown to $OD_{750} = 0.7$ in BG-11. Cells were pelleted and fixed overnight at 4°C with 2.5% formaldehyde/2.5% glutaraldehyde in 0.1 M sodium cacodylate buffer (pH 7.4), suspended into a 2% agarose bead and cut into ~1 mm cubes. Following three washes with 0.1 M sodium cacodylate buffer, cells were suspended in 1% osmium tetroxide/1.5% potassium ferrocyanide and incubated overnight at 4°C. After incubation, cells were washed with HPLC-quality H₂O until clear. Cells were then suspended in 1% uranyl acetate and microwaved for 2 min using a MS-9000 Laboratory Microwave Oven (Electron Microscopy Science), decanted, and washed until clear. Cells were dehydrated in increasing acetone series (microwave 2 min) and then embedded in Spurr's resin (25% increments for 10 min each at 25°C). A final overnight incubation at room temperature in Spurr's resin was done, then cells were embedded in blocks which were polymerized by incubation at 60°C for three days. Thin sections of approximately 50 nm were obtained using an MYX ultramicrotome (RMC Products), post-stained with 1% uranyl acetate and Reynolds lead citrate, and visualized on a JEM 100CX II transmission electron microscope (JEOL) equipped with an Orius SC200-830 CCD camera (Gatan).

MicrobeJ Quantification

Cultures were grown to $OD_{750} = 0.7$ in BG-11. Multiple individual images of the RbcS-mO fluorescent reporter and chlorophyll autofluorescence were obtained for each strain and analyzed using MicrobeJ 5.11n. Cell perimeter detection was performed using the rod-shaped descriptor and default thresholding algorithm. Carboxysome detection was performed using the foci function with a tolerance of 15 and Z-score of 50. Associations, shape descriptors, profiles and distances were recorded for each strain. Heatmaps were automatically generated with counts, contour and a spot size of 5. Mean foci area and standard deviation for each maxima was automatically calculated.

McdA-GFP-His Expression and Purification

The gene sequence, *mcdA-GFP-his₆*, was codon optimized for *E. coli* and synthesized by Genscript. The fragment was inserted into the NcoI/BamHI cloning sites of the expression vector pET15b to create the pAV30 plasmid. pAV30 was transformed into BL21 (AI) cells (Invitrogen) and a 100 mL overnight culture containing 100 µg/mL of carbenicillin was grown at 20°C with shaking at 225 rpm. LB supplemented with 100 µg/mL of carbenicillin and a drop of Antifoam Emulsion (1 L per 2.5 L Fernbach flask × 4) was pre-warmed to 37°C and inoculated with 10 mL of overnight culture per flask. The cells were grown at 37°C with shaking at 225 rpm to an O.D. of 0.4. The flasks were then plunged in an ice bath until the temperature of the culture dropped to 16°C. Protein expression was then induced at O.D. 0.6 by the addition of 10 mL of a 0.1 M IPTG/20% Arabinose solution to each flask. Cells were then grown overnight at 16°C with shaking at 225 rpm (~15 h induction). The cells were transferred to 1 L Beckmann bags and bottles, which were spun in a JLA 8.1 rotor at 4,500 rpm for 1 h. The supernatant was poured out, and the cell pellets were frozen in the bags with liquid nitrogen and stored at -80°C. Frozen cell pellets were combined in a beaker with 10 mL of cold Lysis Buffer (50 mM HEPES-KOH (pH 7.6), 1 M KCl, 10% Glycerol, 20 mM Imidazole (pH 7.4), 2 mM β-mercaptoethanol) per gram of cell pellet (~150 mL total), three Protease Inhibitor Mixture Tablets (Sigma) and 0.1 mg/mL lysozyme (Sigma). A homogenizer was used to ensure that the cell pellets were thoroughly dispersed, and two passes through a Microfluidizer lysed the cells. The lysate was cleared with a 30 min ultracentrifugation at 35,000 rpm and 4°C using a 45Ti rotor. The lysate was then passed through a 0.45 µm syringe filter. Using a peristaltic pump, the cleared lysate (~200 mL) was loaded at a flow rate of 2 mL/min onto a 5 mL HisTRAP HP cassette (GE) and equilibrated with Lysis Buffer. The protein was eluted with a 20 mM to 1 M imidazole gradient (total volume = 60 mL). Peak protein fractions were pooled and concentrated using an Amicon Ultra Centrifugal Device (10 KD MWCO). The sample was passed through a 26/10 salt-exchange column equilibrated in Q-Buffer (50 mM HEPES-KOH (pH 7.5), 200 mM KCl, 10% Glycerol, 0.1 mM EDTA, 2 mM DTT). The sample was then immediately loaded onto a 1 mL Mono Q 5/50 anion exchange column (GE) equilibrated in Q-Buffer. The protein was eluted with a 200 mM to 1 M KCl gradient. Peak fractions were pooled and concentrated to a no more than 100 µM. The sample

was then separated over a 10/300GL Superdex200 gel-filtration column equilibrated in Q Buffer (but with 600 mM KCl). Peak fractions were pooled, concentrated to no more than 100 μ M, frozen with liquid nitrogen, and stored at -80°C .

His-MBP-McdA Expression and Purification

Due to insolubility issues encountered when expressing McdA-His, a construct was designed where a His-MBP-tag was encoded upstream of a Tobacco Etch Virus (TEV) cleavage site and fused to the N-terminus of the *mcdA* gene in a pET15b expression backbone to create pAH2 plasmid. pAH2 was transformed into BL21(AI) cells and protein expression was carried out by growing transformants at 37°C and 225 rpm until an OD_{600} of 0.6-0.8 was reached. Following an ice bath plunge to lower the culture temperature to 15°C , protein expression was induced with the addition of 1 mM IPTG and 0.2 % arabinose. Induction was allowed to continue overnight at 15°C . The cells were pelleted, flash frozen with liquid nitrogen, and stored at -80°C . Cells were then lysed in Buffer A (50 mM HEPES pH 7.6, 50 mM KCl, 10% glycerol, 20 mM imidazole pH 7.4, 5 mM BME, 50 $\mu\text{g}/\text{ml}$ lysozyme, 1.25 kU benzonase, 2 Protease Inhibitor Cocktail tablets) using a probe sonicator with 15s on, 15s off pulsation for 8 min. Cell debris were removed by centrifugation at 14,000 rpm for 40 min in a Fiberlite™ F15-8 x 50cy Fixed Angle Rotor (ThermoFisher Scientific) and the resulting lysate was filtered through a 0.45 μm syringe filter prior to being loaded onto a 5 ml His-Trap Ni-NTA (GE). The protein was eluted with a 20 mM – 1 M imidazole gradient. Peak fractions were pooled and concentrated using Amicon 30KD MWCO filter and separated on a MonoQ 5/50 GL anion exchange column (GE). Peak fractions were further separated by gel filtration on a Superdex200 HiLoad 16/600PG column (GE) pre-equilibrated with 50 mM HEPES pH 7.6, 50 mM KCl, 10% glycerol, 5mM DTT. Peak fractions were concentrated to no higher than 100 μM and frozen aliquots were kept at -80°C .

ATPase Assay

ATPase assays were performed in a buffer containing 50 mM HEPES (pH 7.6), 10 mM MgCl₂, 100 mM KCl, 0.1 mg/ml BSA, 2 mM DTT, and 0.1 mg/ml sonicated salmon sperm DNA (when present). Unlabeled ATP was spiked with [γ -³²P]-ATP and purified from contaminating ³²P_i prior to use with a 1 ml gel filtration (P-2 fine resin, Bio-Rad) column. The radiolabeled ATP mix was added to reactions at 1 mM. Reactions were assembled on ice at the protein concentrations indicated, with the McdA variant being added last. The 20 μ l reactions were incubated for 1 hr at 30°C and immediately quenched by adding 10 μ l of a 1% SDS, 20 mM EDTA solution. Two microliters of the quenched reactions were spotted and analyzed by thin-layer chromatography as previously described (Fung et al., 2001).

DNA Binding Assay

Electrophoretic mobility shift assays were performed in a final reaction volume of 10 μ l in a buffer containing 50 mM HEPES (pH 7.6), 5 mM MgCl₂, and 100 mM KCl. We used pUC19 plasmid (2.8 kb) as the DNA substrate at a final concentration of 10 nM. At the concentrations indicated, McdA-GFP-His was incubated for 10 minutes at 23°C with ADP, ATP or ATP γ S (1 mM). Reactions were then mixed with 1 μ l 80% glycerol, run on 1% agarose gel in 1X TAE at 110V for 1.5 h and stained with ethidium bromide.

TIRFM of McdA-GFP Binding to a DNA-carpeted Flowcell

Quartz flowcell construction and DNA-carpeting of the flowcell surface were performed as previously described (Vecchiarelli et al., 2015). For the imaging of McdA-GFP-His binding to the DNA carpet, prism-type TIRFM was performed using an Eclipse TE2000E microscope (Nikon) with a PlanApo 60 \times NA = 1.40 oil-immersed objective and magnifier setting at 1.5 \times . Movies were acquired using an Andor DU-897E camera (Andor Technology) with integrated shutter. The camera settings were digitizer, 3 MHz (14-bit gray scale); preamplifier gain, 5.2; vertical shift speed, 2 MHz; vertical clock range: normal, electron-multiplying

gain 40, EM CCD temperature set at -98°C , baseline clamp ON, exposure time 100 ms, frame rate 0.5 Hz. The baseline of ~ 100 camera units was subtracted from the intensity data. The excitation for McdA-GFP-His was provided by 488-nm diode-pumped solid-state (Sapphire, Coherent) laser. Total internal reflection fluorescence illumination had a Gaussian shape in the field of view with measured horizontal and vertical half maximum widths of $\sim 65\ \mu\text{m} \times 172\ \mu\text{m}$ at 488 nm. Intensity data for the DNA carpet-bound populations of McdA-GFP were taken from the middle of the illumination profile. The laser power of 488-nm illumination was $15\ \mu\text{W}$. Metamorph 7 software (Molecular Devices) was used for camera control and image acquisition. ImageJ was used for analysis. The display brightness and contrast were set to the same levels for all TIRFM movies. ImageJ was used for conversion of Metamorph movies (.stk) into .avi format and Adobe Premiere was used for added text. Movie accelerations are indicated in the movie and figure legends.

McdA-GFP ($0.5\ \mu\text{M}$) was preincubated in McdA Buffer [50 mM Hepes (pH 7.6), 100 mM KCl, 10% (vol/vol) glycerol, 5 mM MgCl_2 , 2 mM DTT, 0.1 mg/mL α -casein, 0.6 mg/mL ascorbic acid] with 1 mM of the indicated nucleotide (or no nucleotide). The sample was incubated for 15 minutes in a 1 ml syringe connected to one of the two inlets of a Y-shaped flowcell. The sample was infused onto the DNA carpet at a rate of $20\ \mu\text{L}/\text{min}$. The fluorescence intensity of McdA-GFP that bound the DNA carpet was measured over time. At $t = 3$ minutes, flow from the sample inlet was stopped and immediately switched to the second inlet that was connected to a wash buffer (McdA Buffer without McdA-GFP or nucleotide). Wash buffer was flowed at a rate of $20\ \mu\text{L}/\text{min}$, and the decrease in fluorescence intensity was monitored over time. The two-inlet flowcell had a Y-patterned configuration and imaging took place at the point of flow convergence to minimize the effect of protein rebinding to the DNA carpet during dissociation when flow was switched to the wash buffer.

Theoretical Model and Computational Method

We find that McdA, McdB, and the carboxysome cargo show *in vivo* dynamics strikingly similar to that found for ParA-mediated DNA partition systems. Therefore, we leveraged our established Brownian ratchet model

of ParA/ParB-mediated partition (Hu et al., 2015; Hu et al., 2017) to theoretically interrogate the carboxysome positioning process in cyanobacteria.

Briefly, the model describes the mechanochemical interplay between nucleoid-bound McdA and carboxysome-bound McdB. McdA and McdB in the current model fulfil exactly the same roles of ParA and ParB as in the low-copy plasmid partition case, respectively. While carboxysome alone diffuses randomly, its motility can be greatly modulated when carboxysome-bound McdB interacts with nucleoid-bound McdA. Specifically, carboxysome-bound McdB stimulates the ATPase activity of nucleoid-bound McdA, which triggers the dissociation of McdA from the nucleoid substrate surface. The slow rate of dissociated McdA resetting its DNA-binding capability generates an McdA-depleted zone behind the moving cargo. The resulting asymmetric McdA distribution perpetuates the directed movement of the carboxysome cargo. Transient tethering arising from the McdA-McdB contacts collectively drives forward movement of the cargo and also quenches diffusive motion in orthogonal directions. This way, McdA/McdB interaction – when at proper mechanochemical coupling – drives directed and persistent movement of carboxysomes (Hu et al., 2015; Hu et al., 2017).

The model treats carboxysomes as circular disks that move on the nucleoid surface, which is modeled as a 2D simulation domain. The simulation domain is bounded by the reflective boundary condition. To study the effects of nucleoid geometry on carboxysome positioning, we constructed the simulation domains to mimic I.) a circular nucleoid and II.) a more elongated rounded rectangle nucleoid, which consists of a rectangle with two hemi-spherical caps at the ends of its long axis.

We simulated the model by the same kinetic Monte Carlo technique as in (Hu et al., 2015; Hu et al., 2017), which describes the coupling between the stochastic reaction-diffusion processes involving McdA and McdB, and their mechanochemical interplay. Specifically, we investigated the effects of carboxysome number and nucleoid geometry on carboxysome positioning. In each case defined by different carboxysome number and nucleoid geometry, the simulation starts with the initial positions of the carboxysomes that cluster around the center of the simulation domain (see Figure 4.10CE in the main text). For each case, we identify the parameter regime in which the carboxysomes undergo “directed segregation” – a motility mode in which the cargoes move away from each other and then become relatively stationary

(*e.g.*, see Figure 3 in Hu et al., 2017). That is, the carboxysomes are segregated and then stably positioned with a large inter-spacing. We then tracked the time evolutions of each of the simulated trajectories that are 10 minutes long, from which the final positions of, and separation distances between, carboxysomes were then calculated and reported in each case (average \pm standard deviation, $n=36$ trajectories).

REFERENCES

REFERENCES

- Adachi, S., Hori, K., and Hiraga, S. (2006). Subcellular positioning of F plasmid mediated by dynamic localization of SopA and SopB. *J. Mol. Biol.* 356(4):850-63.
- Ah-Seng, Y., Lopez, F., Pasta, F., Lane, D., and Bouet, JY. (2009). Dual role of DNA in regulating ATP hydrolysis by the SopA partition protein. *J. Biol. Chem.* 284(44):30067-75.
- Alvarado, A., Kjær, A., Yang, W., Mann, P., Briegel, A., Waldor, MK., and Ringgaard, S. (2017). Coupling chemosensory array formation and localization. *Elife.* 6:e31058.
- Atmakuri, K., Cascales, E., Burton, OT., Banta, LM., and Christie, PJ. (2007). Agrobacterium ParA/MinD-like VirC1 spatially coordinates early conjugative DNA transfer reactions. *EMBO J.* 26(10):2540-51.
- Axen, SD., Erbilgin, O., and Kerfeld, CA. (2014). A Taxonomy of Bacterial Microcompartment Loci Constructed by a Novel Scoring Method. *PLOS Comput. Biol.* 10(10):e1003898.
- Baxter JC., and Funnell, BE. (2014). Plasmid Partition Mechanisms. *Microbiol. Spectr.* 2(6).
- Bouet, JY., and Funnell, B.E. (1999). P1 ParA interacts with the P1 partition complex at parS and an ATP-ADP switch controls ParA activities. *EMBO J.* 18(5):1415-24.
- Bouet, JY, Surtees, JA, and Funnell, BE. (2000). Stoichiometry of P1 plasmid partition complexes. *Journal of Biological Chemistry. J. Biol. Chem.* 275(11):8213-9.
- Cai, F., Sutter, M., Cameron, JC., Stanley, DN., Kinney, JN., and Kerfeld, CA. (2013). The structure of CcmP, a tandem bacterial microcompartment domain protein from the β -carboxysome, forms a subcompartment within a microcompartment. *J. Biol. Chem.* 288(22):16055-63.
- Cai, F., Sutter, M., Bernstein, SL., Kinney, JN., and Kerfeld, CA. (2015). Engineering bacterial microcompartment shells: chimeric shell proteins and chimeric carboxysome shells. *ACS Synth. Biol.* 4(4):444-53.
- Cameron, J.C., Wilson, S.C., Bernstein, S.L., and Kerfeld, C.A. (2013). Biogenesis of a Bacterial Organelle: The Carboxysome Assembly Pathway. *Cell.* 155(5):1131-40.
- Castaing, JP., Bouet, JY., and Lane, D. (2008). F plasmid partition depends on interaction of SopA with non-specific DNA. *Mol. Microbiol.* 70(4):1000-11.

Chen, AH., Robinson-Mosher, A., Savage, DF., Silver, PA., and Polka, JK. (2013). The Bacterial Carbon-Fixing Organelle Is Formed by Shell Envelopment of Preassembled Cargo. *PLoS One*. 8(9):e76127.

Clerico EM, Ditty JL, and Golden SS. (2007). Specialized techniques for site-directed mutagenesis in cyanobacteria. *Methods Mol. Biol.* 362:155-71.

Cot, SS., So, AK., and Espie, GS. (2008). A multiprotein bicarbonate dehydration complex essential to carboxysome function in cyanobacteria. *Journal of Bacteriology*. *J. Bacteriol.* 190(3):936-45.

Davis, MA., and Austin, SJ. (1988). Recognition of the P1 plasmid centromere analog involves binding of the ParB protein and is modified by a specific host factor. *EMBO J.* 7(6):1881-8.

Davis, MA., Martin, KA., and Austin, SJ. (1992). Biochemical activities of the ParA partition protein of the P1 plasmid. *Mol. Microbiol.* 6(9):1141-7.

Drozdetskiy, A., Cole, C., Procter, J., and Geoffrey, JB. (2015). JPred4: a protein secondary structure prediction server. *Nucleic Acids Res.* 1;43(W1):W389-94.

Ducret, A., Quardokus, EM., and Brun, YV. (2016). MicrobeJ, a tool for high throughput bacterial cell detection and quantitative analysis. *Nat. Microbiol.* 1(7):16077.

Fan, C., Cheng, S., Sinha, S., and Bobik, TA. (2012). Interactions between the termini of lumen enzymes and shell proteins mediate enzyme encapsulation into bacterial microcompartments. *Proc. Natl. Acad. Sci.* 11;109(37):14995-5000.

Fange, D., and Elf, J. (2006). Noise-Induced Min Phenotypes in *E. coli*. *PLoS Comput. Biol.* 2(6):e80.

Faulkner, M., Rodriguez-Ramos, J., Dykes, G.F., Owen, S.V.V., Casella, S., Simpson, D.M., Beynon, R.J., and Liu, L.N. (2017). Direct characterization of the native structure and mechanics of cyanobacterial carboxysomes. *Nanoscale*. 9(30):10662-10673.

Fung, E., Bouet, JY., and Funnell, BE. (2001). Probing the ATP-binding site of P1 ParA: partition and repression have different requirements for ATP binding and hydrolysis. *EMBO J.* 20(17): 4901–4911.

Funnell, BE. (1988). Mini-P1 plasmid partitioning: excess ParB protein destabilizes plasmids containing the centromere parS. *J. Bacteriol.* 170(2):954-60.

Gall, A., Cattoni, DI., Guilhas, B., Mathieu-Demazière, C., Oudjedi, L., Fiche, JB., Rech, J., Abrahamsson, S., Murray, H., Bouet, JY., and Nollmann, M. (2016). Bacterial partition complexes segregate within the volume of the nucleoid. *Nat. Commun.* 7:12107.

Gibson, DG., Young, L., Chuang, RY., Venter, JC., Hutchison, CA., and Smith, HO. (2009). Enzymatic assembly of DNA molecules up to several hundred kilobases. *Nat. Methods*. 6(5):343-5.

Hatano, T., Yamaichi, Y., and Niki, H. (2007). Oscillating focus of SopA associated with filamentous structure guides partitioning of F plasmid. *Mol. Microbiol.* 64(5):1198-213.

Hatano, T., and Niki, H. (2010). Partitioning of P1 plasmids by gradual distribution of the ATPase ParA. *Mol. Microbiol.* 78(5):1182-98.

Hester, CM., and Lutkenhaus, J. (2007). Soj (ParA) DNA binding is mediated by conserved arginines and is essential for plasmid segregation. *Proc. Natl. Acad. Sci.* 104(51):20326-31.

Holthuijzen, YA., Maathuis, FJM., Kuenen, JG., Konings, RNH., and Konings, WN. (1986). Carboxysomes of *Thiobacillus neapolitanus* do not contain extrachromosomal DNA. *FEMS Microbiol. Lett.* 35(2-3):193-198.

Hu, B., Yang, G., Zhao, W., Zhang, Y., and Zhao, J. (2007). MreB is important for cell shape but not for chromosome segregation of the filamentous cyanobacterium *Anabaena* sp. PCC 7120. *Mol. Microbiol.* 63(6):1640-52.

Hu, L., Vecchiarelli, AG., Mizuuchi, K., Neuman, KC., and Liu, J. (2015). Directed and persistent movement arises from mechanochemistry of the ParA/ParB system. *Proc. Natl. Acad. Sci.* 112(51):E7055-64.

Hu, L., Vecchiarelli, AG., Mizuuchi, K., Neuman, KC., and Liu, J. (2017). Brownian Ratchet Mechanism for Faithful Segregation of Low-Copy-Number Plasmids. *Biophys. J.* 112(7):1489-1502.

Hwang, LC., Vecchiarelli, AG., Han, YW., Mizuuchi, M., Harada, Y., Funnell, BE., and Mizuuchi, K. (2013). ParA-mediated plasmid partition driven by protein pattern self-organization. *EMBO J.* 32(9):1238-49.

Jain IH, Vijayan V., and O'Shea, EK. (2012). Spatial ordering of chromosomes enhances the fidelity of chromosome partitioning in cyanobacteria. *Proc. Natl. Acad. Sci.* 109(34):13638-43.

Jordan, A., Chandler, J., MacCready, JS., Huang, J., Osteryoung, KW., and Ducat, DC. (2017). Engineering Cyanobacterial Cell Morphology for Enhanced Recovery and Processing of Biomass. *Appl. Environ. Microbiol.* 83(9). pii: e00053-17.

Karimova, G, Pidoux, J, Ullmann, A, and Ladant, D. (1998). A bacterial two-hybrid system based on a reconstituted signal transduction pathway. *Proc. Natl. Acad. Sci.* 95(10):5752-6.

Kelley, LA., Mezulis, S., Yates, CM., Wass, MN., and Sternberg, MJ. (2015). The Phyre2 web portal for protein modeling, prediction and analysis. *Nat. Protoc.* 10(6):845-58.

- Kerfeld, CA., Sawaya, MR., Tanaka, S., Nguyen, CV., Phillips, M., Beeby, M., and Yeates, TO. (2005). Protein structures forming the shell of primitive bacterial organelles. *Science*. 309(5736):936-8.
- Kerfeld, CA., and Erbilgin, O. (2015). Bacterial microcompartments and the modular construction of microbial metabolism. *Trends Microbiol.* 23(1):22-34.
- Kerfeld, CA., and Melnicki, MR. (2016). Assembly, function and evolution of cyanobacterial carboxysomes. *Curr. Opin. Plant Biol.* 31:66-75.
- Kinney, JN., Salmeen, A., Cai, F, and Kerfeld, CA. (2012). Elucidating essential role of conserved carboxysomal protein CcmN reveals common feature of bacterial microcompartment assembly. *J. Biol. Chem.* 287(21):17729-36.
- Kusumoto, A., Shinohara, A., Terashima, H., Kojima, S., Yakushi, T., and Homma, M. (2008). Collaboration of FlhF and FlhG to regulate polar-flagella number and localization in *Vibrio alginolyticus*. *Microbiology*. 154(Pt 5):1390-9.
- Lasocki, K., Bartosik, AA., Mierzejewska, J., Thomas, CM., and Jagura-Burdzy, G. (2007). Deletion of the *parA* (*soj*) homologue in *Pseudomonas aeruginosa* causes ParB instability and affects growth rate, chromosome segregation, and motility. *J. Bacteriol.* 189(15):5762-72.
- Le Gall, A., Cattoni, DI., Guilhas, B., Mathieu-Demazière, C., Oudjedi, L., Fiche, JB., Rech, J., Abrahamsson, S., Murray, H., Bouet, JY., and Nollmann, M. (2016). Bacterial partition complexes segregate within the volume of the nucleoid. *Nat. Commun.* 7:12107.
- Leonard, TA., Butler, PJ., and Löwe, J. (2005). Bacterial chromosome segregation: structure and DNA binding of the Soj dimer — a conserved biological switch. *EMBO J.* 24(2):270-82.
- Lim, HC., Surovtsev, IV., Beltran, BG., Huang, F., Bewersdorf, J., and Jacobs-Wagner, C. (2014). Evidence for a DNA-relay mechanism in ParABS-mediated chromosome segregation. *Elife*. 3:e02758.
- Long, BM., Badger, MR., Whitney, SM., and Price, GD. (2007). Analysis of carboxysomes from *Synechococcus* PCC7942 reveals multiple Rubisco complexes with carboxysomal proteins CcmM and CcaA. *J. Biol. Chem.* 282(40):29323-35.
- Long, BM., Tucker, L., Badger, MR., and Price, GD. (2010). Functional cyanobacterial β -carboxysomes have an absolute requirement for both long and short forms of the CcmM protein. *Plant Physiol.* 153(1):285-93.

Loose, M., Fischer-Friedrich, E., Ries, J., Kruse, K., and Schwille, P. (2008). Spatial regulators for bacterial cell division self-organize into surface waves in vitro. *Science*. 320(5877):789-92.

Loose, M., Kruse, K., and Schwille, P. (2011). Protein Self-Organization: Lessons from the Min System. *Annu. Rev. Biophys.* 40:315-36.

Lutkenhaus, J. (2007). Assembly dynamics of the bacterial MinCDE system and spatial regulation of the Z ring. *Annu. Rev. Biochem.* 76, 539–562.

MacCready, JS., Schossau, J., Osteryoung, KW., and Ducat, DC. (2017). Robust Min-system oscillation in the presence of internal photosynthetic membranes in cyanobacteria. *Mol. Microbiol.* 103(3):483-503.

Miyagishima, SY., Wolk, CP., and Osteryoung, KW. (2005). Identification of cyanobacterial cell division genes by comparative and mutational analyses. *Mol. Microbiol.* 56(1):126-43.

Montgomery, BL. (2015). Light-dependent governance of cell shape dimensions in cyanobacteria. *Front. Microbiol.* 6:514.

Murat, D., Byrne, M., and Komeili, A. (2010). Cell biology of prokaryotic organelles. Cold Spring Harb. *Perspect. Biol.* 2(10): a000422.

Murata, K., Hagiwara, S., Kimori, Y., and Kaneko, Y. (2016). Ultrastructure of compacted DNA in cyanobacteria by high-voltage cryo-electron tomography. *Sci. Rep.* 6:34934.

Nakahira, Y., Ogawa, A., Asano, H., Oyama, T., and Tozawa, Y. (2013). Theophylline-dependent riboswitch as a novel genetic tool for strict regulation of protein expression in *Cyanobacterium Synechococcus elongatus* PCC 7942. *Plant Cell Physiol.* 54(10):1724-35.

Perez-Cheeks, BA., Planet, PJ., Sarkar, IN., Clock, SA., Xu, Q., and Figurski, DH. (2012). The product of *tadZ*, a new member of the *parA/minD* superfamily, localizes to a pole in *Aggregatibacter actinomycetemcomitans*. *Mol. Microbiol.* 83(4):694-711.

Price, GD., and Badger, MR. (1989). Isolation and Characterization of High CO₂-Requiring-Mutants of the Cyanobacterium *Synechococcus* PCC7942 : Two Phenotypes that Accumulate Inorganic Carbon but Are Apparently Unable to Generate CO₂ within the Carboxysome. *Plant Physiol.* 91(2):514-25.

Price, GD., Howitt SM., Harrison K., and Badger, MR. (1993). Analysis of a genomic DNA region from the cyanobacterium *Synechococcus* sp. strain PCC7942 involved in carboxysome assembly and function. *J. Bacteriol.* 175(10):2871-9.

- Ptacin, J.L., Lee, S.F., Garner, E.C., Toro, E., Eckart, M., Comolli, L.R., Moerner, W.E., and Shapiro, L. (2010). A spindle-like apparatus guides bacterial chromosome segregation. *Nat. Cell. Biol.* 12(8):791-8.
- Rae, B.D., Long, B.M., Badger, M.R., and Price, G.D. (2012). Structural Determinants of the Outer Shell of β -Carboxysomes in *Synechococcus elongatus* PCC 7942: Roles for CcmK2, K3-K4, CcmO, and CcmL. *PLoS One.* 7(8):e43871.
- Rae, B.D., Long, B.M., Badger, M.R., and Price, G.D. (2013). Functions, compositions, and evolution of the two types of carboxysomes: polyhedral microcompartments that facilitate CO₂ fixation in cyanobacteria and some proteobacteria. *Mol. Biol. Rev.* 77(3):357-79.
- Ringgaard, S, van Zon, J, Howard, M., and Gerdes, K. (2009). Movement and equipositioning of plasmids by ParA filament disassembly. *Proc. Natl. Acad. Sci.* 106(46):19369-74.
- Ringgaard, S., Schirner, K., Davis, B.M., and Waldor, M.K. (2011). A family of ParA-like ATPases promotes cell pole maturation by facilitating polar localization of chemotaxis proteins. *Genes Dev.* 25(14):1544-55.
- Savage, D.F., Afonso, B., Chen, A.H., and Silver, P.A. (2010). Spatially Ordered Dynamics of the Bacterial Carbon Fixation Machinery. *Science.* 327(5970):1258-61.
- Schofield, W.B., Lim, H.C., and Jacobs-Wagner, C. (2010). Cell cycle coordination and regulation of bacterial chromosome segregation dynamics by polarly localized proteins. *EMBO J.* 29(18):3068-81.
- Sengupta, M., Nielsen, H.J., Youngren, B., and Austin, S. (2010). P1 plasmid segregation: accurate redistribution by dynamic plasmid pairing and separation. *J. Bacteriol.* 192(5):1175-83.
- Sommer, M., Cai, F., Melnicki, M., Kerfeld, C.A. (2017). β -Carboxysome bioinformatics: identification and evolution of new bacterial microcompartment protein gene classes and core locus constraints. *J. Exp. Bot.* 68(14):3841-3855.
- Sun, Y., Casella, S., Fang, Y., Huang, F., Faulkner, M., Barrett, S., and Liu, L.N. (2016). Light modulates the biosynthesis and organization of cyanobacterial carbon fixation machinery through photosynthetic electron flow. *Plant Physiol.* 171(1):530-41.
- Surovtsev, I.V., Campos, M., and Jacobs-Wagner, C. (2016). DNA-relay mechanism is sufficient to explain ParA-dependent intracellular transport and patterning of single and multiple cargos. *Proc. Natl. Acad. Sci.* 113(46):E7268-E7276.
- Tanaka, S., Kerfeld, C.A., Sawaya, M.R., Cai, F., Heinhorst, S., Cannon, G.C., and Yeates, T.O. (2008). Atomic-level models of the bacterial carboxysome shell. *Science.* 319(5866):1083-6.

Tanaka, S., Sawaya, MR., Phillips, M., and Yeates, TO. (2009). Insights from multiple structures of the shell proteins from the beta-carboxysome. *Protein Sci.* 18(1):108-20.

Thompson, SR., Wadhams, GH., and Armitage, JP. (2006). The positioning of cytoplasmic protein clusters in bacteria. *Proc. Natl. Acad. Sci.* 103(21):8209-14.

Vecchiarelli, AG., Han, YW., Tan, X., Mizuuchi, M., Ghirlando, R., Biertümpfel, C., Funnell, BE., and Mizuuchi, K. (2010). ATP control of dynamic P1 ParA–DNA interactions: a key role for the nucleoid in plasmid partition. *Mol. Microbiol.* 78(1):78-91.

Vecchiarelli, AG., Mizuuchi, K., and Funnell, BE. (2012). Surfing biological surfaces: exploiting the nucleoid for partition and transport in bacteria. *Mol. Microbiol.* 86(3):513-23.

Vecchiarelli, AG., Hwang, LC., and Mizuuchi, K. (2013). Cell-free study of F plasmid partition provides evidence for cargo transport by a diffusion-ratchet mechanism. *Proc. Natl. Acad. Sci.* 110(15):E1390-7.

Vecchiarelli, AG., Neuman, KC., and Mizuuchi, K. (2014). A propagating ATPase gradient drives transport of surface-confined cellular cargo. *Proc. Natl. Acad. Sci.* 111(13):4880-5.

Viollier, PH., Sternheim, N., and Shapiro, L. (2002). A dynamically localized histidine kinase controls the asymmetric distribution of polar pili proteins. *EMBO J.* 21(17):4420-8.

Youderian, P., Burke, N., White, DJ., and Hartzell, PL. (2003). Identification of genes required for adventurous gliding motility in *Myxococcus xanthus* with the transposable element mariner. *Mol. Microbiol.* 49(2):555-70.

Young, EJ., Burton, R., Mahalik, JP., Sumpter, BG., Fuentes-Cabrera, M., Kerfeld, CA., and Ducat, DC. (2017). Engineering the Bacterial Microcompartment Domain for Molecular Scaffolding Applications. *Front. Microbiol.* 8:1441.

Zhang, H., and Schumacher, MA. (2017). Structures of partition protein ParA with nonspecific DNA and ParB effector reveal molecular insights into principles governing Walker-box DNA segregation. *Genes Dev.* 31(5):481-492.

Zieske, K., and Schwille, P. (2014). Reconstitution of self-organizing protein gradients as spatial cues in cell-free systems. *Elife.* 3.

CHAPTER 5

PERSPECTIVES AND FUTURE DIRECTIONS

Cyanobacteria as model systems for studying Min and Par dynamics

During the course of my graduate career, I have thoroughly enjoyed my opportunity to study protein self-organization in cyanobacteria. While the vast majority of studies on the Min and Par systems up to this point have been performed in *B. subtilis* and *E. coli*, cyanobacteria possess many unique features not found in canonical bacteria and which could have broader implications for understanding the robust nature of these biological patterns. Indeed, in chapter 2, I explored how the presence of thylakoid membranes influences Min-system patterning and how perforations across thylakoid layers might contribute to emergent Min oscillation. Likewise, in chapter 4, I detailed a new class of proteins that self-organize to position the carbon-fixing organelles of cyanobacteria, carboxysomes, via a mechanism that shares subtle similarities to systems that partition low-copy number plasmids. Here, I detail some additional features unique to cyanobacteria that could influence Min and Par system function, warranting further investigation.

Circadian Rhythms

Cyanobacteria are the only prokaryotic organisms that perform oxygenic photosynthesis and are known to possess a biological circadian clock that precisely operates on the 24-hour rotational period of the earth. Circadian rhythms primarily enable cyanobacteria to anticipate, adapt and respond to daily light cycles by translating environmental cues into changes in gene expression (reviewed in: Cohen and Golden, 2015) (Figure 5.1ABC). The molecular mechanisms underlying the central time-keeping device have been predominantly studied in *S. elongatus*, where they have been shown to influence the timing of cell division. At the core of the circadian oscillator is the protein KaiC, which possesses autokinase and autophosphatase activities (Nishiwaki et al., 2004; Xu et al., 2004). The phosphorylation and ATPase activities of KaiC, a cyclic process that is mediated by the proteins KaiA and KaiB, are central to the emergent properties of the clock. KaiA promotes the autokinase activity of KaiC, whereas KaiB sequesters KaiA away from KaiC, activating the autophosphatase activity of KaiC (Kim et al., 2008; Chang et al., 2012) (Figure 5.1B). Remarkably, reconstitution of the clock can be performed *in vitro* with as little as KaiA, KaiB, KaiC and ATP

(Nakajima et al., 2005), although additional proteins are necessary to synchronize the phase of the clock to light cycles (input) and relay temporal information from the central oscillator to transcriptional regulators of gene expression (output).

The phosphorylation cycles of KaiC do not intrinsically occur on a 24-hour period; instead, the entrainment of the clock is performed by key input proteins that are tightly coupled to the photosynthetic lifestyle of *S. elongatus*. Indeed, KaiA, the iron-sulfur protein LdpA, and the histidine protein kinase CikA influence KaiC phosphorylation by sensing changes in the redox state of the cell by binding oxidized quinone (KaiA and CikA) and becoming targeted for degradation, or by directly detecting the presence of light (LdpA) (Ivleva et al., 2005; Ivleva et al., 2006; Wood et al., 2010). Additionally, KaiC activity is also modulated by the cellular ATP-ADP pool, a ratio that is highly influenced by photosynthesis during the day (Terauchi et al., 2007; Dong et al., 2010). Lastly, expression of Pex occurs in the absence of light; functioning to downregulate KaiA expression and promote KaiC dephosphorylation (Kutsuna et al., 2007). These three core mechanisms of redox-sensing, ATP pool sensing, and direct environmental light-sensing are thought to entrain the phase of the clock.

In *S. elongatus*, oscillatory patterns of gene expression are driven by the phosphorylation of the transcriptional response regulator RpaA (Figure 5.1C). Phosphorylated RpaA (RpaA~P) binds to the promoters of ~170 characterized sites on the chromosome, including regions important for regulating metabolic, clock, division, elongation, and replication factors, all dependent on the RpaA/RpaA~P ratio (Markson et al., 2013). In day/night cycles, the clock drives expression of two distinct categories of genes, Class I and Class II, where RpaA~P initiates expression of Class I genes. Class I genes have peak expression at subjective night (entrained cells anticipating oncoming dark, but kept in the light) and Class II genes have peak expression at subjective dawn (cells anticipating to enter the light, but are transferred to dark). Deletion of *rpaA* arrests cells in a class II expression dawn-like state and abolishes oscillatory patterns of gene expression (Takai et al., 2006), whereas overexpression of an RpaA phosphomimic (D53E) that mimics RpaA~P switches gene expression to a class I expression dusk-like state, resulting in an inhibition of cell division. The timing of the accumulation of RpaA~P is mediated by the SasA-CikA output pathway, whereby SasA phosphorylates RpaA and CikA dephosphorylates RpaA (Figure 5.1C), resulting

in peak RpaA~P levels at the onset of subjective night (Gutu and O'Shea, 2013). To prevent competition for the stimulation of RpaA, the phosphorylation state of KaiC regulates the timing of SasA and CikA activation. For example, the kinase activity of SasA is only activated following SasA binding to fully phosphorylated KaiC (Iwaski et al., 2000; Takai et al., 2006), occurring late within the light period, and deactivated upon SasA binding to KaiB, occurring early in the dark period (Gutu and O'Shea, 2013; Chang et al., 2015). Alternatively, the phosphatase activity of CikA can only be activated when CikA is bound to fully dephosphorylated KaiC, occurring early within the dark period (Gutu and O'Shea, 2013; Chang et al., 2015).

The inherent simplistic nature of the core KaiABC circadian oscillator has attracted extensive research into the nature of how biological clocks regulate not only global gene expression (Kondo et al., 1993), chromosome compaction (Smith and Williams, 2006; Woelfle et al., 2007) and metabolite partitioning (Diamond et al., 2015), but also cellular division (Mori et al., 1996; Mori and Johnson, 2001). In *S. elongatus*, cell division occurs only in the presence of light, independent of the circadian clock (Mori et al., 1996) (Figure 5.1D). However, the circadian clock is also capable of inhibiting cell division in the presence of light (circadian gating) (Mori et al., 1996) (Figure 5.1E). The gating phenomenon occurs when cells are synchronized in light/dark cycles and released into constant light. When cells anticipate the impending dark periods (subjective night), cell division is inhibited during a 4-6 hour window (Figure 5.1E). By "tricking" the cells in this manner, we are able to disentangle light versus circadian-influenced cell phenotypes since dusk-class genes are expressed, but light is present.

The phenomenon of circadian gating is further illustrated with the deletion of *kaiB* or *cikA*, which produce elongated cells that result from an exaggerated gating period (Dong et al., 2010) (Figure 5.1F). These elongated cells are returned to wild-type cell lengths upon the generation of $\Delta kaiB \Delta sasA$, $\Delta kaiB \Delta rpaA$ or $\Delta cikA \Delta sasA$ double mutants, suggesting that the factor imposing the gate is epistatic to the central oscillator and that RpaA~P is required for gating (Dong et al., 2010; Markson et al., 2013) (Figure 5.1F). Indeed, high expression of RpaA(D53E), which mimics phosphorylated RpaA, extends the gate, whereas high expression of RpaA(D53A), which mimics unphosphorylated RpaA, abolishes the gate (Markson et al., 2013). These RpaA phosphomimics demonstrated that the gating phenomenon is a

consequence of RpaA~P levels (Markson et al., 2013). Additionally, the ATPase activity of KaiC has recently been implicated as the mechanism controlling the gating phenomenon. By mimicking varying levels of ATPase activity through the generation of several KaiC mutants, the timing and the duration of the gating period could be modulated. It now appears that the timing and duration of the gating phenomenon is dictated by the central KaiABC oscillator, but the factor that imposes the gate is a target of RpaA~P (Markson et al., 2013). Indeed, when the ATPase activity of KaiC is high, *S. elongatus* exhibits a mislocalization of FtsZ that is independent of FtsZ levels (Mori and Johnson, 2001; Dong et al., 2010). This suggests that RpaA~P might regulate factors involved in FtsZ positioning during the gating period.

In gating cell division, a likely target of RpaA~P is the Min system. The Min system of *S. elongatus* displays both an *E. coli*-like pole-to-pole oscillation of MinCDE and a *B. subtilis*-like midcell localized pool of Cdv3, MinC and MinD (MacCready et al., 2017). The mislocalization of FtsZ during the circadian gate could result from a loss of MinC oscillation or midcell recruitment. Further analysis is now needed to determine if MinC localization is influenced by RpaA~P and why *S. elongatus* possesses a division gate.

Beyond the cell division gate, how circadian rhythms influence carboxysome biogenesis and positioning remains unclear. Indeed, *mcdA* and *mcdB*, which regulate carboxysome positioning and size, are a direct target of RpaA~P (Markson et al., 2013). It's likely that McdA and McdB protein levels are modulated over the life cycle of *S. elongatus*. This could explain why carboxysomes sometimes display dancing, stochastic rapid lateral movement, while carboxysomes in other cells remain completely static. Indeed, in the ParAB system, lowered ParB levels or increased ParA levels result in plasmids becoming stuck to the nucleoid, unable to move (Vecchiarelli et al., 2013). Moreover, our study also revealed that McdB levels influence carboxysome size. It's possible that the circadian clock is relaying environmental cues to modulate McdB levels, and thus, carboxysome size. Further analysis is now required to elucidate how circadian rhythms influence the McdAB system.

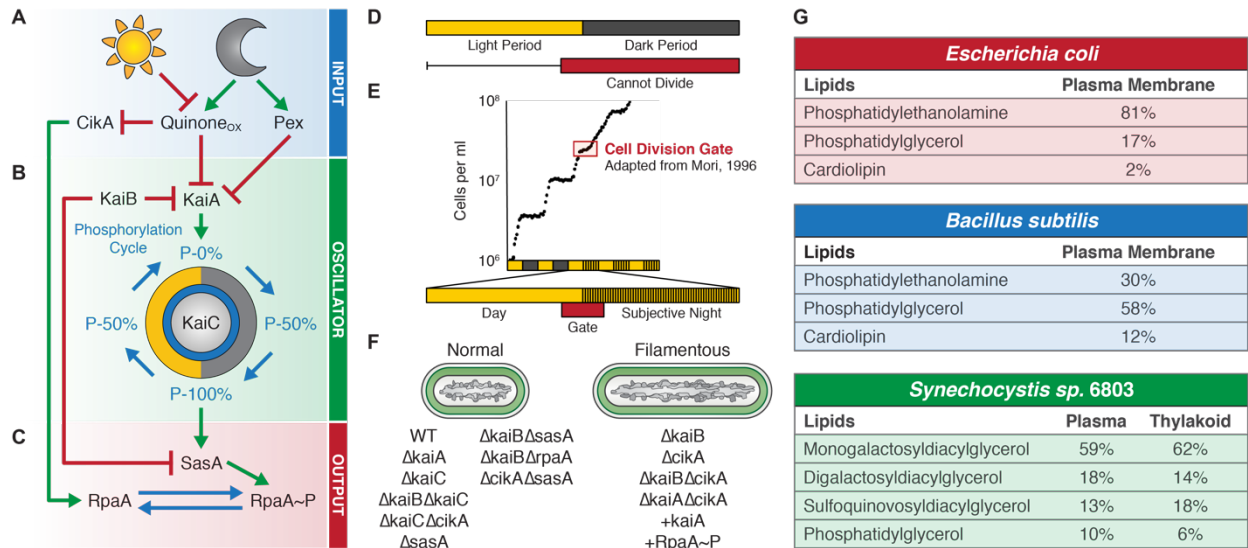


Figure 5.1: Cyanobacterial features possibly influencing Min and Par system function

(A-C) Cartoon depiction of the *S. elongatus* circadian rhythm circuit input (A), core oscillator (B), and output relay (C). (D) *S. elongatus* cannot divide in the absence of light. (E) During repeated 24-hour light/dark cycles, *S. elongatus* does not divide during a ~4-6 hour window around the expected transition into night. Figure Adapted from Mori, 1996. (F) Several clock deletions produce elongated cells due to an exaggerated gating period. All filamentous clock mutants are consistent with elevated RpaA levels. (G) Membrane lipid compositions among *E. coli* (red), *B. subtilis* (blue), and *Synechocystis sp. 6803* (green).

Thylakoid Membranes

Our results from Chapter 2 suggested that cyanobacterial MinD and/or MinE require a mechanism to distinguish between the plasma membrane and thylakoid membrane, though this mechanism is not obvious. Indeed, while the proton motive force across the plasma membrane has previously been shown to be important for membrane binding of *E. coli* MinD and MinE (Strahl and Hamoen, 2010), electrochemical gradients are established across both plasma and thylakoid membranes in cyanobacteria (reviewed in: Hohmann-Marriott and Blankenship, 2011). Therefore, a more likely hypothesis is that slight differences in plasma and thylakoid membrane lipid compositions could provide a mechanism for preferential binding of MinD and/ or MinE to the plasma membrane.

Most bacterial membranes contain phospholipids, two hydrophobic acyl chains connected to a hydrophilic phosphate head by a glycerol molecule, which form a bilayer from their intrinsic amphipathic characteristics. Three main phospholipids make up the plasma membrane in *E. coli* and *B. subtilis*: phosphatidylethanolamine (PE), which is zwitterionic, and phosphatidylglycerol (PG) and cardiolipin (CL), which are anionic (Sohlenkamp and Geiger, 2016). However, the ratio of these lipids greatly differs between these two organisms (Figure 5.1G). In contrast, cyanobacteria largely lack phospholipids, only possessing PG. Instead, the plasma and thylakoid membranes primarily consist of nonionic glycerolipids such as monogalactosyldiacylglycerol (MGDG), digalactosyldiacylglycerol (DGDG), and the sulfur-containing sulfoquinovosyldiacylglycerol (SQDG) (Sohlenkamp and Geiger, 2016) (Figure 5.1G).

Recently, an *in vitro* study reconstituted Min protein dynamics in a lipid-containing synthetic flow cell using purified fluorescent fusions of *E. coli* MinD and MinE to explore the influence of lipid content on emergent Min patterning (Vecchiarelli et al., 2014). Once thought to be important for Min oscillation due to its enrichment at the polar regions of cells, cardiolipin was shown to be dispensable for Min oscillation. Instead, Min proteins bound preferentially to PG, consistent with a previous *in vitro* study (Renner and Weibel, 2012). By varying PG content within the flow cell from high to low, the authors were able to show that Min dynamics were highly dependent on the amount of PG. Indeed, Min dynamics were lost when PG content was above ~60% or below ~13%.

This experiment raises several questions in the context of cyanobacterial Min oscillation. First, while PG content is around 23% in *E. coli*, PG is the least abundant phospholipid in the plasma membrane (~10%) and thylakoid membranes (~6%) of cyanobacteria (Gombos et al., 1996) (Figure 5.1G). Therefore, how Min oscillations occur in cyanobacteria in light of low PG content and whether the nearly two-fold difference in PG content between the plasma membrane and thylakoid membrane network could allow MinD to preferentially bind the plasma membrane over the thylakoid membranes in cyanobacteria remain outstanding questions. Differences in charge of the C-terminal amphipathic helix of *S. elongatus* and *E. coli* MinD may provide a mechanism. Since the amphipathic helix of *S. elongatus* MinD is much more positively charged, this might allow MinD to bind cyanobacterial membranes in the face of low PG content. Additionally, PG in the thylakoid membranes is crucial for the assembly and function of photosystems I and II (Sato et al., 2000; Domonkos et al., 2004; Laczkó-Dobos et al., 2008). Since PG is enriched in and around photosystems and saturated with numerous peripheral phycobilisomes, this feature might limit physical access of MinD to PG in thylakoid membranes. *In vitro* reconstitution is now needed of *S. elongatus* Min dynamics under varying concentrations of PG, MGDG, DGDG and SQDQ to further our understanding of how Min proteins oscillate in cyanobacteria. These results would have further implications for understanding Min system dynamics in the chloroplasts of red/green algae and plants, which have nearly identical lipid compositions as cyanobacteria (Boudière et al., 2014).

Nucleoid Topology

The underlying biological surface upon which MinD/ParA-type ATPases assemble largely influences emergent patterning. To correctly segregate plasmids, the bacterial nucleoid is utilized as a scaffold to drive directed and persistent motion of these cargos towards both polar regions of the cell. While plasmid partitioning has been analyzed in organisms such as *Vibrio cholerae* and *Borrelia burgdorferi*, which possess multiple chromosomes, the vast majority of studies analyzing ParA-mediated segregation have been performed in *E. coli*, which possesses 1-2 chromosomes depending on the life-stage.

Like *V. cholerae* and *B. burgdorferi*, cyanobacteria also carry multiple copies of their chromosome. Indeed, *S. elongatus* possesses between one and 10 identical copies of its circular chromosome (Griese et al., 2011). While genome copy-number can greatly vary among *S. elongatus* cells in a single culture, protein-levels remain consistent across the population (Zheng and O'Shea, 2017). In other words, protein levels are not a consequence of genome copy-number in *S. elongatus*. Since McdAB levels are presumably identical across a population of cells and emergent dynamics of MinD/ParA family proteins are largely influenced by the geometry and area of the biological surface upon which they assemble, whether McdAB system behavior would differ between similarly-sized *S. elongatus* cells as a consequence of the number of chromosomes is an open question.

Confounding the exploration of this question, the nucleoid of *S. elongatus* displays rhythmic condensation and relaxation cycles dependent on the circadian clock (Smith and Williams, 2006; Woelfle et al., 2007). Indeed, over a 24-hour light/dark period, chromosomes are aggregated into a singular nucleoid region during the day and rearrange into multiple “nucleoid islands” prior to transition into night (Woelfle et al., 2007). This phenomenon has important implications for understanding McdAB dynamics, and subsequently carboxysome positioning, over a full circadian cycle. Whether oscillation of McdA can “hop” the gap between adjacent nucleoid islands or whether multiple independent McdA oscillations occur on individual islands remains an outstanding question. Exploration of these fundamental questions will contribute to our understanding of the robust nature of the McdAB systems and provide valuable insight into the connection between nutrient availability, circadian rhythms, stress responses and carboxysome biogenesis/regulation in cyanobacteria.

Future Directions

It has recently become apparent that many bacteria possess specialized protein-based organelles, also known as bacterial microcompartments (BMCs), challenging many long-held views in microbiology (Axen et al., 2014). BMCs are characterized depending on whether they perform anabolic or catabolic reactions. The model anabolic BMC is the carboxysome, classified as α or β depending on the type of Ribulose-1,5-bisphosphate carboxylase/oxygenase (RuBisCO) they encapsulate (Figure 5.2ABEF) (Rae et al., 2013). Since RuBisCO can bind CO_2 or O_2 indiscriminately, carbonic anhydrase creates a high- CO_2 environment within carboxysomes to drive reactions towards the Calvin-Benson-Bassham cycle and away from photorespiration. By this mechanism, carboxysomes contribute to greater than 25% of global carbon-fixation through atmospheric CO_2 assimilation. Alternatively, the model catabolic BMCs are 1,2-propanediol utilization (PDU) (Figure 5.2CG) and ethanolamine utilization (EUT) (Figure 5.2DH) (Chowdhury et al., 2014). These BMCs protect the cell from aldehyde toxicity during catabolism of the target substrate and are important for growth of *Listeria* and enteric pathogenesis by *Salmonella* (Jakobson and Tullman-Ercek, 2016). Recently, several new BMCs have been discovered across a broad evolutionary range and have gained considerable attention for their ability to encapsulate diverse reactions (Figure 5.2I) (Axen et al., 2014). However, although new BMCs are being discovered with increasing frequency, identification of the factors regulating BMC subcellular organization has remained elusive.

In chapter 4, I showed that β -carboxysomes are strategically positioned along the longitudinal axis of the cyanobacterium *Synechococcus elongatus* PCC 7942 by a new class of self-organizing proteins, McdA and McdB, to ensure faithful inheritance of carboxysomes following cell division. While previous models for McdA function proposed a “push-or-pull” self-assembling cytoskeletal mechanism, we showed that McdA is instead part of a self-organizing protein family that does not self-assemble into a higher order structure, but instead forms dynamic oscillatory patterns along nucleoids, by continually hydrolyzing ATP. Mechanistically, we found that McdA is a Walker-A ATPase that non-specifically binds DNA and exploits the nucleoid to position β -carboxysomes equidistantly by a pole-to-pole oscillation (Figure 5.2J). McdB, representing a new family of proteins, localizes to β -carboxysomes through an interaction with shell proteins

and removes McdA from the nucleoid by stimulating its inherent ATPase activity. Consistent with this, we found that in the absence of carboxysomes, site-specificity of McdB is lost and McdA dynamics along the nucleoid collapses. The interaction between β -carboxysome-localized McdB and nucleoid-localized McdA causes: (i) a depletion zone to form within the vicinity of carboxysomes, (ii) a global break in McdA symmetry to occur along the nucleoid, (iii) movement of carboxysomes toward increased McdA concentration, and (iv) emergence of a pole-to-pole oscillation of McdA across space and time (Figure 5.2JK). This behavior can be described as a Brownian-Ratchet, which accounts for directed and persistent movement of carboxysomes towards increased McdA concentration. Moreover, reaction-diffusion simulations, using parameters established for the ParA/ParB system, revealed that a self-organizing pattern could account for linear and hexagonal packing of carboxysomes. Therefore, the McdAB system ensures that cell death does not occur from a lack of carboxysome inheritance following cell division (Figure 5.2L) by spacing carboxysomes equidistantly from each other (Figure 5.2M).

In my future work, I will explore the molecular mechanisms of α - & β -carboxysome subcellular organization using a combination of *in vivo*, *in vitro* and *in silico* approaches. This research is creative & unique because I will be establishing an entirely new multidisciplinary field of study, subcellular organization of bacterial organelles, and my graduate work with protein self-organization and β -carboxysome positioning has perfectly poised me to advance knowledge in this field. I anticipate the expected outcomes of this work will broaden our knowledge of BMC biogenesis, define the kinetics that contribute to subcellular organization of bacterial organelles by emergent protein patterning, and elucidate the coevolution of McdA/McdB and BMC systems across bacterial phyla.

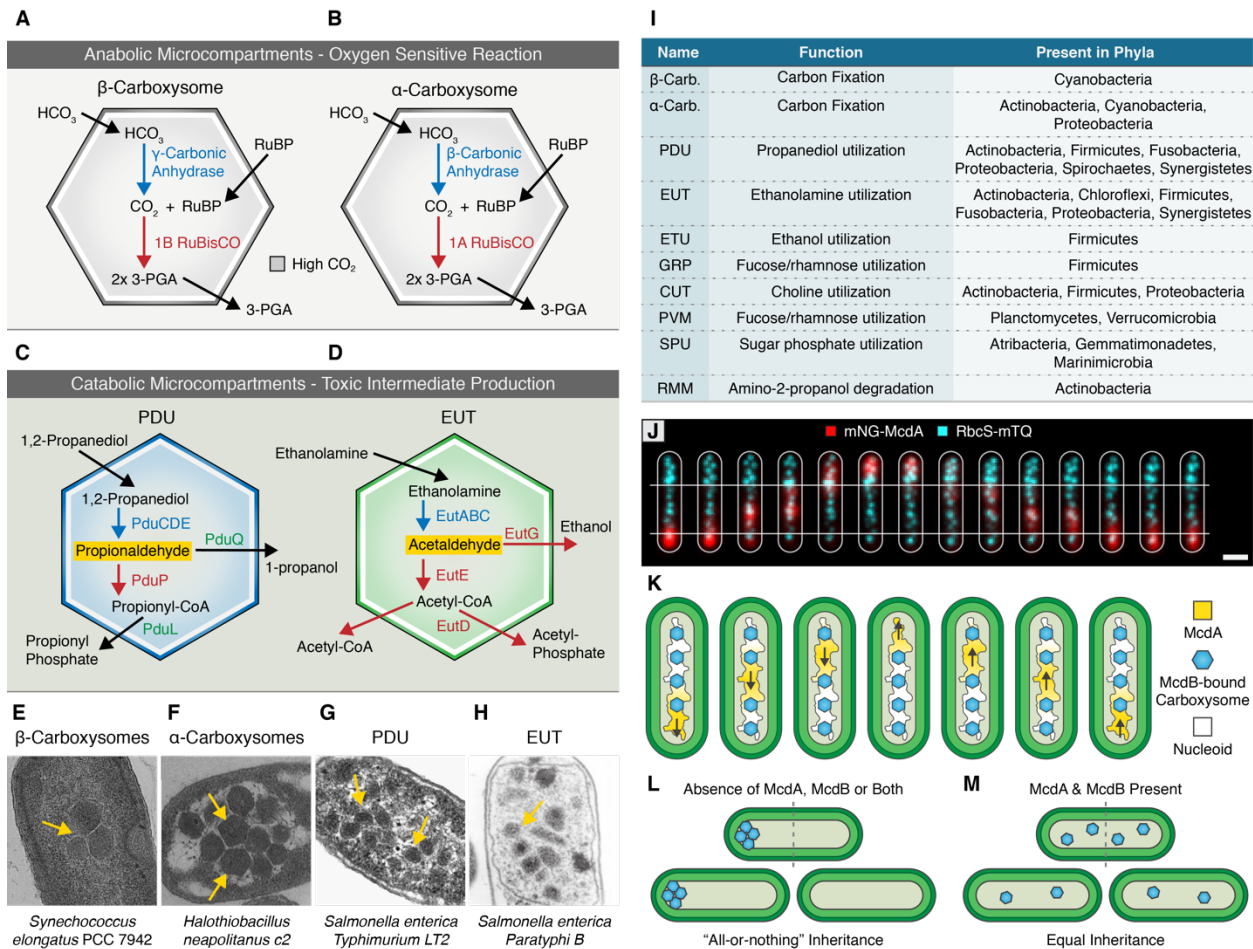


Figure 5.2: Diversity of bacterial microcompartments

(A) Cartoon illustration of the metabolic capacity of β -carboxysome, (B) α -Carboxysome, (C) Propanediol utilization, and (D) ethanolamine utilization microcompartments. (E) Transmission electron micrographs of β -carboxysomes (Chapter 4), (F) α -Carboxysomes (Menon et al., 2008), (G) PDU (Crowley et al., 2008), and (H) EUT microcompartments (Kerfeld et al., 2010). (I) Diverse microcompartments are found across many bacterial phyla. (J) Carboxysomes (blue) are positioned by oscillation of McdA (red). White lines present for guidance. (K) Model for equidistance positioning of carboxysomes. McdB-bound carboxysomes (blue) more towards increased concentrations of McdA (yellow) on the nucleoid (white). Subsequently, McdB removes McdA from the nucleoid. (L) In the absence of McdA, McdB, or both proteins, carboxysomes cluster towards polar regions of the cells, reducing the rate of their inheritance. (M) Alternatively, when carboxysomes are equidistantly spaced, carboxysomes are equally inherited.

Identification & Diversity of BMC Trafficking Systems Across Bacteria

The increasing availability of genomic data, in combination with targeted bioinformatic analyses, has resulted in a wealth of data suggesting that BMCs are present in many bacterial phyla (Figure 5.2I) (Axen et al., 2014). In these organisms, the vast majority of BMC-related genes tend to form operons with their respective encapsulated enzymes. My preliminary bioinformatic analysis of regions near α - & β -carboxysome operons has identified several McdA/B-like sequences, suggesting a possible functional association. In support of this hypothesis, heterologous expression of the *Gloeobacter kilaueensis* JSI McdB-like protein in an *S. elongatus* strain lacking native McdB resulted in colocalization with carboxysomes (Figure 4.12B). However, the *G. kilaueensis* McdB-like protein was unable to remove native McdA from the nucleoid, suggesting a high specificity between McdA/B partners. Moreover, the heterologous expression of several other candidate McdB-like proteins from other cyanobacterial species did not bind *S. elongatus* carboxysomes, suggesting that McdA/McdB and McdB/carboxysome interactions are highly specific and divergent across evolutionary time. Therefore, a more rigorous analysis is warranted.

One possible method for identifying diverse *mcdA/B* sequences would be to perform rigorous neighborhood and co-occurrence analyses to build locus similarity networks that identify putative McdA/B sequences near all known BMC operons across all BMC-containing bacterial genomes. The results would provide strong evidence that the McdA/B subcellular organization system is widespread among BMC-containing bacteria and also provide a foundation for quantifying McdA/B system diversity. Subsequently, Markov Chain Monte Carlo could also be implemented to perform the Bayesian analyses necessary for analyzing the residues or regions of coevolution between McdA/McdB and McdB/Carboxysome interaction. This in-depth analysis might provide the quantitative models needed for identification of protein-protein specificity. Therefore, these comprehensive bioinformatic analyses are critical for not only identifying divergence between McdA/B systems across diverse BMCs, but also for understanding McdA/B coevolution with their respective BMC.

REFERENCES

REFERENCES

- Axen, SD., Erbilgin, O., and Kerfeld, CA. (2014). A taxonomy of bacterial microcompartment loci constructed by a novel scoring method. *PLoS Comput. Biol.* 10(10):e1003898.
- Boudière, L., Michaud, M., Petroustos, D., Rébeillé, F., Falconet, D., Bastien, O., Roy, S., Finazzi, G., Rolland, N., Jouhet, J., et al. (2014). Glycerolipids in photosynthesis: composition, synthesis and trafficking. *Biochim. Biophys. Acta.* 1837(4):470-80.
- Chang, YG., Tseng, R., Kuo, NW., and LiWang, A. (2012). Rhythmic ring-ring stacking drives the circadian oscillator clockwise. *Proc. Natl. Acad. Sci.* 109(42):16847-51.
- Chang, YG., Cohen, S., Phong, C., Myers, W., Kim, YI., Tseng, R., Lin, J., Zhang, L., Boyd, J., Lee, Y., et al. (2015). A protein fold switch joins the circadian oscillator to clock output in cyanobacteria. *Science.* 349, 324–328.
- Chowdhury, C., Sinha, S., Chun, S., Yeates, TO., and Bobik, TA. (2014). Diverse bacterial microcompartment organelles. *Microbiol. Mol. Biol. Rev.* 78(3):438-68.
- Cohen, S., and Golden, SS. (2015). Circadian Rhythms in Cyanobacteria. *Microbiol. Mol. Biol. R.* 79, 373–385.
- Crowley, CS., Sawaya, MR., Bobik, TA., and Yeates, TO. (2008). Structure of the PduU shell protein from the Pdu microcompartment of Salmonella. *Structure.* 16(9):1324-32.
- Domonkos, I., Malec, P., Sallai, A., Kovács, L., Itoh, K., Shen, G., Ughy, B., Bogos, B., Sakurai, I., Kis, M., et al. (2004). Phosphatidylglycerol Is Essential for Oligomerization of Photosystem I Reaction Center. *Plant Physiol.* 134, 1471–1478.
- Dong, G., Yang, Q., Wang, Q., Kim, YI., Wood, T., Osteryoung, KW., Oudenaarden, A., and Golden, SS. (2010). Elevated ATPase Activity of KaiC Applies a Circadian Checkpoint on Cell Division in *Synechococcus elongatus*. *Cell.* 140, 529–539.
- Diamond, S., Jun, D., Rubin, B., and Golden, SS. (2015). The circadian oscillator in *Synechococcus elongatus* controls metabolite partitioning during diurnal growth. *Proc. Natl. Acad. Sci.* 112, E1916–E1925.
- Gombos, Z., Wada, H., Varkonyi, Z., Los, DA., and Murata, N. (1996). Characterization of the Fad12 mutant of *Synechocystis* that is defective in delta 12 acyl-lipid desaturase activity. *Biochim. Biophys. Acta.* 1299(1):117-23.

Griese, M., Lange, C., and Soppa, J. (2011). Ploidy in cyanobacteria. *FEMS Microbiol. Lett.* 323(2):124-31.

Gutu, A., and O'Shea, EK. (2013). Two antagonistic clock-regulated histidine kinases time the activation of circadian gene expression. *Mol. Cell.* 50, 288–294.

Hohmann-Marriott, MF., and Blankenship, RE. (2011). Evolution of photosynthesis. *Annu. Rev. Plant Biol.* 62, 515–548.

Ivleva, NB., Bramlett, MR., Lindahl, PA., and Golden, SS. (2005). LdpA: a component of the circadian clock senses redox state of the cell. *EMBO J.* 24:1202–1210.

Ivleva, NB., Gao, T., LiWang, AC., and Golden, SS. (2006). Quinone sensing by the circadian input kinase of the cyanobacterial circadian clock. *Proc. Natl. Acad. Sci.* 103:17468–17473.

Iwasaki, H., Williams, S., Kitayama, Y., Ishiura, M., Golden, SS., and Kondo, T. (2000). A KaiC-Interacting Sensory Histidine Kinase, SasA, Necessary to Sustain Robust Circadian Oscillation in Cyanobacteria. *Cell.* 101, 223–233.

Jakobson, CM., and Tullman-Ercek, D. (2016). Dumpster Diving in the Gut: Bacterial Microcompartments as Part of a Host-Associated Lifestyle. *PLoS Pathog.* 12(5):e1005558.

Kerfeld, CA., Heinhorst, S., and Cannon, GC. (2010). Bacterial microcompartments. *Annu. Rev. Microbiol.* 64:391-408.

Kim, YI., Dong, G., Carruthers, CW., Golden, SS., and LiWang, A. (2008). The day/night switch in KaiC, a central oscillator component of the circadian clock of cyanobacteria. *Proc. Natl. Acad. Sci.* 105(35):12825-30.

Kondo, T., Strayer, C., Kulkarni, R., Taylor, W., Ishiura, M., Golden, SS., and Johnson, C. (1993). Circadian rhythms in prokaryotes: luciferase as a reporter of circadian gene expression in cyanobacteria. *Proc. Natl. Acad. Sci.* 90, 5672–5676.

Kutsuna, S., Kondo, T., Ikegami, H., Uzumaki, T., Katayama, M., and Ishiura, M. (2007). The circadian clock-related gene pex regulates a negative cis element in the kaiA promoter region. *J. Bacteriol.* 189, 7690–7696.

Laczkó-Dobos, H., Ughy, B., Tóth, S., Komenda, J., Zsiros, O., Domonkos, I., Párducz, Á., Bogos, B., Komura, M., Itoh, S., et al. (2008). Role of phosphatidylglycerol in the function and assembly of Photosystem II reaction center, studied in a cdsA-inactivated PAL mutant strain of Synechocystis sp. PCC 6803 that lacks phycobilisomes. *Biochim. Biophys. Acta.* 1777, 1184–1194.

- MacCready, JS., Schossau, J., Osteryoung, KW., and Ducat, DC. (2016). Robust Min-system oscillation in the presence of internal photosynthetic membranes in cyanobacteria. *Mol. Microbiol.* 103, 483–503.
- Markson, JS., Piechura, JR., Puszynska, AM., and O’Shea, EK. (2013). Circadian Control of Global Gene Expression by the Cyanobacterial Master Regulator RpaA. *Cell.* 155, 1396–1408.
- Menon, BB., Dou, Z., Heinhorst, S., Shively, JM., and Cannon, GC. (2008). Halothiobacillus neapolitanus carboxysomes sequester heterologous and chimeric RubisCO species. *PLoS One.* 3(10):e3570.
- Mori, T., Binder, B., and Johnson, C. (1996). Circadian gating of cell division in cyanobacteria growing with average doubling times of less than 24 hours. *Proc. Natl. Acad. Sci.* 93, 10183–10188.
- Mori, T., and Johnson, C. (2001). Independence of Circadian Timing from Cell Division in Cyanobacteria. *J. Bacteriol.* 183(8): 2439-2444.
- Nakajima, M., Imai, K., Ito, H., Nishiwaki, T., Murayama, Y., Iwasaki, H., Oyama, T., and Kondo, T. (2005). Reconstitution of circadian oscillation of cyanobacterial KaiC phosphorylation in vitro. *Science.* 308(5720):414-5.
- Nishiwaki, T., Satomi, Y., Nakajima, M., Lee, C., Kiyohara, R., Kageyama, H., Kitayama, Y., Temamoto, M., Yamaguchi, A., Hijikata, A., et al. (2004). Role of KaiC phosphorylation in the circadian clock system of *Synechococcus elongatus* PCC 7942. *Proc. Natl. Acad. Sci.* 101:13927-13932.
- Rae, BD., Long, BM., Badger, MR., and Price, GD. (2013). Functions, compositions, and evolution of the two types of carboxysomes: polyhedral microcompartments that facilitate CO₂ fixation in cyanobacteria and some proteobacteria. *Microbiol. Mol. Biol. Rev.* 77(3):357-79.
- Renner, L., and Weibel, D. (2012). MinD and MinE Interact with Anionic Phospholipids and Regulate Division Plane Formation in *Escherichia coli*. *J. Biol. Chem.* 287, 38835–38844.
- Sato, N., Hagio, M., Wada, H., and Tsuzuki, M. (2000). Requirement of phosphatidylglycerol for photosynthetic function in thylakoid membranes. *Proc. Natl. Acad. Sci.* 97(19):10655-60.
- Sohlenkamp, C., and Geiger, O. (2016). Bacterial membrane lipids: diversity in structures and pathways. *FEMS Microbiol. Rev.* 40(1):133-59.
- Smith, RM., and Williams, SB. (2006). Circadian rhythms in gene transcription imparted by chromosome compaction in the cyanobacterium *Synechococcus elongatus*. *Proc. Natl. Acad. Sci.* 103:8564–8569.
- Strahl, H., and Hamoen, L. (2010). Membrane potential is important for bacterial cell division. *Proc. Natl. Acad. Sci.* 107, 12281–12286.

Takai, N., Nakajima, M., Oyama, T., Kito, R., Sugita, C., Sugita, M., Kondo, T., and Iwasaki, H. (2006). A KaiC-associating SasA-RpaA two-component regulatory system as a major circadian timing mediator in cyanobacteria. *Proc. Natl. Acad. Sci.* 103, 12109-12114.

Terauchi, K., Kitayama, Y., Nishiwaki, T., Miwa, K., Murayama, Y., Oyama, T., and Kondo, T. (2007). ATPase activity of KaiC determines the basic timing for circadian clock of cyanobacteria. *Proc. Natl. Acad. Sci.* 104, 16377–16381.

Tsai, Y., Sawaya, MR., Cannon, GC., Cai, F., Williams, EB., Heinhorst, S., Kerfeld, CA., and Yeates, TO. (2007). Structural analysis of CsoS1A and the protein shell of the Halothiobacillus neapolitanus carboxysome. *PLoS Biol.* 5(6):e144.

Vecchiarelli, AG., Hwang, LC., and Mizuuchi, K. (2013). Cell-free study of F plasmid partition provides evidence for cargo transport by a diffusion-ratchet mechanism. *Proc. Natl. Acad. Sci.* 110(15):E1390-7.

Vecchiarelli, AG., Li, M., Mizuuchi, M., and Mizuuchi, K. (2014). Differential affinities of MinD and MinE to anionic phospholipid influence Min patterning dynamics in vitro. *Mol. Microbiol.* 93, 453–463.

Woelfle, MA., Xu, Y., Qin, X., and Johnson, CH. (2007). Circadian rhythms of superhelical status of DNA in cyanobacteria. *Proc. Natl. Acad. Sci.* 104(47):18819-24.

Wood, TL., Bridwell-Rabb, J., Kim, YI., Gao, T., Chang, YG., LiWang, A., Barondeau, DP., and Golden, SS. (2010). The KaiA protein of the cyanobacterial circadian oscillator is modulated by a redox-active cofactor. *Proc. Natl. Acad. Sci.* 107(13):5804-9.

Xu, Y., Mori, T., Pattanayek, R., Pattanayek, S., Egli, M., and Johnson, CH. (2004). Identification of key phosphorylation sites in the circadian clock protein KaiC by crystallographic and mutagenetic analyses. *Proc. Natl. Acad. Sci.* 10: 13933–13938.

Zheng, XY., and O'Shea, EK. (2017). Cyanobacteria Maintain Constant Protein Concentration despite Genome Copy-Number Variation. *Cell Rep.* 19(3):497-504.